

In presenting this thesis in partial fulfillment of the requirements for an advanced degree at Idaho State University, I agree that the Library shall make it freely available for inspection. I further state that permission for extensive copying of my thesis for scholarly purposes may be granted by the Dean of the Graduate School, Dean of my academic division, or by the University Librarian. It is understood that any copying or publication of this thesis for financial gain shall not be allowed without my written permission.

Signature _____

Date _____

Verification of the 3-Region Advanced Test Reactor MCNP Model

by

Brenna Carbno

A thesis

submitted in partial fulfillment

of the requirements for the degree of

Master of Science in the Department of Nuclear Science and Engineering

Idaho State University

Fall 2022

To the Graduate Faculty:

The members of the committee appointed to examine the thesis of Brenna Carbno find it satisfactory and recommend that it be accepted.

Chad L Pope, PhD PE

Major Advisor

Joshua Peterson-Droogh,

Committee Member

Dr. Leslie Kerby,

Graduate Faculty Representative

TABLE OF CONTENTS

List of Figures	vi
List of Tables	vii
Abstract	viii
Chapter I: Introduction	1
Chapter II: Background	1
2.1 Verification and Validation	1
2.2 Advanced Test Reactor	7
2.3 MCNP	8
2.4 MCCAFE	10
2.5 CIC-94	11
2.6 Three Region Model	14
Chapter III: Updating the 3-region MCNP model	18
3.1 The Unchanged 3-Region Model	20
3.2 Updating the OSCC's	24
3.3 Updating the Neck Shims.	25
3.4 Combining Neck Shim and OSCC Updates	28
3.5 Removing Experiments	29
3.5.1 Changing Surface Numbers and Adding Tallies.	31
3.6 Updating Fuel Materials	33
3.7 sensitivity	34
3.8 Center Flux Trap Error	43
3.9 Tallies	50
Chapter 4: Conclusions	55
Chapter V: Future Work	56
A Tally Graphs	59
B Percent Error by Cell	130

List of Figures

Figure 1	Phases of modeling and simulation and the role of V&V [14]	2
Figure 2	Verification process [1]	4
Figure 3	Validation process [1]	5
Figure 4	Verification and validation activities and products [2].	6
Figure 5	Cross-sectional view of the ATR core. [9]	8
Figure 6	MCNP Full core 19-plate model	12
Figure 7	19-plate model fuel element	14
Figure 8	Axial view of 19-plate model fuel element.	14
Figure 9	MCNP full core 3region	15
Figure 10	Radial view of 3-region model fuel element.	18
Figure 11	Axial view of 3-region model fuel element.	18
Figure 12	19-Plate model mesh tally	19
Figure 13	3-region model mesh tally.	20
Figure 14	20% agreement between the 19-plate model and the original 3-region model.	22
Figure 15	ATR map overlay of 20% agreement between the 19-plate model and the original 3-region model.	22
Figure 16	agree within two standard deviations.	23
Figure 17	Surfaces that define the OSCC's in the original 3-region model.	24
Figure 18	Surfaces that define the OSCC's in the 19-plate model.	24
Figure 19	20% agreement between the two models after updating the OSCC's	25
Figure 20	Where the two models agree within two standard deviations after updating the OSCC rotations.	25
Figure 21	Original cells for regulation rods and shim rods.	26
Figure 22	MCCAFE generated cells for the neck shims and regulation rod cells.	27
Figure 23	20% agreement between the two models after updating the neck shims.	27
Figure 24	Where the two models agree within two standard deviations after updating the neck shim positions.	28
Figure 25	20% agreement between the two models after updating the neck shims and OSCC's.	29
Figure 26	Where the two models agree within two standard deviations after updating the neck shims and OSCC's.	29
Figure 27	20% agreement between the two models after removing the experiments.	30
Figure 28	Where the two models agree within two standard deviations after removing the experiments.	30
Figure 29	MCCAFE generated cells for the neck shims and regulation rod cells.	31
Figure 30	Fixed 3-region surfaces.	32
Figure 31	20% agreement between the two models after updating fuel material.	33
Figure 32	Where the two models agree within two standard deviations after updating the fuel materials.	34
Figure 33	3-region center flux trap with error compared to 19-plate center flux trap.	43
Figure 34	20% agreement between the two models after updating the center flux trap.	44
Figure 35	Where the two models agree within two standard deviations after updating the center flux trap.	44
Figure 36	Reactivity curves for OSCC's.	50
Figure 37	Flux and heat generation for the A1 position.	52
Figure 38	Flux and heat generation for the B10 position.	52
Figure 39	Energy deposition for 19-plate model.	53
Figure 40	energy deposition for 3-region model	53
Figure 41	fission energy deposition mesh tall of 19-plate model	54
Figure 42	fission energy deposition mesh tall of 3-region model	54
Figure 43	20% agreement between energy deposition of both models.	55
Figure 44	20% agreement between fission energy deposition of both models.	55
Figure 45	Updated 3-region model	56

Figure 46	Flux and heat generation for the A1 position.	59
Figure 47	Flux and heat generation for the A2 position.	60
Figure 48	Flux and heat generation for the A3 position.	61
Figure 49	Flux and heat generation for the A4 position.	62
Figure 50	Flux and heat generation for the A5 position.	63
Figure 51	Flux and heat generation for the A6 position.	64
Figure 52	Flux and heat generation for the A7 position.	65
Figure 53	Flux and heat generation for the A8 position.	66
Figure 54	Flux and heat generation for the A9 position.	67
Figure 55	Flux and heat generation for the A10 position.	68
Figure 56	Flux and heat generation for the A11 position.	69
Figure 57	Flux and heat generation for the A12 position.	70
Figure 58	Flux and heat generation for the B1 position.	71
Figure 59	Flux and heat generation for the B2 position.	72
Figure 60	Flux and heat generation for the B3 position.	73
Figure 61	Flux and heat generation for the B5 position.	74
Figure 62	Flux and heat generation for the B6 position.	75
Figure 63	Flux and heat generation for the B7 position.	76
Figure 64	Flux and heat generation for the B8 position.	77
Figure 65	Flux and heat generation for the B9 position.	78
Figure 66	Flux and heat generation for the B10 position.	79
Figure 67	Flux and heat generation for the B11 position.	80
Figure 68	Flux and heat generation for the B12 position.	81
Figure 69	Flux and heat generation for the I1 position.	82
Figure 70	Flux and heat generation for the I2 position.	83
Figure 71	Flux and heat generation for the I3 position.	84
Figure 72	Flux and heat generation for the I4 position.	85
Figure 73	Flux and heat generation for the I5 position.	86
Figure 74	Flux and heat generation for the I6 position.	87
Figure 75	Flux and heat generation for the I7 position.	88
Figure 76	Flux and heat generation for the I8 position.	89
Figure 77	Flux and heat generation for the I9 position.	90
Figure 78	Flux and heat generation for the I10 position.	91
Figure 79	Flux and heat generation for the I11 position.	92
Figure 80	Flux and heat generation for the I12 position.	93
Figure 81	Flux and heat generation for the I13 position.	94
Figure 82	Flux and heat generation for the I14 position.	95
Figure 83	Flux and heat generation for the I15 position.	96
Figure 84	Flux and heat generation for the I16 position.	97
Figure 85	Flux and heat generation for the I17 position.	98
Figure 86	Flux and heat generation for the I18 position.	99
Figure 87	Flux and heat generation for the I19 position.	100
Figure 88	Flux and heat generation for the I20 position.	101
Figure 89	Flux and heat generation for the I21 position.	102
Figure 90	Flux and heat generation for the I22 position.	103
Figure 91	Flux and heat generation for the I23 position.	104
Figure 92	Flux and heat generation for the I24 position.	105
Figure 93	Flux and heat generation for the H1 position.	106
Figure 94	Flux and heat generation for the H2 position.	107
Figure 95	Flux and heat generation for the H3 position.	108
Figure 96	Flux and heat generation for the H4 position.	109
Figure 97	Flux and heat generation for the H5 position.	110
Figure 98	Flux and heat generation for the H6 position.	111
Figure 99	Flux and heat generation for the H7 position.	112

Figure 100	Flux and heat generation for the H8 position.	113
Figure 101	Flux and heat generation for the H9 position.	114
Figure 102	Flux and heat generation for the H10 position.	115
Figure 103	Flux and heat generation for the H11 position.	116
Figure 104	Flux and heat generation for the H12 position.	117
Figure 105	Flux and heat generation for the H13 position.	118
Figure 106	Flux and heat generation for the H14 position.	119
Figure 107	Flux and heat generation for the H15 position.	120
Figure 108	Flux and heat generation for the H16 position.	121
Figure 109	Flux and heat generation for the CFT position.	122
Figure 110	Flux and heat generation for the NEFT position.	123
Figure 111	Flux and heat generation for the EFT position.	124
Figure 112	Flux and heat generation for the SEFT position.	125
Figure 113	Flux and heat generation for the SFT position.	126
Figure 114	Flux and heat generation for the SWFT position.	127
Figure 115	Flux and heat generation for the WFT position.	128
Figure 116	Flux and heat generation for the NWFT position.	129
Figure 117	Flux and heat generation for the NFT position.	130

List of Tables

Table 1	Summary of symbols used in tally equations.	10
Table 2	Summary of what is modeled in the 19-plate MCNP model.	13
Table 3	Summary of what is modeled in the 3-region MCNP model.	17
Table 4	Description of colors used in mesh tally data.	21
Table 5	Summary of changes to k-effective in the 3-region model.	23
Table 6	Summary of surface and cell numbers.	32
Table 7	Values for the 19-plate model sensitivity study.	35
Table 8	Values for the 19-plate model sensitivity study.	36
Table 9	Values for the 19-plate model sensitivity study.	37
Table 10	Values for the 3region model sensitivity study with incorrect center flux trap geometry.	38
Table 11	Values for the 3-region model sensitivity study with incorrect center flux trap geometry.	39
Table 12	Values for the 3-region model sensitivity study.	40
Table 13	Difference between the 19-plate model and the 3-region model with incorrect center flux trap geometry.	41
Table 14	Difference between the 19-plate model and the 3-region model with incorrect center flux trap geometry.	42
Table 15	Difference between the 19-plate model and the 3-region model with incorrect center flux trap geometry.	42
Table 16	Values for the 3-region model sensitivity study with corrected center flux trap geometry.	45
Table 17	Values for the 3region model sensitivity study with corrected center flux trap geometry.	46
Table 18	Values for the 3-region model sensitivity study with corrected center flux trap geometry.	47
Table 19	Difference between the 19-plate model and the 3-region model with correct center flux trap geometry.	48
Table 20	Difference between the 19-plate model and the 3-region model with correct center flux trap geometry.	49
Table 21	Difference between the 19-plate model and the 3-region model with correct center flux trap geometry.	49
Table 22	Summary of power scaled to each lobe in the 19-plate and 3-region models.	51
Table 23	Percent error for flux and heating tallies.	52
Table 24	Percent error for flux and heating tallies.	131
Table 25	Percent error for flux and heating tallies.	132
Table 26	Percent error for flux and heating tallies.	133
Table 27	Percent error for flux and heating tallies.	134
Table 28	Percent error for flux and heating tallies.	135
Table 29	Percent error for flux and heating tallies.	136
Table 30	Percent error for flux and heating tallies.	137
Table 31	Percent error for flux and heating tallies.	138
Table 32	Percent error for flux and heating tallies.	139
Table 33	Percent error for flux and heating tallies.	140
Table 34	Percent error for flux and heating tallies.	141
Table 35	Percent error for flux and heating tallies.	142
Table 36	Percent error for flux and heating tallies.	143
Table 37	Percent error for flux and heating tallies.	144
Table 38	Percent error for flux and heating tallies.	145
Table 39	Percent error for flux and heating tallies.	146
Table 40	Percent error for flux and heating tallies.	147
Table 41	Percent error for flux and heating tallies.	148
Table 42	Percent error for flux and heating tallies.	149
Table 43	Percent error for flux and heating tallies.	150

Verification of the 3-Region Advanced Test Reactor MCNP Model

Thesis Abstract–Idaho State University (2022)

The verification of the 3-region homogenized fuel Advanced Test Reactor MCNP model. The 3- region model was compared to the 19-plate model found in the 94-CIC report. Flux tallies, energy deposition tallies, and quarter core mesh tallies were used to compare the two models. The 3-region model needed updating in order to make good comparisons between the models. The percent error from the flux and energy deposition tallies data shows that experiment positions inside the flux trap have higher errors than positions outside the fuel ring. The standard deviation data obtained from the mesh tallies shows that the two models agree within two standard deviations throughout the reactor. It is concluded that the model works adequately for what it is used for.

Key words: Key Words: MCNP, Verification, Advanced Test Reactor

1 Introduction

The Idaho National Laboratory (INL) strives for safety and excellence in nuclear research. This is possible with the support of the thousands of people employed by the laboratory. The neutronics analysis department contributes to the culture of excellence by conducting safety analysis for experiments that will go into the nuclear test reactors. To ensure the highest quality analysis, the software used must go through a thorough software quality assurance (SQA) process. Included in the SQA of the software is verification and validation (V&V) of the computer models used for the simulations. In a recent audit of the department SQA program, it was noticed that the 3-region computer model for the advanced test reactor was not properly verified or validated.

2 Background

2.1 Verification and Validation

A discussion of verification would be incomplete without also discussing validation. V&V can have different definitions depending on what is being verified/validated and who is performing the work. A formal definition of V&V is needed.

A formal definition of V&V was first published by the Society for Computer Simulation (SCS) in 1979. The SCS defines model verification as, "substantiation that a computerized model represents a conceptual model within specified limits of accuracy," and defines model validation as, "substantiation that a computerized model within its domain of applicability possesses a satisfactory range of accuracy consistent with the intended application of the model" [14]. The main implication from the verification definition is the computerized model, or the computer code, must accurately mimic the model that was originally conceptualized. The validation definition is admittedly rather vague but does tell us that the computerized model needs to have some level of accuracy. Both definitions have one concept in common: the need substantiation or evidence of correctness. In addition to the definitions, the SCS included a helpful diagram that shows the role of V&V in modeling and simulation and is included here as figure 1.

The diagram depicted in figure 1 identifies two different types of models. The first is a conceptual model. This model includes modeling assumptions, mathematical equations, and any other relevant information that describes the physical system or process of interest. Analysis and observation of the physical system is the primary source of the conceptual model. The second model is the computerized model. This model is the computer program that implements the conceptual model. This model is also referred to as the computer model or the code. Figure 1 shows that verification is the relationship between the conceptual model and

the computerized model validation is the relationship between the conceptual model and reality. The SCS defines qualification as "determination of adequacy of the conceptual model to provide an acceptable level of agreement for the domain of intended application" [13]. Figure 1 shows model qualification is the link between reality and the conceptual model.

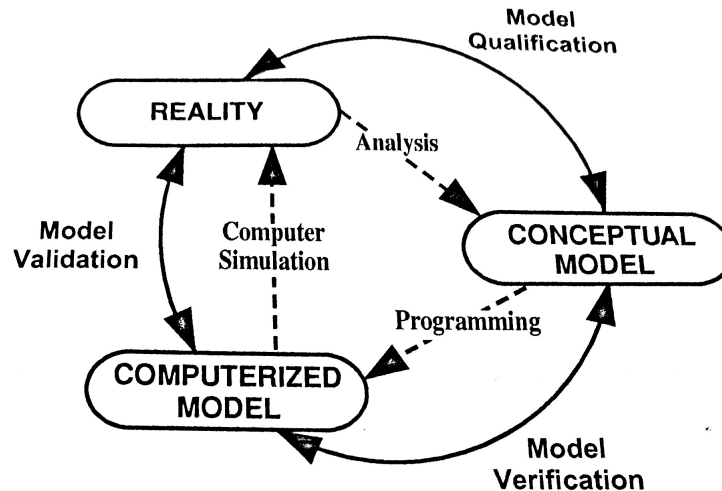


Figure 1: Phases of modeling and simulation and the role of V&V [14]

These definitions of V&V show that V&V are tools used for assessing the accuracy of the conceptual and computerized model. In practice, the assessment of accuracy was so difficult that V&V became more associated with credibility, or if the model was worthy of belief. Unfortunately, in science and engineering a quantitative assessment of accuracy is mandatory for important physical cases related to the intended application.

In 1991 the Institute of Electrical and Electronics Engineers (IEEE) introduced new definitions for V&V. Verification was defined as "the process of evaluating the products of a software development phase to provide assurance that they meet the requirements defined for them by the previous phase," and validation was defined as "the process of testing a computer program and evaluation the results to ensure compliance with specific requirements" [7]. The value of the verification definition is directly dependent on the requirements that have been defined before the verification process begins [13]. Similarly, the validation definition relies on requirements that are defined before the validation phase starts, however without defining those requirements the validation definition lacks substance. Having the requirements defined in a preceding phase and not in the V&V definitions gives the IEEE V&V definitions the flexibility to apply to a wide variety of modeling and simulation applications. Both definitions emphasize that V&V is an ongoing process of activities. These definitions are useful as they "provide a distinctly different perspective toward the entire issue of V&V than

what is needed in scientific computing” [13]. Consequently, the IEEE definitions are more prevalently used in engineering. The computer science community, software quality assurance community, the American Nuclear Society, and the International Organization for Standardization also use the IEEE definitions [13].

The US Department of Defense (DoD) came up with their own V&V definitions in the mid 1990’s. Verification is ”the process of determining that a model implantation accurately represents the developer’s conceptual description of the model,” and validation is ”the process of determining the degree to which a model is an accurate representation of the real world from the perspective of the intended uses of the model” [6]. There is a critical difference between the DoD definitions and the IEEE definitions. The DoD definition can be thought of as *model V&V* and the IEEE definitions can be thought of as *software V&V* [13]. The DoD definitions and IEEE definitions are similar in that they both stress that V&V are ongoing processes. It should be noted that the V&V process does not have a clearly defined end point, however an end point can be established if ”additional specifications are given in terms of intended use of the model and adequacy” [13]. The ongoing nature of V&V brings to light the issue that correctness and accuracy of any given computational model cannot be determined for every possible application. This means that, like many applications in science, these models cannot be proven correct, but they can be proven incorrect. If accuracy cannot be completely determined, then the DoD’s emphasis on accuracy in their definitions may seem strange. However, a measure of accuracy can be determined for specific applications. For verification, accuracy can be determined be either a well-accepted solutions to simplified model problems or an expert opinion on the reasonableness of the solution. For validation, accuracy can be determined by either experimentally measured data or an expert opinion on the credibility of the results [13].

The American Institute of Aeronautics and Astronautics (AIAA) published their own definitions for V&V in 1998. The validation definition is the same as the DoD’s, but verification is defined as, ”the process of determining that a model implementation accurately represents the developer’s conceptual description of the model and the solution to the model” [1]. The AIAA definition of verification clarifies the DoD verification definition by stating that the accuracy of the numerical model to the conceptual model should be included in the definition. This addition to the definition shows that the identification, qualification, and reduction of errors in the conceptual model and numerical solution is the main goal of verification [13]. In other words, ” Verification provides evidence or substantiation that the conceptual...model is solved accurately by the discrete mathematics model embodied in the computer code” [13]. The issue now is that highly accurate solutions can only be found for simplified models. It is important to note that verification deals only with mathematics. The relationship between the conceptual model and the real world is handled by validation. The question, ”Does my model accurately solve the physics of this situation?” is answered in the validation process.

In addition to the definitions of V&V The AIAA guide also provided diagrams of the verification and validation processes. Figure 2 shows the verification process. The process begins with the conceptual model. The conceptual model is broken down into two distinct parts. On the left we see the computational model which in turn leads to the computational solution. On the right we see the highly accurate solutions. The link between the computational solutions and the highly accurate solutions is verification.

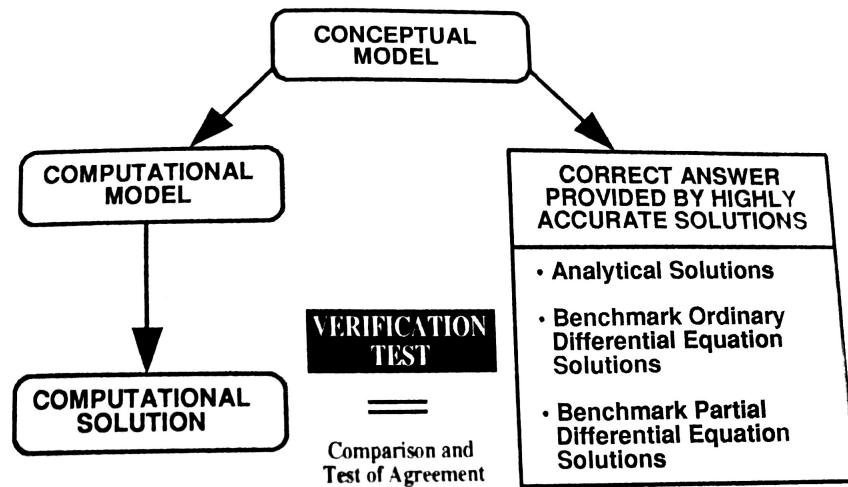


Figure 2: Verification process [1]

While the AIAA definition of validation is the same as the DoD's, the perspective of the AIAA definition is different. Specifically, the perspective on what types of comparisons should be allowed in validation. The AIAA guide states that the assessment of the conceptual model to the real world be made only with experimental measurements. The "fundamental strategy of validation involves identification and quantification of the error and uncertainty in the conceptual and mathematical models" [13]. This compares the quantified error in the numerical solution and the estimated uncertainty in the experimental data. The AIAA perspective on validation sees experimental data as the best measure of reality however this perspective does not assume that experimental data is more accurate than computational results. Figure 3 shows the AIAA validation process. Validation starts with the real world. On the left, the real world leads to the conceptual model. The conceptual model leads to the computational model which in turn leads to the conceptual solution. On the right of the real world is the experimental data. The link between the computational solution and the experimental data is validation.

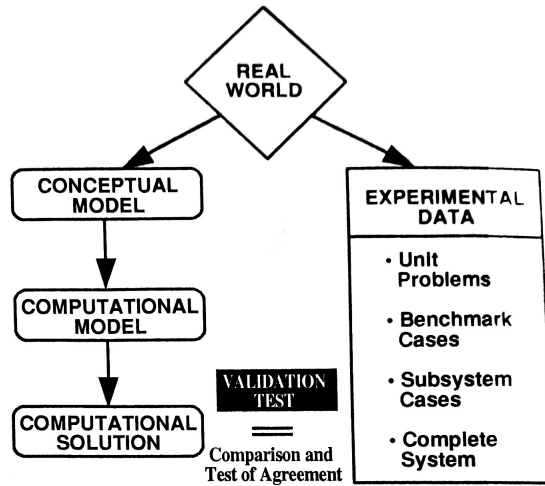


Figure 3: Validation process [1]

The AIAA perspective on validation naturally leads to the discussion of prediction, which the AIAA has defined as, "use of a computational model to foretell the state of a physical system under conditions for which the computational model has not been validated" [1]. An important distinction between validation and prediction is that predictions must be for a specific case that is different in some way to other cases that have been validated. If this distinction is not made, then predictions are no more than replications of previously obtained results.

The American Society of Mechanical Engineers (ASME) published their definitions of V&V in 2006. Once again, the validation definition is the same as the DoD definition. However, verification is defined as, "the process of determining that a computational model accurately represents the underlying mathematical model and it's solution" [2]. The ASME Guide also included a helpful diagram with their definitions, which can be seen here as figure 4. This diagram differs from the AIAA figures because the ASME diagram shows verification and validation activities in the same figure.

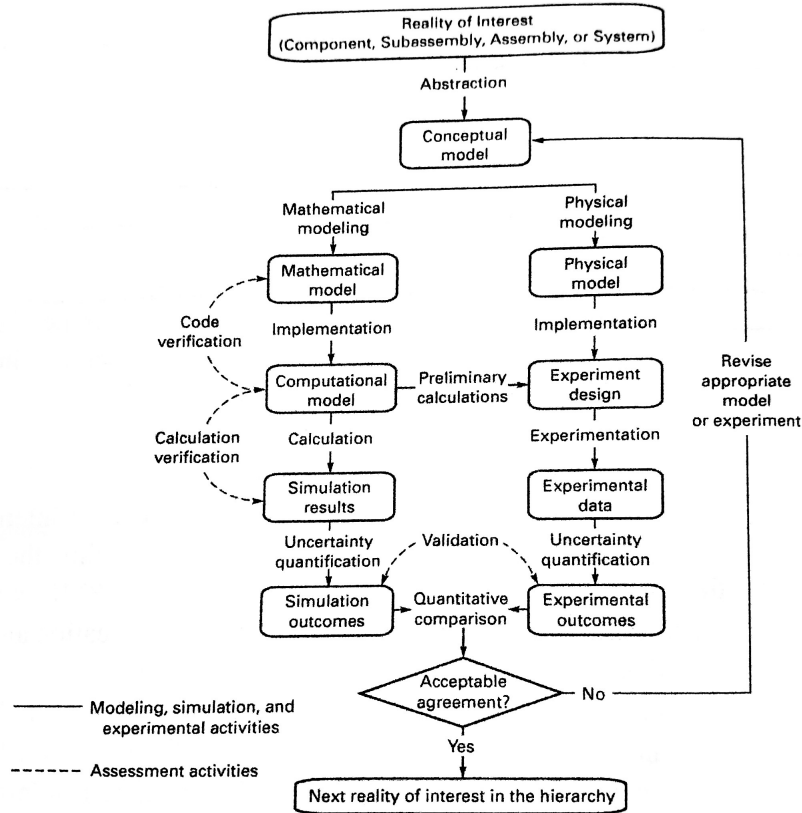


Figure 4: Verification and validation activities and products [2].

Figure 4 can be applied to any aspect of a system, whether that be the complete system, a subsystem, benchmark cases, or unit problems. Figure 4 shows a separation of verification activities. This separation of verification activities allows for improved coding reliability and improved assessments of the numerical accuracy of the computational model. Figure 4 also shows a critical decision at the end of the V&V process, which is, "Is there acceptable agreement between the computational results and the experimental measurements?" The answer to this important question should be made with the intended use of the model in mind. To help answer this question, the conceptual model should be made with a few things in mind. The first is which "physical processes in the reality are anticipated to have significant effects on the responses of interest and which processes are not expected to be important" [13]. The second is what requirements are needed to demonstrate the accuracy and predictive capability of the model. Without these accuracy requirements the question of "How good is good enough?" cannot be answered and an acceptance of the model cannot be made. Lastly, the intended use of the model should be specified.

This project will focus on the verification of the 3-region MCNP model. It is assumed that MCNP correctly solves the underlying mathematical model. It is also assumed that the 94-CIC model is properly

verified and validated.

2.2 Advanced Test Reactor

The Advanced Test Reactor (ATR), located at the INL, is a 250-MW thermal, high flux test reactor. Construction on the ATR began in November of 1961 and completed in 1965. Fuel loading began in 1967 and core testing of the ATR was completed in 1969. The ATR started full power operations later in the year of 1969 and since has been used for research of the effects of radiation on reactor structure and fuel materials as well as production of medical and industrial isotopes.

The ATR core contains 40 fuel elements arranged in a serpentine annulus in and around nine flux traps. Each fuel element consists of 19 curved plates attached to side plates, forming a 45-degree sector of a circular cross section in cross section. The fuel is highly enriched, 93 wt%, uranium aluminum fuel powder dispersed in aluminum [9].

The reactor is moderated by light water and reflected by beryllium. There are 16 Outer shim control cylinders and 24 neck shims [9]. The ATR has nine flux traps, eight inner A experiment positions, eight outer A experiment positions, eight small B experiment positions, four large B experiment positions, 20 large and medium I experiment positions, four small I experiment positions, and 16 H experiment positions. Figure 5 shows a cross section of the ATR core.

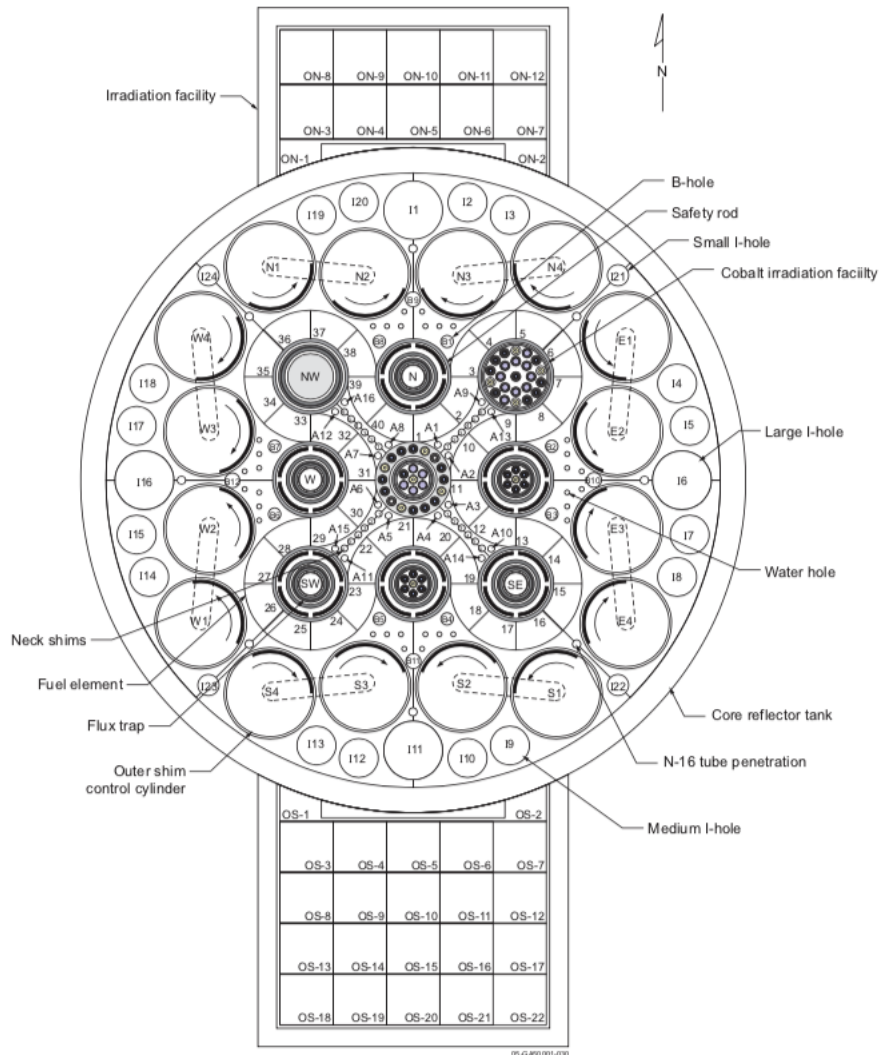


Figure 5: Cross-sectional view of the ATR core. [9]

2.3 MCNP

The software used in this project was MCNP6.2. "MCNP is a general-purpose, continuous-energy, generalized-geometry, time-dependent, Monte Carlo radiation-transport code designed to track many particle types over broad ranges of energies [16]. MCNP is used by neutronic analysts at INL to model experiments that will go into the ATR.

MCNP automatically creates standard summary information that gives the user a better insight into the physics of the problem and the adequacy of the Monte Carlo simulation [17]. In addition, MCNP has seven standard tallies available to users. Of these seven basic tallies, the three used in this project are track length

estimate of cell flux, track length estimate of energy deposition, and track length estimate of fission energy deposition. The models used in this were ran as KCODE criticality problems. In this mode particles are, "normalized to be per fission neutron generation" [17].

The physical quantity of the flux tally is given by equation 1 [17].

$$\bar{\phi}_V = \frac{1}{V} \int dE \int dt \int dV \int d\Omega \Psi(\vec{r}, \Omega, E, t) \quad (1)$$

The units given by MCNP for the flux tally are *particles/cm²*. The physical quantity of energy deposition is given by equation 2 [17].

$$H_t = \frac{\rho_a}{m} \int dE \int dt \int dV \int d\Omega \sigma_t(E) H(E) \Psi(\vec{r}, \hat{\Omega}, E, t) \quad (2)$$

The units of the energy deposition tally are *MeV/g*. The physical quantity of the fission energy deposition is given by equation 3 [17].

$$H_f = \frac{\rho_a}{m} Q \int dE \int dt \int dV \int d\Omega \sigma_f(E) \Psi(\vec{r}, \hat{\Omega}, E, t) \quad (3)$$

The units for fission energy given by MCNP are by *MeV/g*. Table 1 defines what each symbol in equations 1, 2, and 3 represent.

Symbol	Meaning
$\vec{r}, \hat{\Omega}, E, t$	particle position vector (cm), direction vector, energy (MeV), and time
$\sigma_t(E)$	microscopic total cross section (barns)
$\sigma_f(E)$	microscopic fission cross section (barns)
$H(E)$	heating number (MeV/collision)
ρ_a	atom density (atoms/barn-cm)
m	cell mass (g)
V	volume (cm ³)
Q	fission heating Q-value (MeV)
Ψ	angular flux familiar from nuclear reactor theory
$\bar{\phi}_V$	average flux in a cell (volume)
H_t	total energy deposition in a cell (MeV/g)
H_f	total fission energy deposition in a cell (MeV/g)

Table 1: Summary of symbols used in tally equations.

MCNP also has a superimposed mesh tally. Rather than tallying particles in a cell, the mesh tally "allows the user to tally particles on a mesh independent of the problem geometry" [17]. Currently the mesh tally is only available for track length flux. Because the energy deposition and fission energy deposition tallies are track length tallies, a tally multiplier card can be added to a track length flux mesh tally to transform the flux mesh tally to a energy deposition or fission energy deposition mesh tally. Examination of equations 1, 2, and 3 will show that they are, in fact, the same equation with different multipliers. It is assumed that MCNP works as expected.

2.4 MCCAFE

The Monte Carlo Constructor of Advanced Test Reactor Fuel Elements (MCCAFE) is software developed at the INL. MCCAFE is available at https://hpcgitlab.hpc.inl.gov/experiment_analysis/mccafe. A HPC account and access to the experiment analysis group is needed to use it. MCCAFE is used to generate MCNP input decks.

MCCAFE requires a minimum of five files to operate. The first is a 3-region MCNP input deck. This is the base that MCCAFE will build from. The second file is a spreadsheet with data from the most recent

ATR cycle. This data includes time stamps, neck shim positions, and control drum rotations. Editing this spreadsheet will change the control drum and neck shim positions in the new MCNP input decks that MCCAFE generates. The third file is another spreadsheet with uranium-235 mass for each time step in the ATR cycle data. The fourth file is a spreadsheet with boron mass for each time step in the ATR cycle data. Together the uranium-235 and boron spreadsheets dictate whether the MCCAFE generated fuel is depleted or fresh. The final file is a yaml file. This is the file that MCCAFE uses to find the previous four files. Also, the yaml file is where the user defines which cross section library MCCAFE should use when generating new materials.

MCCAFE has other uses, but MCACFE was only used to make new control drum rotations, neck shim positions, and fuel materials for this project. The MCNP input deck that is used with MCCAFE cannot have cells or surface cards already generated by MCCAFE. Otherwise MCCAFE will not generate new surface or cell cards. It is assumed that MCCAFE works as expected.

2.5 CIC-94

The evaluation "ADVANCED TEST REACTOR: SERPENTINE ARRANGEMENT OF HIGHLY ENRICHED WATER-MODERATED URANIUM-ALUMINIDE FUEL PLATES REFLECTED BY BERYLLIUM" is published in volume II of the "International Handbook of Evaluated Criticality Safety Benchmark Experiments" (ICSBEP) under the label "HEU-MET-THERM-022." The MCNP model used in the ICSBEP is the benchmark model used to verify the 3-region model in this project and will be referred to as the 19-plate model. Access to the ICSBEP can be requested at https://www.oecd-nea.org/jcms/pl_24498/international-criticality-safety-benchmark-evaluation-project-icsbep. Figure 6 shows the 19-plate MCNP model of the ATR. Data for the 19-plate model was taken from the 1994 core internal change-out (CIC) [9]. Table 2 summarizes what is modeled in each position in the 19-plate model.

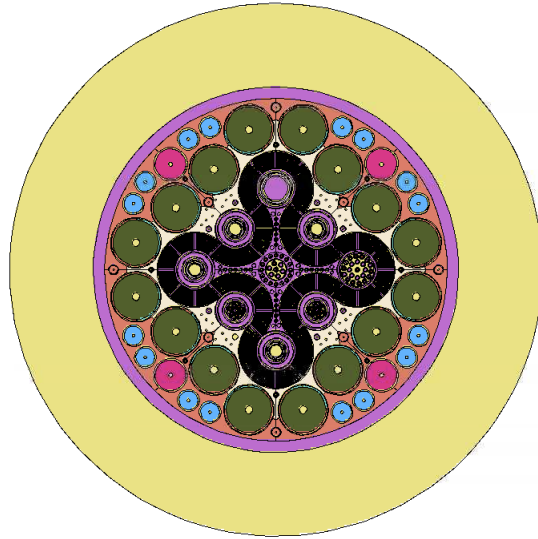


Figure 6: MCNP Full core 19-plate model

Position	What is Modeled
Center Flux Trap	Cobalt targets
Northeast Flux Trap	Cobalt targets
East Flux Trap	Cobalt targets
Southeast Flux Trap	Aluminum baffle and a hafnium safety rod
South Flux Trap	Cobalt targets
Southwest Flux Trap	Aluminum baffle and a hafnium safety rod
West Flux Trap	Aluminum baffle and a hafnium safety rod
Northwest Flux Trap	Aluminum baffle
North Flux Trap	Aluminum baffle and a hafnium safety rod
All A	Aluminum flow restrictors
Small B	Aluminum flow restrictors
Large B	Beryllium fillers
All I	Beryllium fillers
H	H2,H6, H10, and H14 have flux monitor holders. H3 and H11 have flux wire tubes. The remaining H positions have cobalt targets.

Table 2: Summary of what is modeled in the 19-plate MCNP model.

The important thing to note about this model is that each of the 19 plates is modeled individually. This is shown in figure 7. Also note that each plate has a different material defined in it.

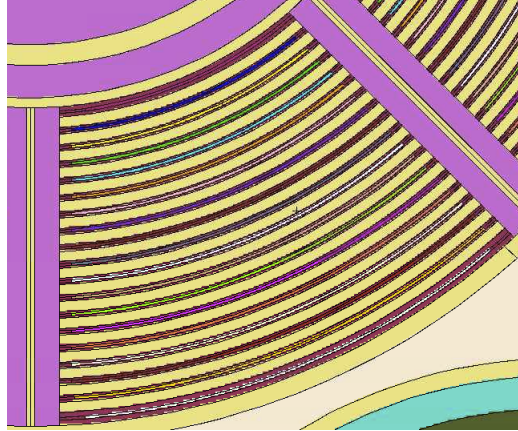


Figure 7: 19-plate model fuel element

An axial view of a 19-plate model fuel element is shown in figure 8. Take note that only one material is used though out the entire viable plate. Since the 19-plate model models fresh fuel, only 19 different material definitions are needed, one for each of the plates. Boron is used in the first four and last four of the 19 plates in each fuel element.



Figure 8: Axial view of 19-plate model fuel element.

2.6 Three Region Model

Versions of the 3-region model have used at the INL for many years now. Unfortunately, the documentation for any of these models is lacking. Figure 9 shows a full core view of the current 3-region model.

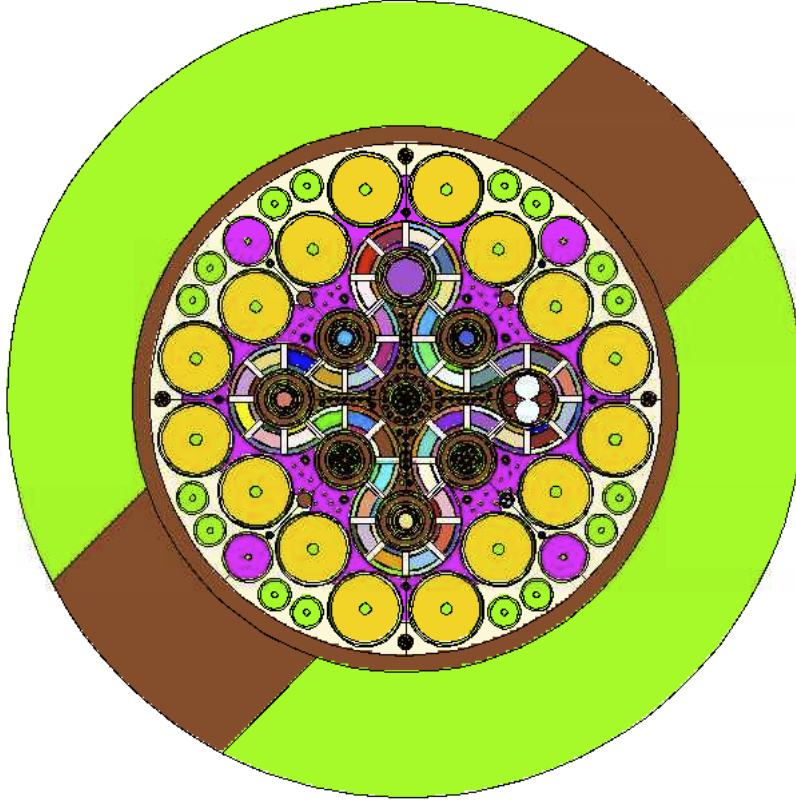


Figure 9: MCNP full core 3region

Experiment reports for the INL usually have a section that covers what software and model was used. For example, section four of the depletion report for the AGR-2 experiment states that MCNP is used [15]. Though which model used is never explicitly stated, the first figure in the report shows the 3-region model. The reactor physics report for the AGR-2 experiment is much the same. MCNP was used and a figure shows the 3-region model [10]. Unsurprisingly, reports for the AGR-1 experiment are similar. They report using the MCNP software and images of the 3-region model are shown [5], [4]. None of these experiment reports justify the use of MCNP or the use of the 3-region model. More recent experiments, such as the MVP experiment, outline the V&V process used for MCNP, but do not include justification for the model used.

In 2014 an update to the ATR core model was published [12]. Both the 19-plate model and the 3-region model received updates. The updates primarily updated geometry around the flux traps and removed unneeded tallies and cells. This report does briefly describe the V&V efforts for MCNP and has a lengthy section on validation for the methods used. However, the 19-plate model was used for the validation and no verification of the 3-region model was done.

An attempt at verification to a 3-region model was done in 2006 [3]. The report compares the k-effective of the 19-plate model to a 3-region model and single radial region model. Careful examination of the MCNP

output files from this project show that the 3-region model used is not the same 3-region model used in this verification project. The input deck for the 3-region used in the 2006 project could be found.

Because of the lack of documentation for the 3-region model, there is no base model to start comparing the 3-region model to the 19-plate model. Therefore, it was decided that the model used in the ATF-1 experiment would be a good starting place. Table 3 summarizes what was in each experiment position of the 3-region model.

Position	What is Modeled
Center Flux Trap	Cobalt targets
Northeast Flux Trap	Aluminum baffle
East Flux Trap	Aluminum Filler
Southeast Flux Trap	Aluminum baffle, hafnium safety rod, and an experiment shroud
South Flux Trap	Cobalt targets
Southwest Flux Trap	Aluminum baffle, hafnium safety rod, and an experiment shroud
West Flux Trap	Aluminum baffle, hafnium safety rod, and an experiment shroud
Northwest Flux Trap	Aluminum baffle and an experiment shroud
North Flux Trap	An experiment shroud
All A	A1-A11 cobalt targets, A12 FAST experiment
Small B	cobalt targets
Large B	B9, B11, B12 Aluminum fillers. B12 AGR-1
Large and Medium I	Beryllium fillers
Small I	I21 ATF, I22 FAST, I23 ATF, I24 ATF
H	H1, H4, H5, H7, H8, H9, H12, H13, H15, H16 depleted fixed shim rods. H3, H2, H6, H10, H11, H14 flux wire holder.

Table 3: Summary of what is modeled in the 3-region MCNP model.

The most significant difference between the two models is the way the fuel is modeled. In the 3-region model, the fuel plates in a fuel element are divided into three radial groups based on their boron content. Plates 1-4 are in group one, plates 5-14 are in group two and plates 15-19 are in group three. The fuel has been homogenized into one material in each of the three different radial groups. Figure 10 shows the three

radial groups.

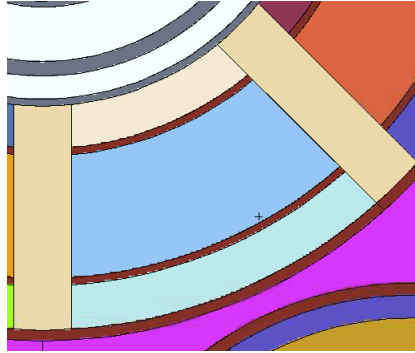


Figure 10: Radial view of 3-region model fuel element.

In the axial direction, each 3-region model fuel element is divided into seven regions. This is helpful when modeling depleted fuel. Figure 11 shows the axial view of two 3-region model fuel elements. Each fuel element has 21 total regions, three radial and seven axial, with 21 different fuel materials defined. With 40 fuel elements there are 840 material definitions for the fuel in the 3-region model.

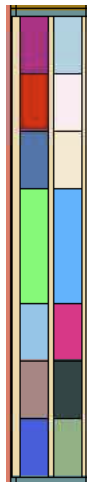


Figure 11: Axial view of 3-region model fuel element.

3 Updating the 3-region MCNP model

This project made use of INL's High Performance Computing (HPC) resources. Both models were run on HPC's Sawtooth supercomputer. Sawtooth is an HP SGI 8600-based system with 99,792 cores, 99,792 TB of memory and a LINPACK rating of 5,600.00 TFlop/s. Sawtooth's network is an enhanced hypercube utilizing EDR/HDR InfiniBand. Individual compute nodes contain dual Xeon Platinum 8268 processors with 24 cores each and a total of 192GB of memory. Some nodes also have 4 NVIDIA V100 GPUs and an

additional 192 GB of RAM for a total of 384 GB of memory. Sawtooth came online in Fall 2019 and ranked 37 on the November 2019 TOP500 list.

Each model was run with a kcode card. Each run had 50 skipped cycles and 700 active cycles. Each cycle tracked 50,000 neutrons.

A superimposed mesh tally was placed over the southeast lobe of both the 3-region and 19-plate model to gather more information about the models. The ATR is symmetrical, so it is assumed that a mesh tally over a quarter of the core is sufficient. The tally on both models was a 500 by 500 by 100 mesh that started just below the fuel and ended right above the fuel. The mesh tally on the 19-plate model is shown in figure 12 and the mesh tally on the 3-region model is shown in figure 13.

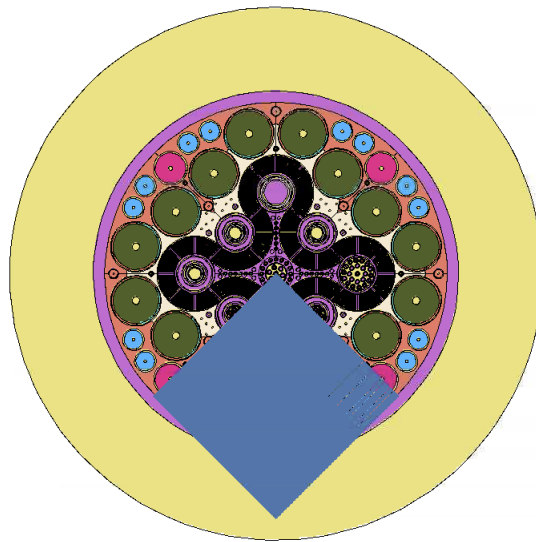


Figure 12: 19-Plate model mesh tally

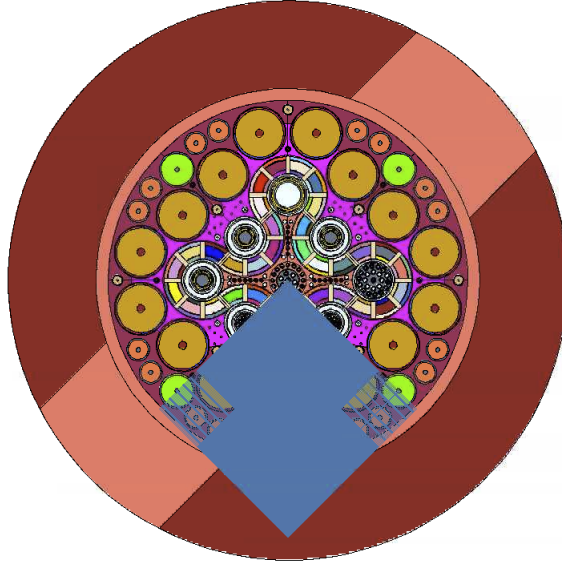


Figure 13: 3-region model mesh tally.

Information from the output and mesh tally files was extracted using Jupyter notebooks. A python script would read through the output file and find and display the tallies. Another script would read in the mesh tally information and store it in a pandas data frame. mesh tally data from the center plane of the fuel was extracted from the mesh tally files. The 19-plate tally was divided by the 3-region tally to see where the two models agreed.

Another Jupyter notebook was used to find and plot the standard deviation of both mesh tallies from the models. This was done by multiplying the tally result by the error. After the standard deviation was calculated the script would check if the tally result of 3-region model was within the standard deviation of the 19-plate model and if the tally result of the 3-region model was within the standard deviation of the 19-plate model.

3.1 The Unchanged 3-Region Model

Because the original 3-region model was a conglomerate of different experiments, it was not expected that results from the unchanged model would resemble the 19-plate model at all. Indeed, the 3-region model gave an overall k-effective of 1.05755 with a standard deviation of 0.00014 while the 19-plate model gave an overall k-effective of 0.99951 with a standard deviation of 0.00015. A summary of k-effective changes can be found in table 5.

Figure 14 shows the mesh tally data for the 19-plate model and the unchanged 3-region model. Table 4 shows what each color of the mesh represents. The mesh data shows where the two models agree within $\pm 10\%$. This data in the mesh figures was is the 19-plate tally value divided by the 3-region tally value. Some

notable feature of figure 14 is that the models have large disagreements in the center flux trap, the neck shims, the southeast flux trap, the south flux trap, and the OSCC's. This was expected from the unchanged model. The unchanged model had 24% of the bins agree within 20% of the 19-plate model.

Color	Representation
Yellow	Greater than 10% difference where the 3-region model predicts a greater value than the 19-plate model.
Red	Less than 10% difference where the 3-region model predicts a greater value than the 19-plate model.
Green	Less than 10% difference where the 3-region model predicts a smaller value than the 19-plate model.
Black	Greater than 10% difference where the 3-region model predicts a smaller value than the 19-plate model.

Table 4: Description of colors used in mesh tally data.

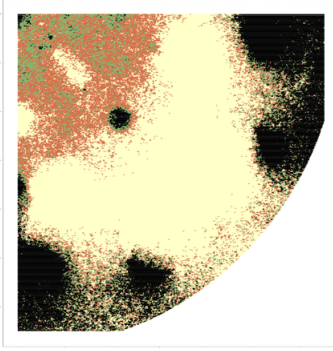


Figure 14: 20% agreement between the 19-plate model and the original 3-region model.

It might be difficult to see exactly where the different experiment positions are in the mesh tally plots. Figure 15 shows a map of the ATR over the mesh tally plot. This is the same for all the mesh tally plots.

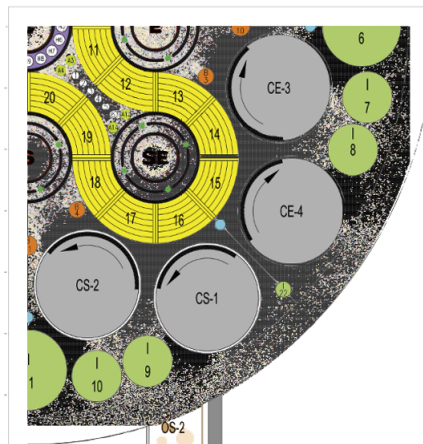


Figure 15: ATR map overlay of 20% agreement between the 19-plate model and the original 3-region model.

Figure 16 show where the two models agree within two standard deviations. The blue show where the models agree. For the most part, the agreement for two standard deviations and agreement within $\pm 10\%$ are the same except towards the outside of the reactor they only agree within two standard deviations. The is understandable because there is greater statistical uncertainty further from the core. The unchanged model had 31% of the bins within two standard deviations of the 19-plate model.

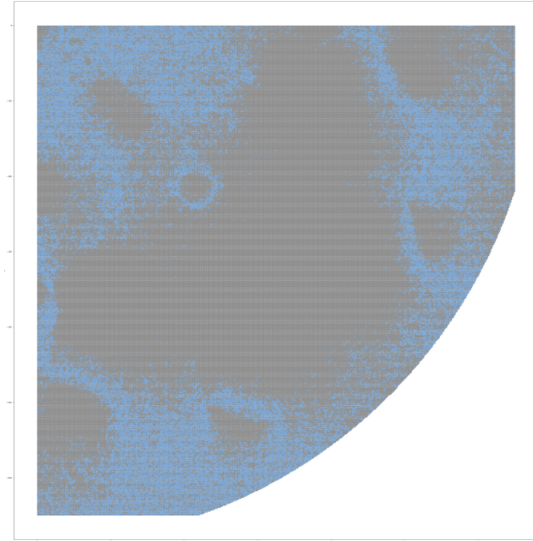


Figure 16: agree within two standard deviations.

Description of changes	K-effective	Standard Deviation
19-Plate Model	0.99951	0.00015
Unchanged 3-region model	1.05755	0.00014
Changing OSCC positions in the 3-region model	1.02422	0.00015
Changing Neck shim positions in the 3-region model	1.01417	0.00014
Changing both OSCC and neck shim position in the 3-region model	0.97130	0.00015
Removing experiments from the 3-region model	0.97632	0.00015
Modeling fresh fuel in the 3-region model	0.98097	0.00015
Correcting center flux trap geometry in the 3-region model	0.97819	0.00015

Table 5: Summary of changes to k-effective in the 3-region model.

3.2 Updating the OSCC's

There was hope when we started this project that adjusting the OSCC's, and neck shims would resolve the difference in k-effective. Therefore, the first step in this verification process was to adjust the OSCC's in the 3-region model so that they matched the positions of the OSCC's in the 19-plate model. To achieve this the surfaces that define the OSCC's needed to be changed. Figure 17 shows the surface definitions in the 3-region model and figure 18 shows the surface definitions for the 19-plate model. The surface numbers were also changed to reflect the order that is used in the 19-plate model.

```

c ***** Begin Control Surfaces *****
c
c          CONTROL DRUM POSITION SURFACES
c
c mopyBEGIN CONTROL DRUM POSITION SURFACES
996 c/z 45.391 15.870 9.195 $ N4, NE shim position = 63.13
995 c/z 29.281 27.124 9.195 $ N3, NE shim position = 63.13
994 c/z 31.091 32.844 9.195 $ N2, NW shim position = 96.84
993 c/z 18.908 49.773 9.195 $ N1, NW shim position = 96.84
981 c/z 45.391 -15.870 9.195 $ E1, NE shim position = 63.13
982 c/z 29.281 -27.124 9.195 $ E2, NE shim position = 63.13
991 c/z -31.091 32.844 9.195 $ W3, NW shim position = 96.84
992 c/z -18.908 49.773 9.195 $ W4, NW shim position = 96.84
988 c/z -50.353 -19.074 9.195 $ S4, SW shim position = 100.60
987 c/z -33.370 -31.387 9.195 $ S3, SW shim position = 100.60
986 c/z -31.646 -33.911 9.195 $ S2, SE shim position = 104.34
985 c/z -19.202 -50.939 9.195 $ S1, SE shim position = 104.34
989 c/z -50.353 19.074 9.195 $ W1, SW shim position = 100.60
990 c/z -33.370 31.387 9.195 $ W2, SW shim position = 100.60
983 c/z 31.646 -33.911 9.195 $ E3, SE shim position = 104.34
984 c/z 19.202 -50.939 9.195 $ E4, SE shim position = 104.34
c mopyEND CONTROL DRUM POSITION SURFACES
c
c
c ***** End Control Surfaces *****

```

Figure 17: Surfaces that define the OSCC's in the original 3-region model.

```

c -----
c
c          CONTROL DRUM POSITION SURFACES
c
981 c/z 44.4092 -14.3428 9.1948 $ DRUM E1 AT 51.8 DEGREES
982 c/z 28.6783 -25.4119 9.1948 $ DRUM E2 AT 51.8 DEGREES
983 c/z 25.4119 -28.6783 9.1948 $ DRUM E3 AT 51.8 DEGREES
984 c/z 14.3428 -44.4092 9.1948 $ DRUM E4 AT 51.8 DEGREES
985 c/z -14.3428 -44.4092 9.1948 $ DRUM S1 AT 51.8 DEGREES
986 c/z -25.4119 -28.6783 9.1948 $ DRUM S2 AT 51.8 DEGREES
987 c/z -28.6783 -25.4119 9.1948 $ DRUM S3 AT 51.8 DEGREES
988 c/z -44.4092 -14.3428 9.1948 $ DRUM S4 AT 51.8 DEGREES
989 c/z -44.4092 14.3428 9.1948 $ DRUM W1 AT 51.8 DEGREES
990 c/z -28.6783 25.4119 9.1948 $ DRUM W2 AT 51.8 DEGREES
991 c/z -25.4119 28.6783 9.1948 $ DRUM W3 AT 51.8 DEGREES
992 c/z -14.3428 44.4092 9.1948 $ DRUM W4 AT 51.8 DEGREES
993 c/z 14.3428 44.4092 9.1948 $ DRUM N1 AT 51.8 DEGREES
994 c/z 25.4119 28.6783 9.1948 $ DRUM N2 AT 51.8 DEGREES
995 c/z 28.6783 25.4119 9.1948 $ DRUM N3 AT 51.8 DEGREES
996 c/z 44.4092 14.3428 9.1948 $ DRUM N4 AT 51.8 DEGREES
c
c
c -----

```

Figure 18: Surfaces that define the OSCC's in the 19-plate model.

With the changes to the OSCC's, the new k-effective is 1.02422 with a standard deviation of 0.00015. While still much larger than the 19-plate model, the k-effective did go down as expected. Figure 19 shows the new mesh tally data after changing the OSCC positions in the 3-region model. This change improves the 20% agreement between the two models in the area between the fuel and the OSCC's, but does not improve

agreement in the flux traps, neck shims, the H positions, and the B positions. The 3-region model now has 57% of the bins agreeing within 20% of the 19-plate model.

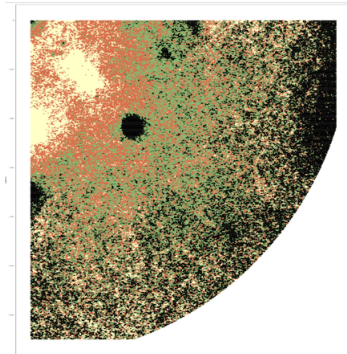


Figure 19: 20% agreement between the two models after updating the OSCC's

The agreement in the standard deviation, seen in figure 20, improved around the OSCC's. Interestingly, there is greater disagreement in the area inside the fuel. The inner A positions are now within two standard deviations after the change in the OSCC's. The flux traps and B positions, however, are still not in agreement. With updates to the OSCC's, 69% of the bins agree within two standard deviations.

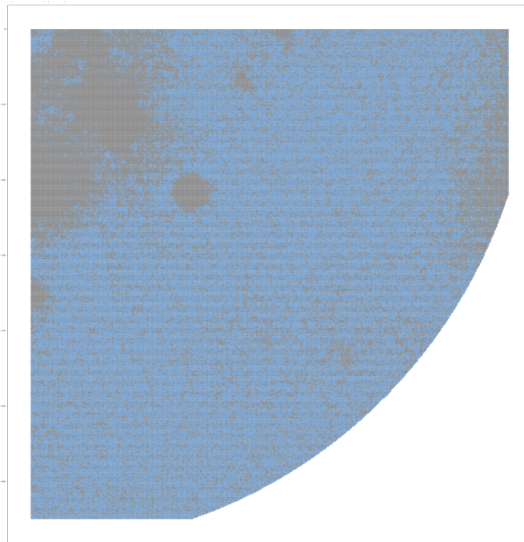


Figure 20: Where the two models agree within two standard deviations after updating the OSCC rotations.

3.3 Updating the Neck Shims.

The next step was to adjust the neck shims. This is done by adjusting the cell card for the shims. This is not as easy as adjusting the surface cards for the OSCC's, so MCCAFFE was used to generate new cell cards for the 22 neck shims. The Original shim rod cell cards are show in figure 21. Most of the cells stayed the

same so only the affected cells are shown in the figures. The regulation rods are defined differently from the rest of the neck shims. The cells specific to the two regulation rods can be seen in figures 21b and 21c.

```

c -----
c ---      NE      NW      SW      SE
c ---      1----6  1----6  1----6  1--r-6
c ---      000000  000000  000000  100200
702 030 6.02136-2 701 -702 100 -200    $ NE 1 Hf neck shim = 0
707 030 6.02136-2 706 -707 100 -200    $ NE 2 Hf neck shim = 0
712 030 6.02136-2 711 -712 100 -200    $ NE 3 Hf neck shim = 0
717 030 6.02136-2 716 -717 100 -200    $ NE 4 Hf neck shim = 0
722 030 6.02136-2 721 -722 100 -200    $ NE 5 Hf neck shim = 0
727 030 6.02136-2 726 -727 100 -200    $ NE 6 Hf neck shim = 0
732 030 6.02136-2 731 -732 100 -200    $ NW 1 Hf neck shim = 0
737 030 6.02136-2 736 -737 100 -200    $ NW 2 Hf neck shim = 0
742 030 6.02136-2 741 -742 100 -200    $ NW 3 Hf neck shim = 0
747 030 6.02136-2 746 -747 100 -200    $ NW 4 Hf neck shim = 0
752 030 6.02136-2 751 -752 100 -200    $ NW 5 Hf neck shim = 0
757 030 6.02136-2 756 -757 100 -200    $ NW 6 Hf neck shim = 0
762 030 6.02136-2 761 -762 100 -200    $ SW 1 Hf neck shim = 0
767 030 6.02136-2 766 -767 100 -200    $ SW 2 Hf neck shim = 0
772 030 6.02136-2 771 -772 100 -200    $ SW 3 Hf neck shim = 0
777 030 6.02136-2 776 -777 150 -200    $ SW 4 Hf neck shim = 0
782 030 6.02136-2 781 -782 100 -200    $ SW 5 Hf neck shim = 0
787 030 6.02136-2 786 -787 100 -200    $ SW 6 Hf neck shim = 0
792 070 -13.36 791 -792 100 -200    $ SE 1 Hf neck shim = 0
797 030 6.02136-2 796 -797 100 -200    $ SE 2 Hf neck shim = 0
802 030 6.02136-2 801 -802 100 -200    $ SE 3 Hf neck shim = 0
807 070 -13.36 806 -807 150 -200    $ SE 4 Hf neck shim = 0
812 030 6.02136-2 811 -812 100 -200    $ SE 5 Hf neck shim = 0
817 030 6.02136-2 816 -817 100 -200    $ SE 6 Hf neck shim = 0
c
c mopyEND NECKSHIMS

```

(a) Original shim rod cells.

```

776 010 1.00276-1 -776 100 -200    $ SW 4 water inside shim
888 070 -13.36 776 -777 100 -150    $ SW 4 water filler
778 010 1.00276-1 777 -778 100 -200    $ SW 4 water outside shim
779 010 1.00276-1 -778 96 -100    $ SW 4 water below shim
780 010 1.00276-1 -778 200 -204    $ SW 4 water above shim

```

(b) Original southwest regulation rod cells.

```

806 010 1.00276-1 -806 100 -200    $ SE 4 water inside shim
889 010 1.00276-1 806 -807 100 -150    $ SE 4 water filler
808 010 1.00276-1 807 -808 100 -200    $ SE 4 water outside shim
809 010 1.00276-1 -808 96 -100    $ SE 4 water below shim
810 010 1.00276-1 -808 200 -204    $ SE 4 water above shim

```

(c) Southeast regulation rod cells.

Figure 21: Original cells for regulation rods and shim rods.

After running MCCAFAE it was simply a matter of copying the new cells from the MCCAFAE output and pasting them into the 3-region model. Looking at figure 22a, you can see that the materials for the shims have changed to material 70, which is hafnium. Since the regulation rods are trickier to change those were updated by taking the cells directly from the 19-plate model. These new cells are pictured in figure 22b and figure 22c.

```

c -----
c ---      NE      NW      SW      SE
c ---      1----6  1----6  1----6  1--r-6
c ---      000000  000000  000000  100200
702  70      -13.36  701 -702 +100 -200      $ (shim inserted)
707  70      -13.36  706 -707 +100 -200      $ (shim inserted)
712  70      -13.36  711 -712 +100 -200      $ (shim inserted)
717  70      -13.36  716 -717 +100 -200      $ (shim inserted)
722  70      -13.36  721 -722 +100 -200      $ (shim inserted)
727  70      -13.36  726 -727 +100 -200      $ (shim inserted)
732  70      -13.36  731 -732 +100 -200      $ (shim inserted)
737  70      -13.36  736 -737 +100 -200      $ (shim inserted)
742  70      -13.36  741 -742 +100 -200      $ (shim inserted)
747  70      -13.36  746 -747 +100 -200      $ (shim inserted)
752  70      -13.36  751 -752 +100 -200      $ (shim inserted)
757  70      -13.36  756 -757 +100 -200      $ (shim inserted)
762  70      -13.36  761 -762 +100 -200      $ (shim inserted)
767  70      -13.36  766 -767 +100 -200      $ (shim inserted)
772  70      -13.36  771 -772 +100 -200      $ (shim inserted)
782  70      -13.36  781 -782 +100 -200      $ (shim inserted)
787  70      -13.36  786 -787 +100 -200      $ (shim inserted)
792  70      -13.36  791 -792 +100 -200      $ (shim inserted)
797  70      -13.36  796 -797 +100 -200      $ (shim inserted)
802  70      -13.36  801 -802 +100 -200      $ (shim inserted)
812  70      -13.36  811 -812 +100 -200      $ (shim inserted)
817  70      -13.36  816 -817 +100 -200      $ (shim inserted)
c
c mopyEND NECKSHIMS
c ***** End Control Cells *****

```

(a) MCCAFAE generated cells for 22 neck shims

776	130	0.099581	-776	100	-200	\$ SW 4 water inside shim
777	147	0.044868	-777	150	-200	\$ SW 4 Hf reg rod
888	130	0.099581	776	-777	100 -150	\$ SW 4 water filler
778	130	0.099581	777	-778	100 -200	\$ SW 4 water outside shim
779	130	0.099581	-778	96	-100	\$ SW 4 water below shim
780	130	0.099581	-778	200	-204	\$ SW 4 water above shim

(b) Southwest regulation rod cells.

806	130	0.099581	-806	100	-200	\$ SE 4 water inside shim
807	147	0.044868	806	-807	150 -200	\$ SE 4 Hf neck shim
889	130	0.099581	806	-807	100 -150	\$ SE 4 water filler
808	130	0.099581	807	-808	100 -200	\$ SE 4 water outside shim
809	130	0.099581	-808	96	-100	\$ SE 4 water below shim
810	130	0.099581	-808	200	-204	\$ SE 4 water above shim

(c) Southeast regulation rod cells.

Figure 22: MCCAFAE generated cells for the neck shims and regulation rod cells.

The resulting k-effective from this change was 1.01417 with a standard deviation of 0.00014. The mesh tally data from this change can be seen in figure 23. This data looks very similar to the data in figure 14. The most notable changes are that there is more agreement in the neck shim area and the agreement in the southeast flux trap, which has not been seen yet. 18% of the bins agree within 20% after updating the neck shims.

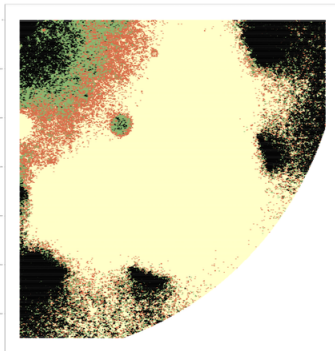


Figure 23: 20% agreement between the two models after updating the neck shims.

The standard deviation data for this change can be seen figure 24. This also closely resembles the standard deviation data from the unchanged 3-region model. The neck shims are visible now, though the agreement

within two standard deviations has only improved for the last two neck shims. There is new agreement in the southeast flux trap. Only 25% of the bins agree within two standard deviations after updating the neck shims.

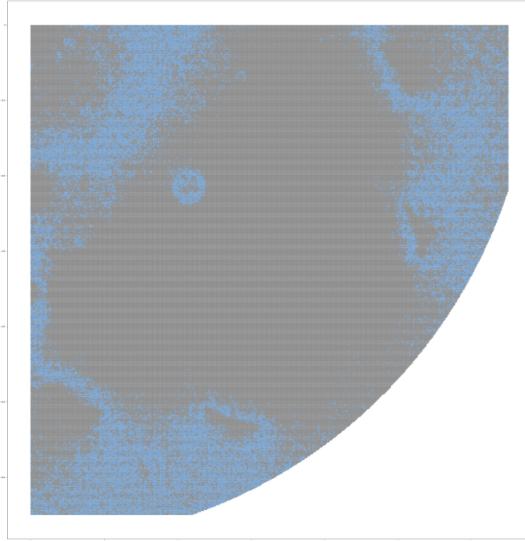


Figure 24: Where the two models agree within two standard deviations after updating the neck shim positions.

3.4 Combining Neck Shim and OSCC Updates

After looking at the OSCC's and neck shims separately, I combined the two changes and ran the model again. This was done by simply combining the changes made in the previous two steps. The new k-effective from this combination is 0.97130 with a standard deviation of 0.00015.

The mesh tally data in from this is shown in figure 25. As expected, combining these changes significantly improved where the two models have 20% agreement. At this point the two models still have disagreements in the flux traps, large B positions, inner A positions, and H positions. Updating both the neck shims and OSCC's brings the 20% agreement between the two models to 35%.

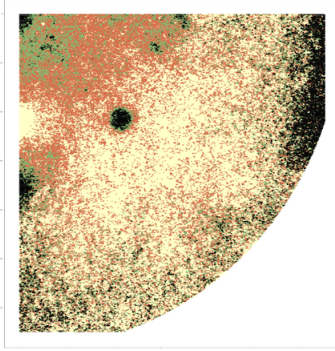


Figure 25: 20% agreement between the two models after updating the neck shims and OSCC's.

The standard deviation data, seen in figure 26 reveals more information on the two models. The flux traps and fuel do not agree within two standard deviations while most other areas of the reactor do have agreement. This is unsurprising because the 3-region models depleted fuel while the 19-plate model uses fresh fuel. 49% of the bins agree within two standard deviations.

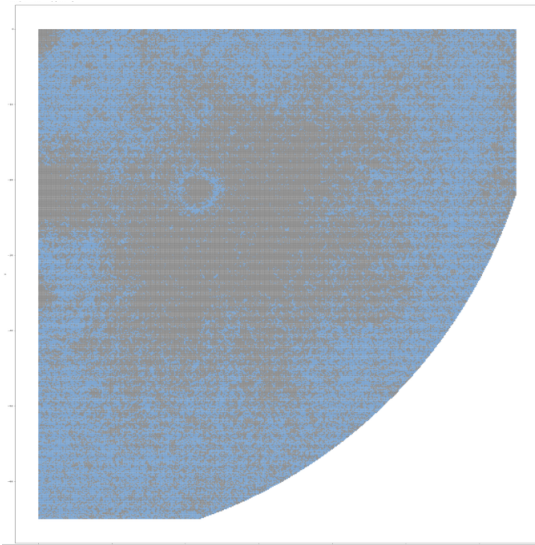


Figure 26: Where the two models agree within two standard deviations after updating the neck shims and OSCC's.

3.5 Removing Experiments

At this point it was clear that there was more going on, so to make a better comparison the experiments that were in the 3-region model were removed or changed to match what was modeled in the 19-plate model. The experiment positions are modeled almost identically in the two models, so it was relatively simple, if time consuming, matter to change the cells and surfaces in the 3-region model to resemble those in the 19-plate model. Any tallies and material associated with the old experiments were also removed from the model.

During this process, the materials for water, hafnium, cobalt, beryllium, and aluminum were updated to match what is used in the 19-plate model.

The mesh tally data from the 3-region model after all the old experiments were removed is shown in figure 27. Where the two models have 20% agreement now covers most of the reactor. Disagreements in all the flux traps, except for the center flux trap, and experiment positions have been fixed. There are disagreements in the hafnium portions of the OSCC's as well as generally less agreement further from the core. Removing the experiments brings the 20% agreement to 55%.

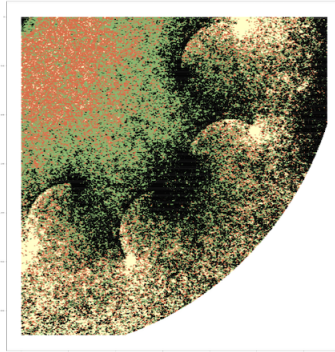


Figure 27: 20% agreement between the two models after removing the experiments.

Figure 28 shows the standard deviation of the two models after removing the experiments from the 3-region model. There is more agreement in the fuel surrounding the southeast flux trap and in the experiment positions. There are still gaps around the center flux trap, OSCC's, and the center flux trap. 66% of the bins agree within two standard deviations.

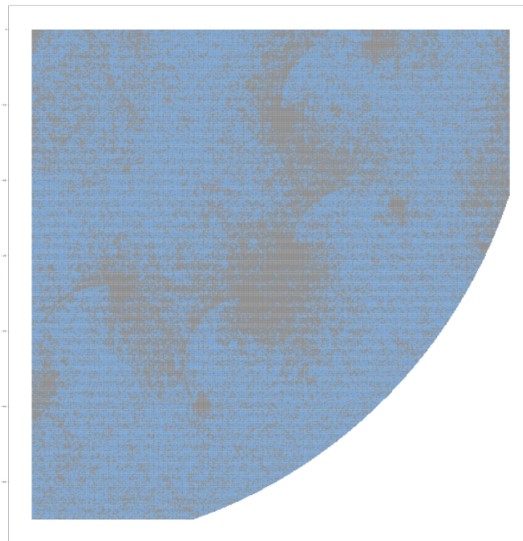


Figure 28: Where the two models agree within two standard deviations after removing the experiments.

3.5.1 Changing Surface Numbers and Adding Tallies.

There are some important differences in surface numbers between the 3-region and 19-plate models. Specifically, the surfaces that define the top and bottom of the fuel. In the 19-plate model surface 97, shown in figure 29a, defines the bottom of the fuel elements. The 3-region model also has a surface 97 that defines the bottom of the fuel element, shown in figure 29b. The difference is that the 3-region model also has a surface 96 that defines the bottom of the shim housing. The 3-region model uses surface 96 to define flux traps, A positions, H positions, and the shim housing. The 19-plate model does not have corresponding surface. When porting geometry over to the 3-region model, MCNP would not give any geometry errors but would quickly crash after starting a run. A similar problem was encountered with surface 203. The defines the top of the fuel elements in both models. The 3-region model has a surface 204 which defines the top of the shim housing. Surface 204 is used the same way as surface 96 but at the top of the reactor.

97	pz	-20.955	\$ bottom of fuel element	95	pz	-64.540	\$ bottom of H2O reflector
98	pz	-2.540	\$ bottom of Be reflector	96	pz	-41.540	\$ bottom of shim housing
99	pz	-1.905	\$ bottom of fuel plates	97	pz	-20.955	\$ bottom of fuel element
100	pz	0.000	\$ bottom of fuel meat	98	pz	-2.540	\$ bottom of Be reflector
101	pz	5.080	\$ bottom of Hf shim on drums	99	pz	-1.905	\$ bottom of fuel plates
102	pz	3.0163	\$ used for below OSC Hf region	100	pz	0.000	\$ bottom of fuel meat
150	pz	60.960	\$ middle of active fuel	101	pz	5.080	\$ bottom of Hf shim on drums
185	pz	114.30	\$ bottom of safety rod	102	pz	3.0163	\$ used for below OSC Hf region
200	pz	121.920	\$ top of fuel meat	110	pz	15.240	\$ fuel segmentation plane
201	pz	123.825	\$ top of fuel plates	120	pz	30.480	\$ fuel segmentation plane
202	pz	127.0000	\$ top of Be reflector	130	pz	45.720	\$ fuel segmentation plane
203	pz	147.32	\$ top of fuel element	150	pz	60.960	\$ middle of active fuel
208	pz	137.1600	\$ used for above OSC region	151	pz	64.770	\$ tally plane 1.5 in above midplane
209	pz	-8.255	\$ bottom of core reflector tank	160	pz	76.200	\$ fuel segmentation plane
210	pz	139.7	\$ top of core reflector tank	170	pz	91.440	\$ fuel segmentation plane
				180	pz	106.680	\$ fuel segmentation plane
				185	pz	114.30	\$ bottom of safety rod
				200	pz	121.920	\$ top of fuel meat
				201	pz	123.825	\$ top of fuel plates
				202	pz	127.0000	\$ top of Be reflector
				203	pz	147.320	\$ top of fuel element
				204	pz	166.0000	\$ top of shim housing
				205	pz	187.0000	\$ top of H2O reflector
				208	pz	137.1600	\$ used for above OSC region

(a) 19-plate model surfaces.

(b) 3-region model surfaces.

Figure 29: MCCAFE generated cells for the neck shims and regulation rod cells.

The problem was fixed by changing surface 96 and surface 204 to 97 and 203. The original surfaces 97 and 203 were changed to 197 and 2203. These changes are shown in figure 30. With these changes geometry can be moved between the two models without errors.

95	pz	-64.540	\$ bottom of H2O reflector
97	pz	-41.540	\$ bottom of shim housing
197	pz	-20.955	\$ bottom of fuel element
98	pz	-2.540	\$ bottom of Be reflector
99	pz	-1.905	\$ bottom of fuel plates
100	pz	0.000	\$ bottom of fuel meat
101	pz	5.080	\$ bottom of Hf shim on drums
102	pz	3.0163	\$ used for below OSC Hf region
110	pz	15.240	\$ fuel segmentation plane
120	pz	30.480	\$ fuel segmentation plane
130	pz	45.720	\$ fuel segmentation plane
150	pz	60.960	\$ middle of active fuel
151	pz	64.770	\$ tally plane 1.5 in above midplane
160	pz	76.200	\$ fuel segmentation plane
170	pz	91.440	\$ fuel segmentation plane
180	pz	106.680	\$ fuel segmentation plane
185	pz	114.30	\$ bottom of safety rod
200	pz	121.920	\$ top of fuel meat
201	pz	123.825	\$ top of fuel plates
202	pz	127.0000	\$ top of Be reflector
2203	pz	147.320	\$ top of fuel element
203	pz	166.0000	\$ top of shim housing
205	pz	187.0000	\$ top of H2O reflector
208	pz	137.1600	\$ used for above OSC region

Figure 30: Fixed 3-region surfaces.

Surface and cell numbers for the experiment positions were changed to match those in the 19-plate model to make it easy to change between the two models. Table 6 has a summary of what cell and surface numbers are used for the experiment positions and flux traps.

Position	Cell Numbers	Surface Numbers
Inner A	31000-38000	21000-28000
Outer A	41000-44000	31000-34000
A13-16	49000	39000
Small B	51000-58000	41000-48000
Large B	61000-64000	51000-54000
Large and Medium I	71000-90000	61000-80000
Small I	91000-94000	81000-84000
H	95000-97000	90000-92000
Flux Traps	21000-29000	1200-1700/11000- 15000

Table 6: Summary of surface and cell numbers.

In addition to changing the surface and cell numbers, tallies were added to all experiment positions and flux traps for both models. Each position got a total flux and total energy deposition tally as well as an energy tally divided into six energy bins. The energy bins are from the lower cut off to 0.1 MeV, 0.1 MeV to 0.5 MeV, 0.5 MeV to 1 MeV, 1 MeV to 5 MeV, 5 MeV to 10 MeV, and 10 MeV to 20 MeV. The fuel cells in

both models received a fission energy deposition tally.

3.6 Updating Fuel Materials

The fuel materials were the next thing to be updated. MCCAFF was once again utilized for this change. The U-235 mass, 1075.0 g, and Boron, 660 g, mass needed for this were taken from the 94-CIC documentation. The structure of the fuel was unchanged, so MCCAFF generated 840 new fuel materials to model fresh fuel the entire length of the fuel elements. This resulted in a k-effective of 0.98097 with a standard deviation of 0.00015.

The mesh tally data from this run can be seen in in figure 31. Most noticeably, this still has significant disagreement in the center flux trap. The rest of the flux traps, fuel, A positions, B positions, and H positions all have excellent agreement. As the data goes beyond the OSCC's and into the I positions the models agree less, but this is expected towards the outside of the reactor. Updating the fuel materials brings the 20% agreement to 65%.

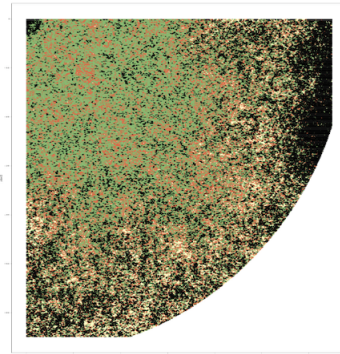


Figure 31: 20% agreement between the two models after updating fuel material.

The standard deviation, shown in figure 32, shows the two models are in general agreement throughout the entire reactor. Even though the tallies do not exactly agree, the standard deviation shows the models to agree. The only spot of disagreement is in the center flux trap. 76% of the reactor models agree within two standard deviations.

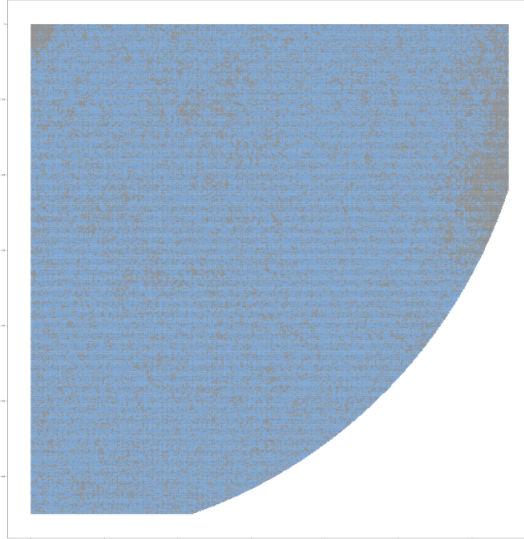


Figure 32: Where the two models agree within two standard deviations after updating the fuel materials.

3.7 sensitivity

A sensitivity study was to see how both models reacted to change. Ideally the reactivity in both models would change by the same amount. This was done by replacing what was in the experiment position with hafnium. This was done only on the southeast lobe because of the symmetry of the reactor. In the A, small B, and H6 positions the aluminum filler was replaced with hafnium. In the large B, and all I positions the beryllium was replaced. In the H5, H7, H8, and H9 positions the cobalt was replaced. In the center flux trap, only the cobalt was replaced. In the east and south flux traps the cobalt was replaced. In the southeast flux trap the aluminum was replaced. The materials in the neck shims and OSCC's were not changed. Instead, the drums were rotated to 10, 30, 50, 70, 90, 110, 130, and 150 degrees. The shims were withdrawn individually.

This method caught an input error in the benchmark model table on the 90-degree OSCC rotation as well as error in the input deck of the southeast flux trap. In both cases the difference in reactivity between the two models was an order of magnitude greater than the rest of the data.

Tables 7, 9, and 8 show the reactivity change in the 19-plate model. Tables 10, 11, and 12 show the reactivity change in 3-region model.

19-Plate Model				
Position	K-effective value	Error	Change in reactivity (\$)	Change in reactivity error (\$)
Center Flux Trap	0.99879	0.00014	-0.10	0.029
East Flux Trap	0.99751	0.00014	-0.28	0.029
Southeast Flux Trap	0.97766	0.00015	-3.11	0.030
South Flux Trap	0.99739	0.00014	-0.30	0.029

Table 7: Values for the 19-plate model sensitivity study.

Position	K-effective value	Error	Change in reactivity (\$)	Change in reactivity error (\$)
19-plate model	0.99951	0.00015	NA	NA
A3	0.99517	0.00014	-0.61	0.029
A4	0.99557	0.00014	-0.55	0.029
A10	0.99549	0.00014	-0.56	0.029
A14	0.99622	0.00014	-0.46	0.029
B3	0.99651	0.00014	-0.42	0.029
B4	0.99624	0.00014	-0.46	0.029
B10	0.99901	0.00014	-0.070	0.029
B11	0.99864	0.00014	-0.12	0.029
H5	0.99865	0.00014	-0.12	0.029
H6	0.99634	0.00014	-0.44	0.029
H7	0.99887	0.00014	-0.089	0.029
H8	0.99883	0.00014	-0.095	0.029
H9	0.99879	0.00014	-0.10	0.029
I6	0.99916	0.00014	-0.049	0.029
I7	0.99937	0.00014	-0.019	0.029
I8	0.99897	0.00014	-0.075	0.029
I9	0.99903	0.00014	-0.067	0.029
I10	0.99911	0.00014	-0.056	0.029
I11	0.99893	0.00015	-0.081	0.030
I22	0.99897	0.00014	-0.075	0.029

Table 8: Values for the 19-plate model sensitivity study.

Position	K-effective	Error	Change in reactivity (\$)	Change in reactivity error (\$)
Shim 1	1.00158	0.00014	0.29	0.028
Shim 2	1.00151	0.00014	0.28	0.028
Shim 3	1.00147	0.00015	0.27	0.029
Shim 4	0.99782	0.00014	-0.24	0.029
Shim 5	1.0016	0.00015	0.29	0.029
Shim 6	1.00177	0.00015	0.31	0.029
OSCC 10 Degrees	0.9923	0.00014	-1.00	0.029
OSCC 30 Degrees	0.99418	0.00015	-0.74	0.030
OSCC 50 Degrees	0.99847	0.00015	-0.14	0.030
OSCC 70 Degrees	1.00509	0.00015	0.77	0.029
OSCC 90 Degrees	1.01376	0.00014	1.95	0.028
OSCC 110 Degrees	1.0224	0.00014	3.11	0.028
OSCC 130 Degrees	1.02838	0.00014	3.90	0.028
OSCC 150 Degrees	1.03137	0.00014	4.29	0.028

Table 9: Values for the 19-plate model sensitivity study.

3-Region Model with Incorrect Center Flux Trap Geometry				
Position	K-effective value	Error	Change in reactivity (\$)	Change in reactivity error (\$)
3-region model	0.98097	0.00015	NA	NA
A3	0.97781	0.00015	-0.46	0.031
A4	0.97762	0.00014	-0.49	0.030
A10	0.97745	0.00015	-0.51	0.031
A14	0.97869	0.00014	-0.33	0.030
B3	0.97803	0.00015	-0.43	0.031
B4	0.97823	0.00014	-0.40	0.030
B10	0.97698	0.00014	-0.58	0.030
B11	0.98049	0.00014	-0.069	0.030
H5	0.98024	0.00015	-0.11	0.031
H6	0.97843	0.00014	-0.37	0.030
H7	0.98096	0.00014	-0.0014	0.030
H8	0.98069	0.00015	-0.040	0.031
H9	0.98063	0.00015	-0.049	0.031
I6	0.98131	0.00014	0.049	0.030
I7	0.98143	0.00015	0.066	0.031
I8	0.98085	0.00015	-0.017	0.031
I9	0.98125	0.00014	0.040	0.030
I10	0.98104	0.00014	0.010	0.030
I11	0.98115	0.00015	0.026	0.031
I22	0.98125	0.00015	0.040	0.031

Table 10: Values for the 3region model sensitivity study with incorrect center flux trap geometry.

Position	K-effective	Error	Change in reactivity (\$)	Change in reactivity error (\$)
Shim 1	0.98329	0.00015	0.33	0.031
Shim 2	0.98306	0.00015	0.30	0.031
Shim 3	0.98331	0.00015	0.34	0.031
Shim 4	0.98011	0.00015	-0.12	0.031
Shim 5	0.98315	0.00014	0.31	0.030
Shim 6	0.98317	0.00014	0.32	0.030
OSCC 10 Degrees	0.97472	0.00016	-0.91	0.032
OSCC 30 Degrees	0.97682	0.00015	-0.60	0.031
OSCC 50 Degrees	0.98029	0.00014	-0.098	0.030
OSCC 70 Degrees	0.98661	0.00014	0.81	0.029
OSCC 90 Degrees	0.99456	0.00014	1.93	0.029
OSCC 110 Degrees	1.00232	0.00015	3.02	0.030
OSCC 130 Degrees	1.00815	0.00015	3.82	0.030
OSCC 150 Degrees	1.01087	0.00014	4.19	0.029

Table 11: Values for the 3-region model sensitivity study with incorrect center flux trap geometry.

Position	K-effective value	Error	Change in reactivity (\$)	Change in reactivity error (\$)
Center Flux Trap	0.98077	0.00015	-0.029	0.031
East Flux Trap	0.97971	0.00015	-0.18	0.031
Southeast Flux Trap	0.9611	0.00014	-2.93	0.030
South Flux Trap	0.97956	0.00014	-0.20	0.030

Table 12: Values for the 3-region model sensitivity study.

Tables 13, 14, and 15 show the difference in reactivity between the two models. The majority of the experiment positions and drum rotations have a greater than 0.05\$ difference between the models.

Position	Reactivity Change Difference (19-plate - 3 region \$)
A3	-0.15
A4	-0.065
A10	-0.051
A14	-0.13
B3	0.0073
B4	-0.060
B10	0.51
B11	-0.052
H5	-0.014
H6	-0.075
H7	-0.090
H8	-0.054
H9	-0.051
I6	-0.10
I7	-0.086
I8	-0.058
I9	-0.11
I10	-0.066
I11	-0.11
I22	-0.12

Table 13: Difference between the 19-plate model and the 3-region model with incorrect center flux trap geometry.

Position	Reactivity Change Difference (19-plate - 3 region \$)
Shim 1	-0.047
Shim 2	-0.024
Shim 3	-0.065
Shim 4	-0.11
Shim 5	-0.024
Shim 6	-0.0033
OSCC 10 Degrees	-0.10
OSCC 30 Degrees	-0.14
OSCC 50 Degrees	-0.047
OSCC 70 Degrees	-0.038
OSCC 90 Degrees	0.019
OSCC 110 Degrees	0.095
OSCC 130 Degrees	0.084
OSCC 150 Degrees	0.10

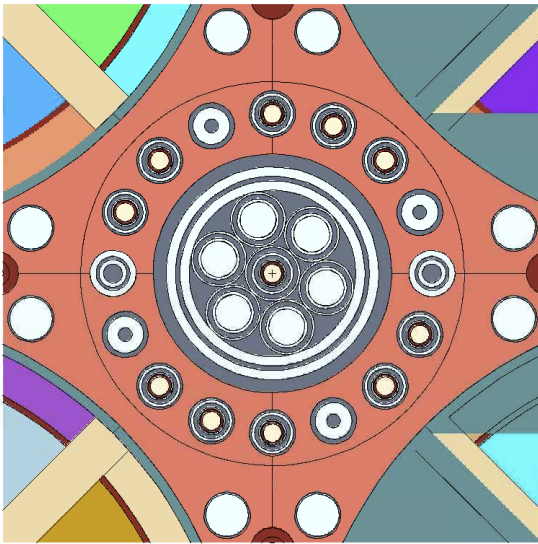
Table 14: Difference between the 19-plate model and the 3-region model with incorrect center flux trap geometry.

Position	Reactivity Change Difference (19-plate - 3 region \$)
Center Flux Trap	-0.071
East Flux Trap	-0.097
Southeast Flux Trap	-0.18
South Flux Trap	-0.092

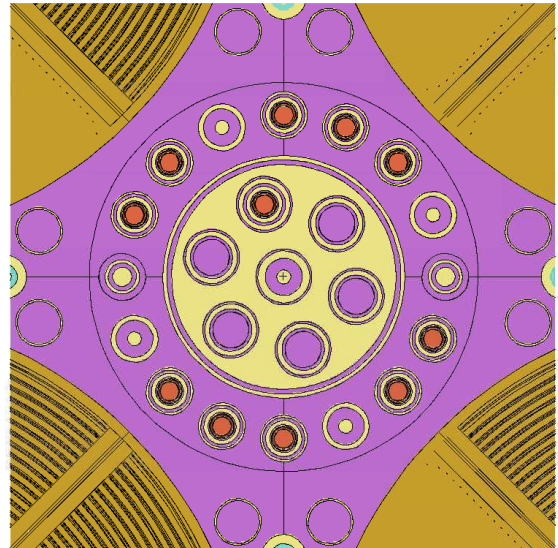
Table 15: Difference between the 19-plate model and the 3-region model with incorrect center flux trap geometry.

3.8 Center Flux Trap Error

After the initial sensitivity study on the two models, it was discovered that the geometry in the two models did not exactly match. Figure 33a shows what was used in the 3-region model and figure 33b shows what was used in the 19-plate model. Visually it is easy to see the differences between the two center flux traps. In figure 33a the seven smaller cylinders are closer together to accommodate extra aluminum and water rings and the cobalt is in the middle cylinder instead of a side cylinder. This error occurred when the old experiments were being removed. When looking at the cells that define these two center flux traps, there is almost no difference. In addition, the outermost water and aluminum ring that surround the center flux trap in the 3-region model are not defined with the center flux trap. Instead, they are defined with the shim housing surfaces. In addition to being in a different part of the model, the outer water and aluminum ring are thicker in the 3-region model and needed to have their radii adjusted.



(a) 3-region center flux trap with error.



(b) 19-plate center flux trap with correct geometry.

Figure 33: 3-region center flux trap with error compared to 19-plate center flux trap.

After correcting the center flux trap geometry, the 3-region model was rerun. The k-effective for the model with correct geometry is 0.97819 with a standard deviation of 0.00015. The new mesh tally data, figure 34 shows the disagreement in the center flux is gone. Now the only areas of disagreement in the tally results are at the edge of the reactor. After all the updates, 60% of the models agree within 20%

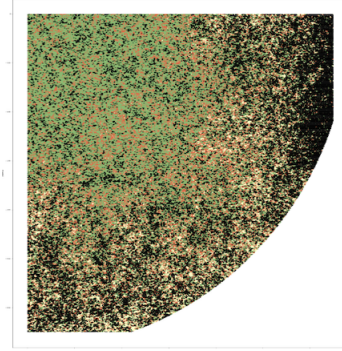


Figure 34: 20% agreement between the two models after updating the center flux trap.

The standard deviation data shows, figure 35, shows agreement across the entire reactor. There are no large areas of disagreement. 79% of the bins agree within two standard deviations after all updates to the 3-region model.

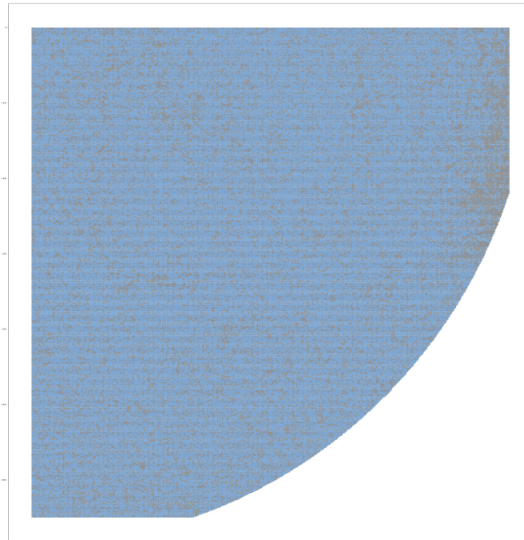


Figure 35: Where the two models agree within two standard deviations after updating the center flux trap.

With the center flux trap geometry fixed, the sensitivity study was rerun. The new 3-region data is shown in tables 16, 18, 17.

3-Region Model with Corrected Center Flux Trap Geometry				
Position	K-effective value	Error	Change in reactivity (\$)	Change in reactivity error (\$)
Center Flux Trap	0.97753	0.00014	-0.096	0.030
East Flux Trap	0.97679	0.00015	-0.20	0.031
Southeast Flux Trap	0.95786	0.00014	-3.01	0.030
South Flux Trap	0.97659	0.00015	-0.23	0.031

Table 16: Values for the 3-region model sensitivity study with corrected center flux trap geometry.

Position	K-effective value	Error	Change in reactivity (\$)	Change in reactivity error (\$)
3-region model	0.97819	0.00015	NA	NA
A3	0.97453	0.00015	-0.53	0.031
A4	0.97481	0.00015	-0.49	0.031
A10	0.97462	0.00014	-0.52	0.030
A14	0.9753	0.00015	-0.42	0.031
B3	0.97529	0.00015	-0.42	0.031
B4	0.97547	0.00014	-0.40	0.030
B10	0.97756	0.00015	-0.092	0.031
B11	0.97746	0.00015	-0.11	0.031
H5	0.97791	0.00015	-0.041	0.031
H6	0.97506	0.00015	-0.46	0.031
H7	0.97774	0.00015	-0.065	0.031
H8	0.9771	0.00015	-0.16	0.031
H9	0.97744	0.00015	-0.11	0.031
I6	0.97797	0.00015	-0.032	0.031
I7	0.97833	0.00015	0.020	0.031
I8	0.97806	0.00015	-0.019	0.031
I9	0.97775	0.00016	-0.064	0.032
I10	0.97791	0.00015	-0.041	0.031
I11	0.97833	0.00015	0.020	0.031
I22	0.97813	0.00014	-0.0087	0.030

Table 17: Values for the 3region model sensitivity study with corrected center flux trap geometry.

Position	K-effective	Error	Change in reactivity (\$)	Change in reactivity error (\$)
Shim 1	0.98	0.00014	0.26	0.030
Shim 2	0.98004	0.00014	0.27	0.030
Shim 3	0.98033	0.00015	0.31	0.031
Shim 4	0.97682	0.00015	-0.20	0.031
Shim 5	0.98051	0.00015	0.34	0.031
Shim 6	0.98033	0.00015	0.31	0.031
OSCC 10 Degrees	0.97177	0.00015	-0.94	0.031
OSCC 30 Degrees	0.97361	0.00014	-0.67	0.030
OSCC 50 Degrees	0.97729	0.00014	-0.13	0.030
OSCC 70 Degrees	0.98385	0.00015	0.82	0.031
OSCC 90 Degrees	0.99184	0.00014	1.95	0.029
OSCC 110 Degrees	0.99985	0.00015	3.08	0.030
OSCC 130 Degrees	1.00581	0.00015	3.90	0.030
OSCC 150 Degrees	1.00849	0.00015	4.29	0.030

Table 18: Values for the 3-region model sensitivity study with corrected center flux trap geometry.

With correct geometry the difference in reactivity between the two models was much closer. The largest difference is 0.10\$ in the I11 position. All the shim movements match within 0.05\$. Tables 19, 20, and 21 show a complete list of differences.

Position	Reactivity Change Difference (19-plate - 3 region \$)
A3	-0.073
A4	-0.058
A10	-0.041
A14	-0.038
B3	0.0039
B4	-0.060
B10	0.022
B11	-0.015
H5	-0.079
H6	0.014
H7	-0.024
H8	0.064
H9	0.0088
I6	-0.017
I7	-0.040
I8	-0.056
I9	-0.0029
I10	-0.015
I11	-0.10
I22	-0.066

Table 19: Difference between the 19-plate model and the 3-region model with correct center flux trap geometry.

Position	Reactivity Change Difference (19-plate - 3 region \$)
Shim 1	0.025
Shim 2	0.0095
Shim 3	-0.038
Shim 4	-0.036
Shim 5	-0.046
Shim 6	0.0035
OSCC 10 Degrees	-0.072
OSCC 30 Degrees	-0.077
OSCC 50 Degrees	-0.014
OSCC 70 Degrees	-0.045
OSCC 90 Degrees	-0.00079
OSCC 110 Degrees	0.035
OSCC 130 Degrees	0.0020
OSCC 150 Degrees	0.027

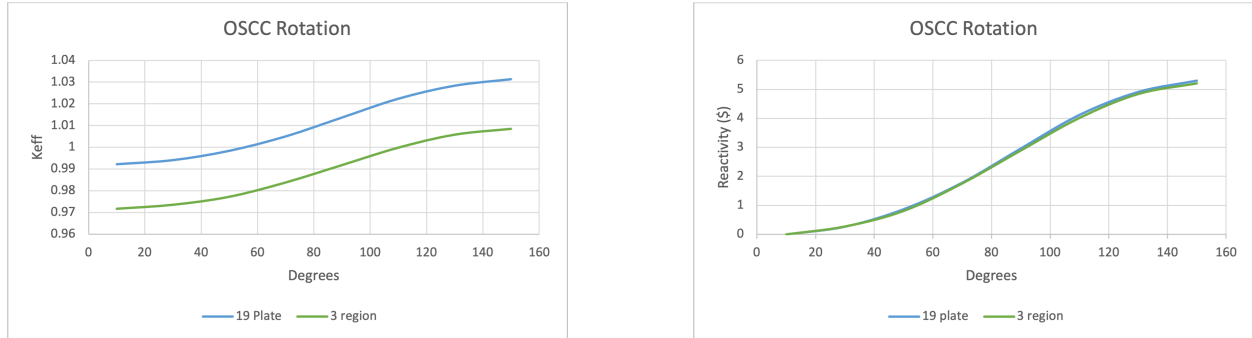
Table 20: Difference between the 19-plate model and the 3-region model with correct center flux trap geometry.

Position	Reactivity Change Difference (19-plate - 3 region \$)
Center Flux Trap	-0.0043
East Flux Trap	-0.075
Southeast Flux Trap	-0.092
South Flux Trap	-0.063

Table 21: Difference between the 19-plate model and the 3-region model with correct center flux trap geometry.

Looking at the reactivity from the OSCC rotations gives more insight into how the models behave. Figure 36a shows the k-effective of the OSCC rotations of both models. The two curves look very similar, but the

3-region curve is lower than the 19-plate model. Figure 36b show the adjusted reactivity of the k-effective curves. They were adjusted to both start at zero to see how well the curves match. The curves do match remarkably well, with only a slight difference at the larger rotations.



(a) K-effective for the OSCC rotations.

(b) Adjusted Reactivity for the OSCC's.

Figure 36: Reactivity curves for OSCC's.

3.9 Tallies

The tally values given by MCNP are not always useful in their raw form. The first step is scaling the power of the ATR to each lobe. The results of a fission energy deposition tally and the mass given in the output file are needed. The tally and mass are multiplied to get energy as seen in equation 4.

$$Energy_{lobe} = mass * tally \quad (4)$$

Next the energy for each lobe is divided by the sum of all the lobes.

$$Energy_{scaled} = \frac{Energy_{lobe}}{\sum_1^5 Energy_{lobe}} \quad (5)$$

Last the scaled energy is divided by the power in each lobe.

$$Power_{scaled} = \frac{Power_{lobe}}{Energy_{scaled}} \quad (6)$$

Power data was taken from the 169A ATR cycle. The power for the northwest lobe was 20 MW, the northeast lobe was 19 MW, the center lobe was 21.6 MW, the southeast lobe was 24 MW, and the southwest lobe was 23 MW. The power scaled to each lobe is shown in table 22.

Lobe	19-plate Model Power (MW)	3-region Model Power (MW)
Northwest	109	108
Northeast	115	115
Center	90.1	90.5
Southeast	117	112
Southwest	111	117

Table 22: Summary of power scaled to each lobe in the 19-plate and 3-region models.

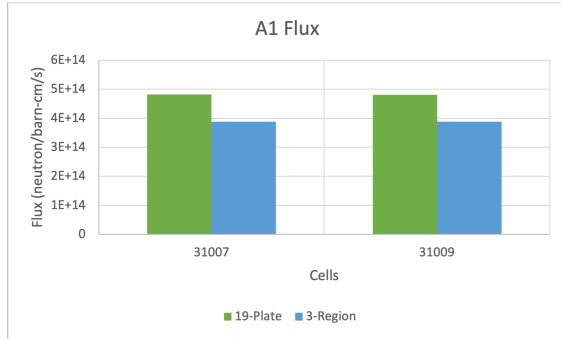
With the scaled power, it is now possible to get the neutron heat generation rates from the energy tallies. Equation 7 shows how to do this with the energy tallies.

$$NHGR = (tally \frac{MEV}{g - neutron})(1.215 \times 10^4 \frac{neutrons - W}{MeV - MW})(Power MW) \quad (7)$$

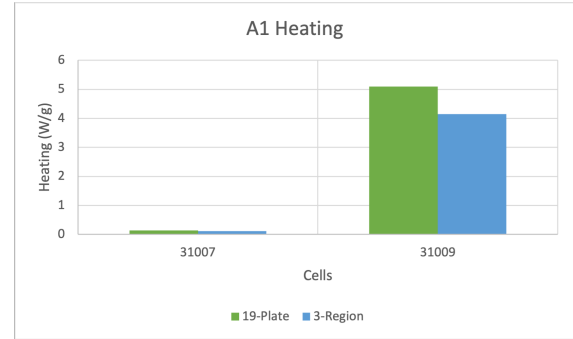
The tallies shown in figures 37 and 38 are examples of the information gathered from the flux and energy deposition tallies. The graphs are a cell-by-cell comparison for each position in the ATR. The heat and flux inside the fuel loop have percent errors greater than 20% while outside the fuel loop the percent error is usually below 5%. The percent error for the B10 and A1 positions can be seen in table 23. When looking at the flux graphs, figures 38a and 37a, take note of the scale. The 3-region data looks as if it half the value of the 19-plate data, when the numbers are close in value. In the two examples provided here the 3-region model under predicts flux and heat. This is generally true outside the fuel, but inside the fuel the 3-region generally over predicts. All the tally graphs can be found in appendix A. The complete percent error tables can be seen in appendix B.

Position	Cell	Flux error	Heat error
A1	31007	19.48	18.33
A1	31009	19.42	18.70
B10	62006	2.84	5.56
B10	62007	2.92	2.76
B10	62008	2.81	2.32
B10	62009	2.94	3.22

Table 23: Percent error for flux and heating tallies.

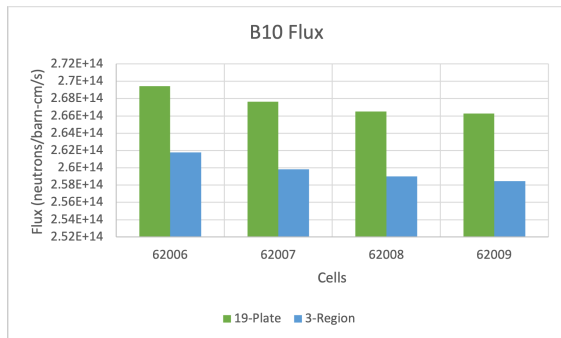


(a) Flux for the A1 position

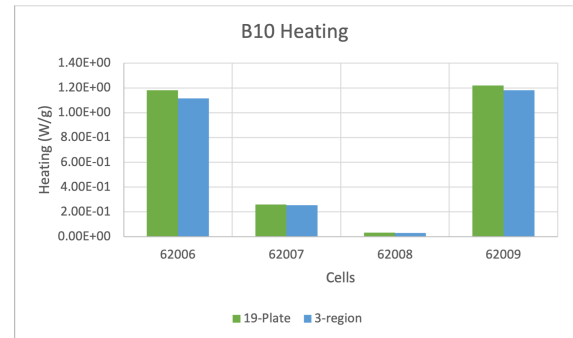


(b) Heat generation rates for the A1 position.

Figure 37: Flux and heat generation for the A1 position.



(a) Flux for the B10 position



(b) Heat generation rates for the B10 position.

Figure 38: Flux and heat generation for the B10 position.

In addition to the experiment position tallies, a tally multiplier was added to the mesh tally to get an energy deposition mesh tally and a fission energy deposition mesh tally on both models. Figure 39 shows the energy deposition in the 19-plate model. This image shows that most of the energy is deposited in the fuel and cobalt near the fuel. The 19 plates in each fuel element are visible as well as each spot of cobalt. Figure 40 shows the energy deposition in the 3-region model. This figure shows the energy is deposited in the fuel, cobalt, and hafnium in the neck shims and OSCC's. The 3 radial regions in each fuel element are clearly visible as well as the hafnium portions of the drums.



Figure 39: Energy deposition for 19-plate model.

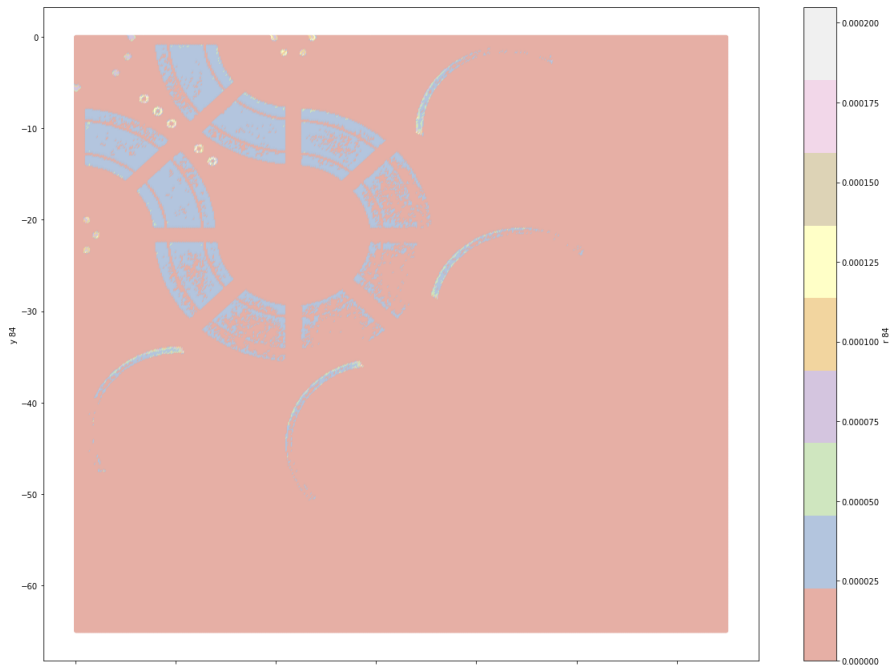


Figure 40: energy deposition for 3-region model

Figures 41 and 42 show fission energy mesh tallies for the 19-plate model and 3-region model respectively. The fission energy mesh tally shows the continuous energy flux scaled by the energy dependent uranium-235 cross section. The result is proportional to the expected fission rate in uranium-235. The similarity between

the two figures shows that the models can produce similar results for more complex values than one group flux.

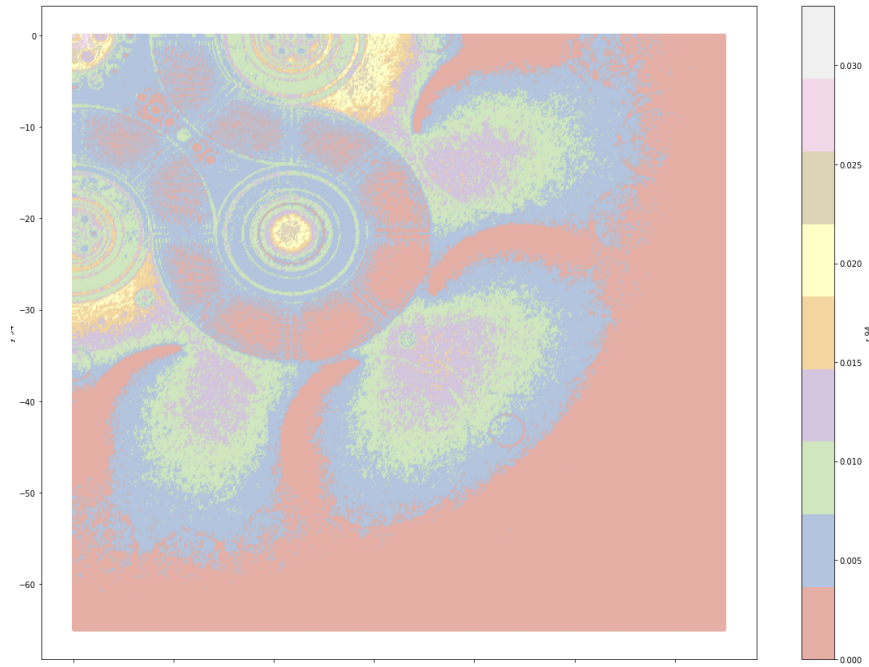


Figure 41: fission energy deposition mesh tall of 19-plate model

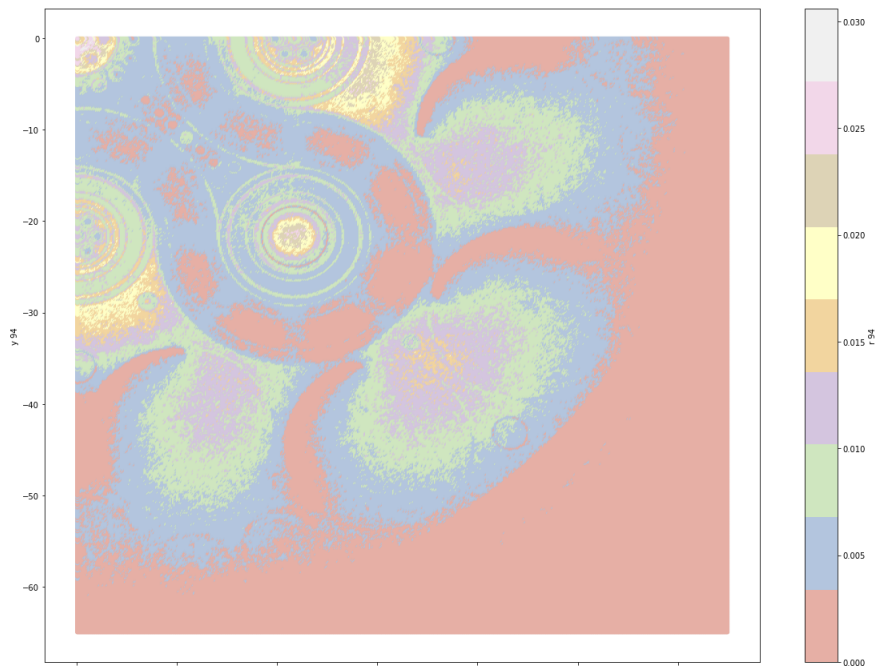


Figure 42: fission energy deposition mesh tall of 3-region model

Figure 43 shows where the two energy deposition mesh tallies agree within $\pm 10\%$. Most notably is the

disagreement in the fuel. Since the fuel is modeled differently it is expected that the energy deposition would not agree. There is also in the areas with hafnium. This could be due to a difference in cross-sections in the material definitions for each model. This difference could cause MCNP to treat hafnium a little differently in the 3-region model.



Figure 43: 20% agreement between energy deposition of both models.

Figure 44 shows where the two fission energy mesh tallies agree within $\pm 10\%$. Again, the fuel is where the greatest discrepancies lie. The 3-region model fuel is visible here because it has been homogenized.

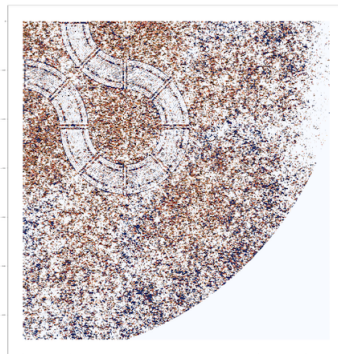


Figure 44: 20% agreement between fission energy deposition of both models.

4 Conclusions

Figure 45 shows the new 3-region model. This new model can be found at <https://hpcgitlab.hpc.inl.gov/> under the project "atr_model_tracking." A HPC account and access to the experiment analysis group is needed to view the model. Based on the data analyzed here, the 3-region model works adequately for the

work it is being used for. It is not recommended to use the 3-region model for an eigenvalue (k-effective) run. Analysts who model experiments in the flux traps or the A positions should be aware of the higher errors associated with the region inside the fuel and should consider using the 19-plate model if possible.

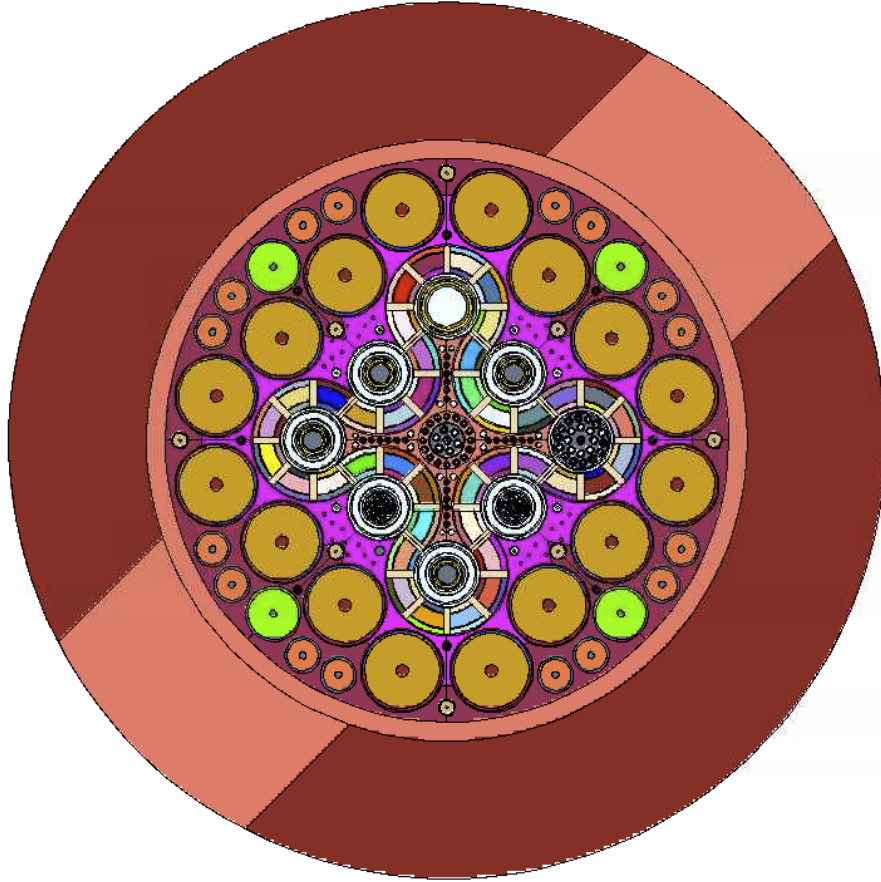


Figure 45: Updated 3-region model

5 Future Work

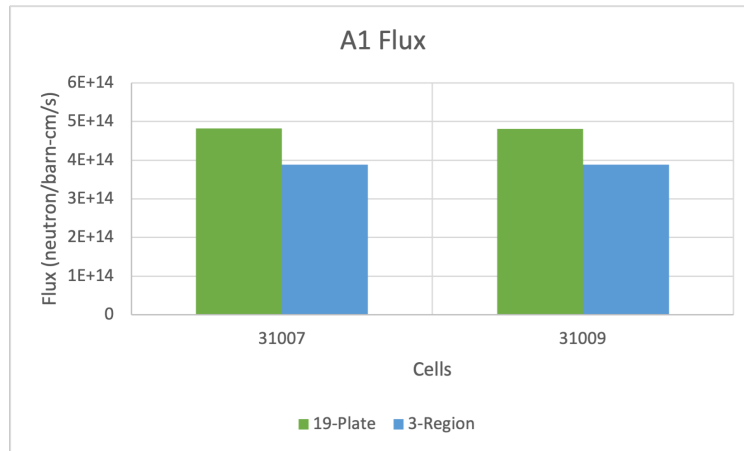
Future work includes updating cross-section in the 3-region and 19-plate models to the newest set, ENDF-VIII. This will make the materials in both models match. This change will show if there was any disagreement due to cross-sections. In addition, the materials in the 3-region model will need to be updated to completely match the 19-plate model. An investigation and resolution into the cause of the greater error seen inside the fuel ring is needed. After cross-sections are updated, it will be time to validate the model. There is plentiful experiment data to use as well as 2022 CIC data.

References

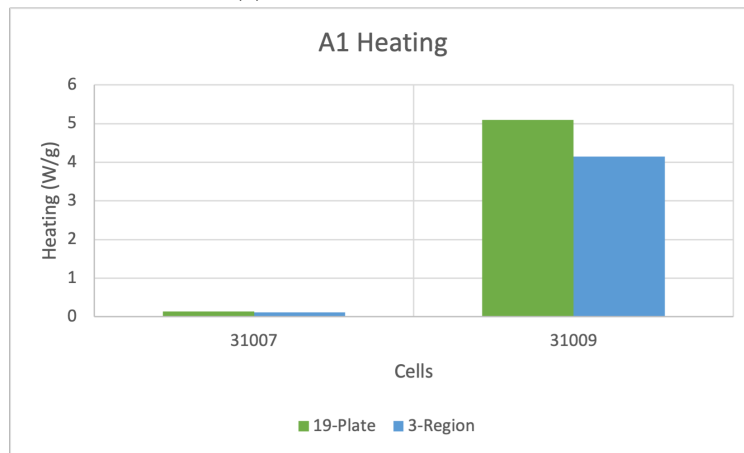
- [1] AIAA (1998) Guide for the verification and validation of computational fluid dynamics simulations. *American Institute of Aeronautics and Astronautics, AIAA-G-077-1998*, Reston, Va.
- [2] ASME (2006). Guide for verification and validation in computational solid mechanics. *American Society of Mechanical Engineers, ASME Standard V&V10-2006*, New York, NY.
- [3] (2006). ATR base model report. Idaho National Laboratory.
- [4] Chang, G. S. & Lillo, M. A. (2003). Confirmatory neutronics Analysis of the AGR-1 experiment irradiated in ATR B-10 position. Idaho National Laboratory.
- [5] Chang, G. S. & Lillo, M. A. (2017). Cycle 140A physics evaluations of AGR-1 experiment in ATR B-10 position. Idaho National Laboratory.
- [6] *DoD Directive No. 5000.59: Modeling and Simulation (M&S) Management.*
- [7] (1991). *IEEE Standard Glossary of Software Engineering Terminology*. IEEE std 610.12-1990, New York.
- [8] (2017). *Experiment Design and Analysis Guide-Neutronics and Physics*. INL gde-594, Idaho.
- [9] Kim, S. S., & Schnitzler B. G. (2005). ADVANCED TEST REACTOR: SERPENTINE ARRANGEMENT OF HIGHLY ENRICHED WATER-MODERATED URANIUM-ALUMINIDE FUEL PLATES REFLECTED BY BERYLLIUM, Department of Energy.
- [10] Parry, J. R., & Chang, G. S. (2010). Reactor physics analysis for the AGR-2 experiment irradiated in the ATR B-12 position. Idaho National Laboratory.
- [11] Peterson-Droogh, J. L. (2019). Physics analysis for the NSUF experiment MVP (Marmot Validation Plan). Idaho National Laboratory.
- [12] Nigg, D. W., & Steuhm K A. (2014). Advanced test reactor core modeling update project. Idaho National Laboratory.
- [13] Oberkampf, W. L., & Roy, C. J. (2010). *Verification and validation in scientific computing*, Cambridge University Press.
- [14] Schlesinger, S. (1979). Terminology for model credibility. *Simulation*.
- [15] Sterbentz, J. W. (2014). JMOCUP As-Run daily depletion calculation for the AGR-2 experiment in ATR B-12 position. Idaho National Laboratory.

- [16] Werner, C. J. (Ed.). (2018). MCNP - Los Alamos National Laboratory. User's Manual Code Version 6.2. Retrieved September 30, 2022, from https://mcnp.lanl.gov/pdf_files/la-ur-17-29981.pdf
- [17] X-5 Monte Carlo Team. (2003). MCNP^o - Los Alamos National Laboratory. MCNP — A General Monte CarloN-Particle Transport Code, Overview and Theory. **32**(3), 103-104.

A Tally Graphs



(a) Flux for the A1 position

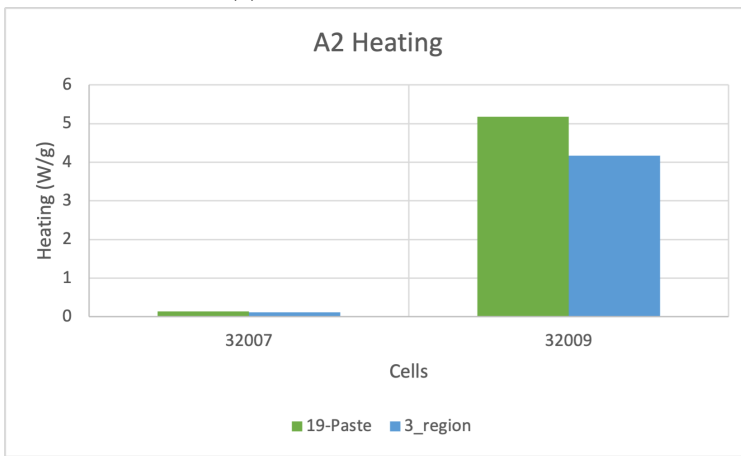


(b) Heat generation rates for the A1 position.

Figure 46: Flux and heat generation for the A1 position.

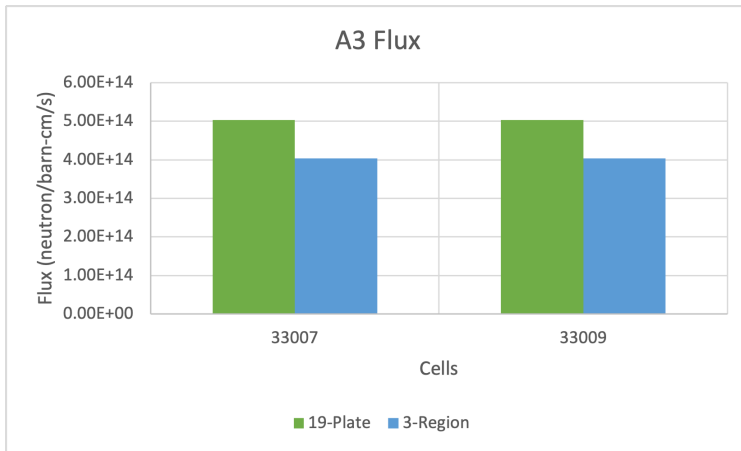


(a) Flux for the A2 position

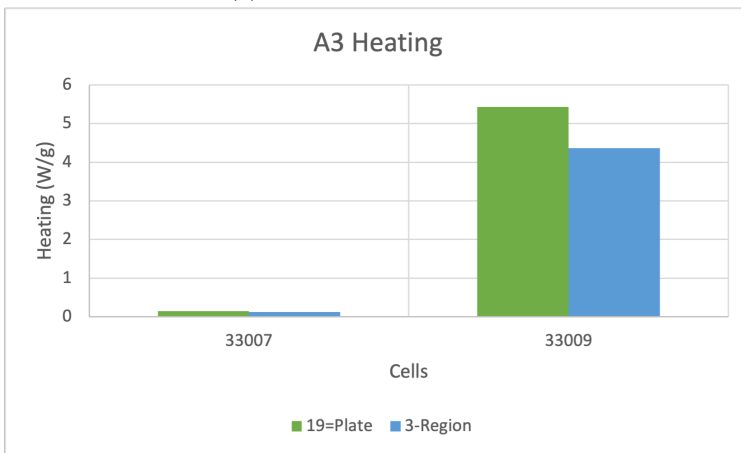


(b) Heat generation rates for the A2 position.

Figure 47: Flux and heat generation for the A2 position.

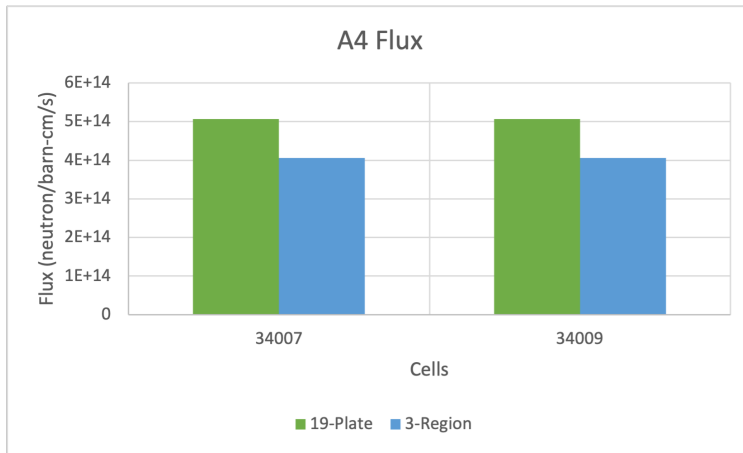


(a) Flux for the A3 position

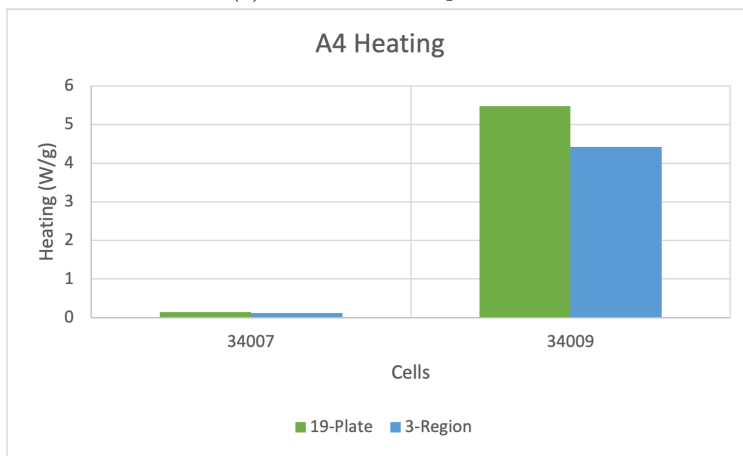


(b) Heat generation rates for the A3 position.

Figure 48: Flux and heat generation for the A3 position.

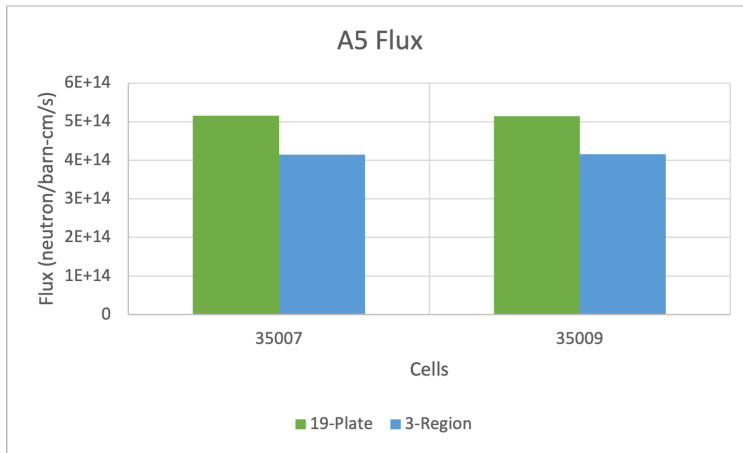


(a) Flux for the A4 position

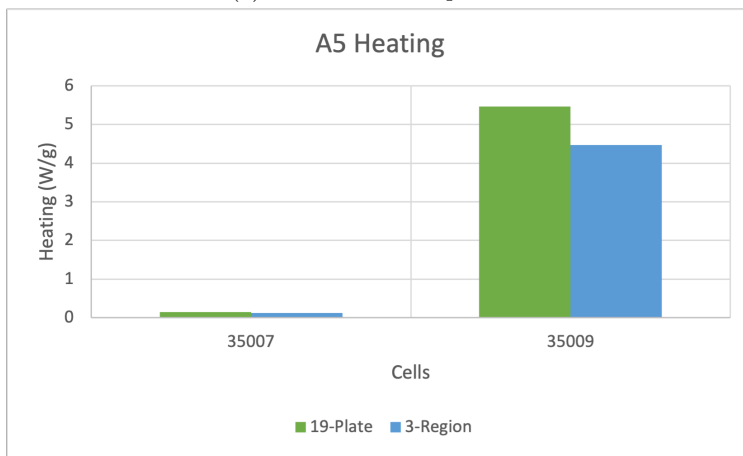


(b) Heat generation rates for the A4 position.

Figure 49: Flux and heat generation for the A4 position.

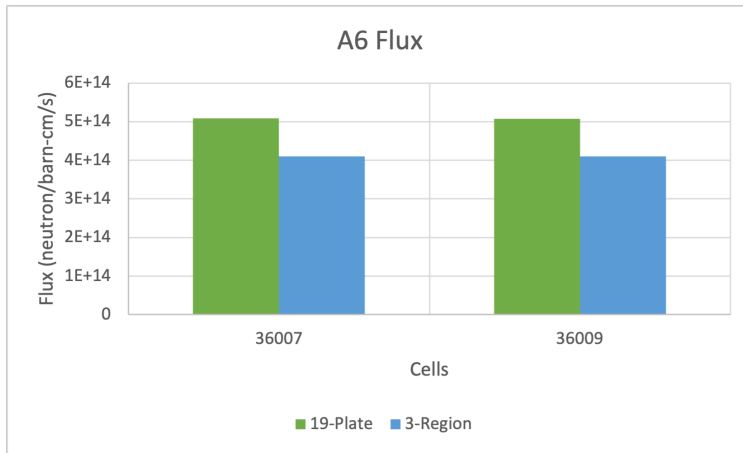


(a) Flux for the A5 position

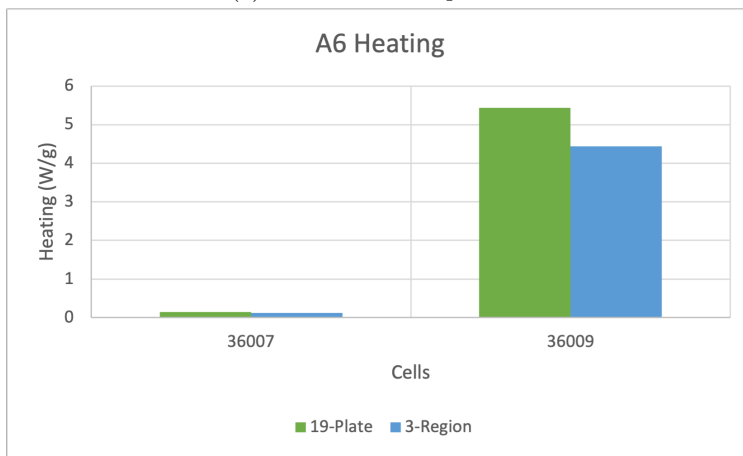


(b) Heat generation rates for the A5 position.

Figure 50: Flux and heat generation for the A5 position.

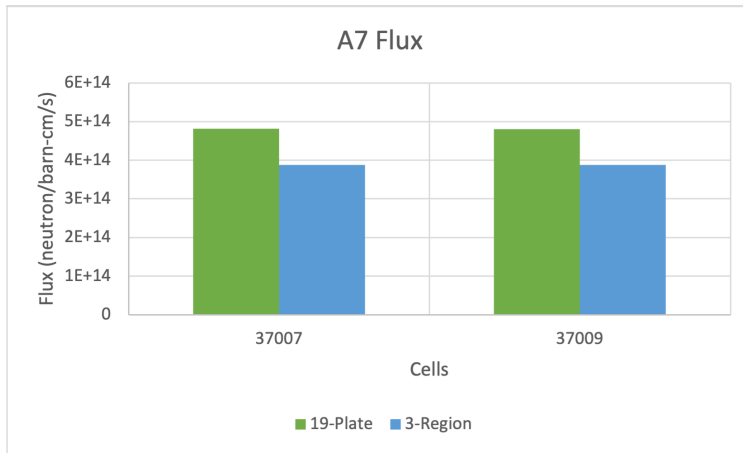


(a) Flux for the A6 position

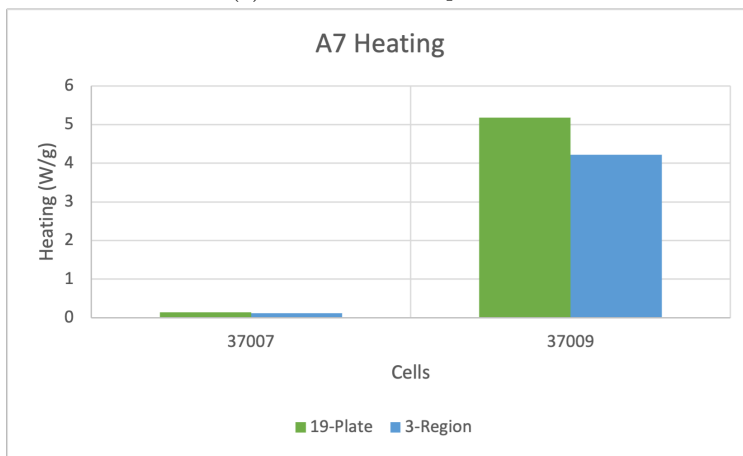


(b) Heat generation rates for the A6 position.

Figure 51: Flux and heat generation for the A6 position.

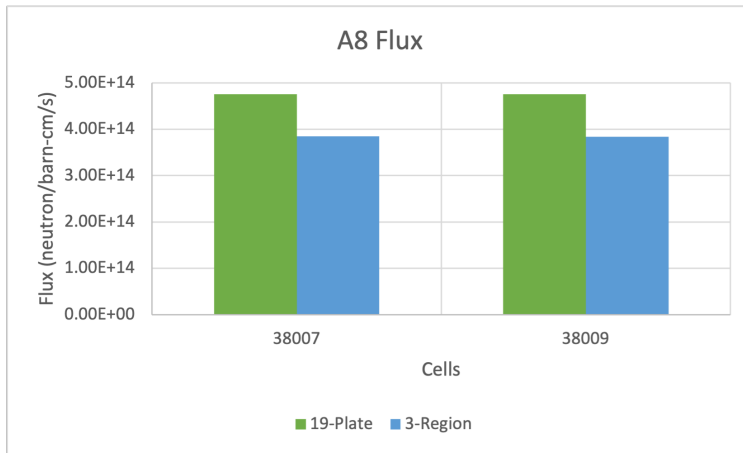


(a) Flux for the A7 position

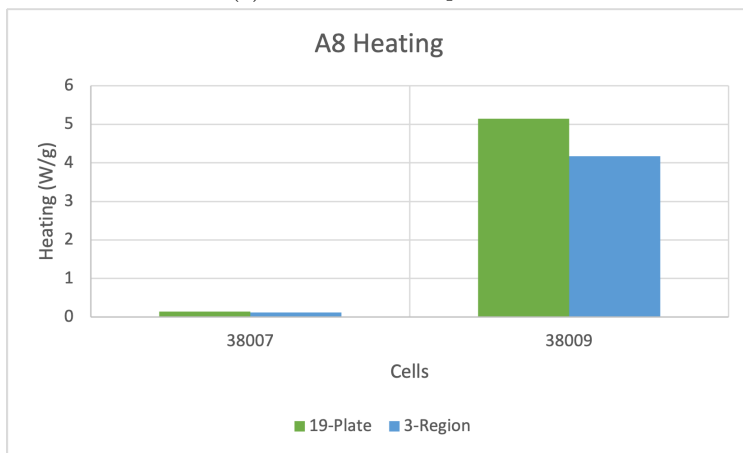


(b) Heat generation rates for the A7 position.

Figure 52: Flux and heat generation for the A7 position.

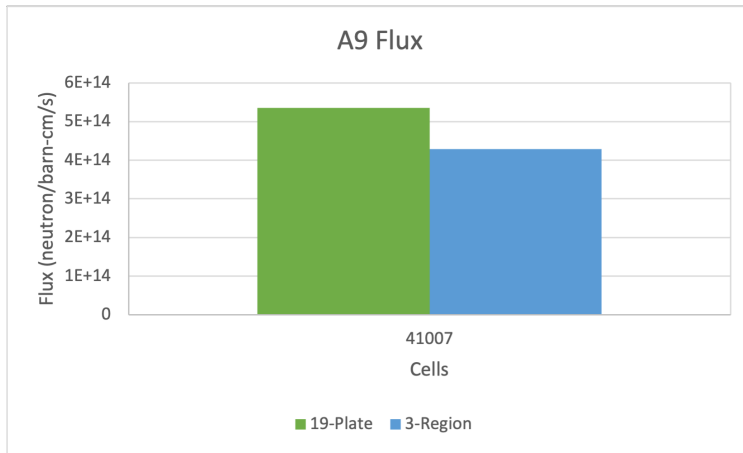


(a) Flux for the A8 position

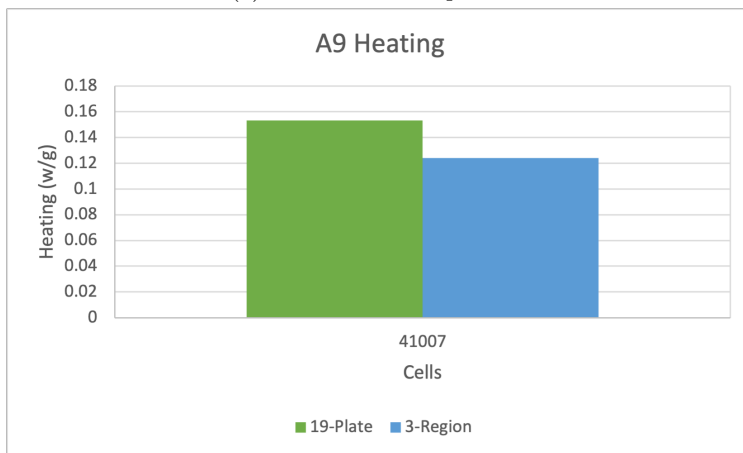


(b) Heat generation rates for the A8 position.

Figure 53: Flux and heat generation for the A8 position.

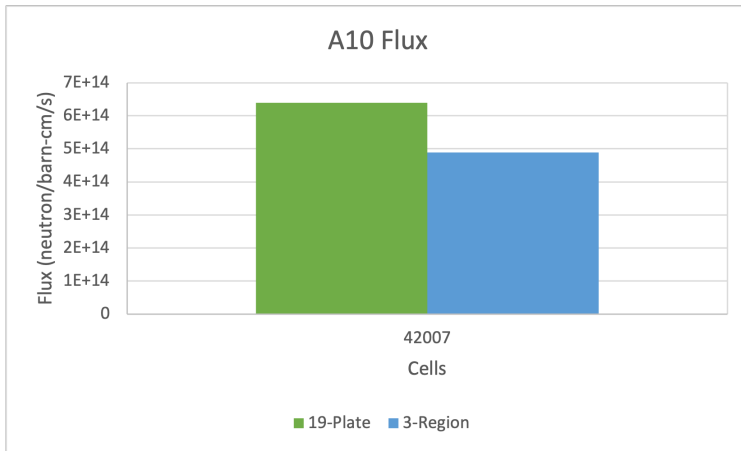


(a) Flux for the A9 position

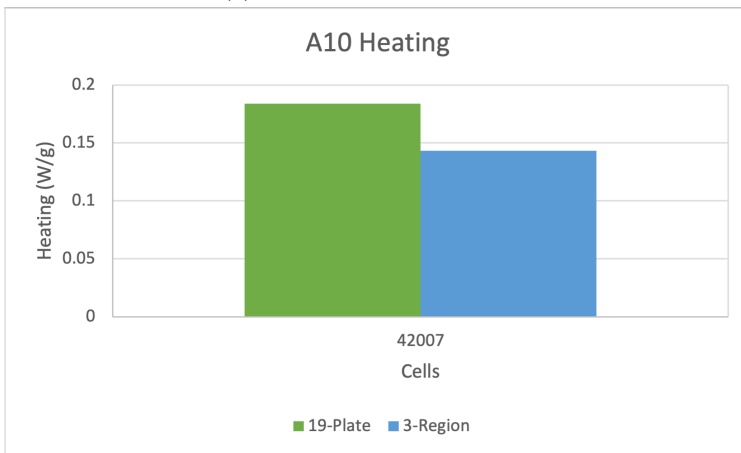


(b) Heat generation rates for the A9 position.

Figure 54: Flux and heat generation for the A9 position.

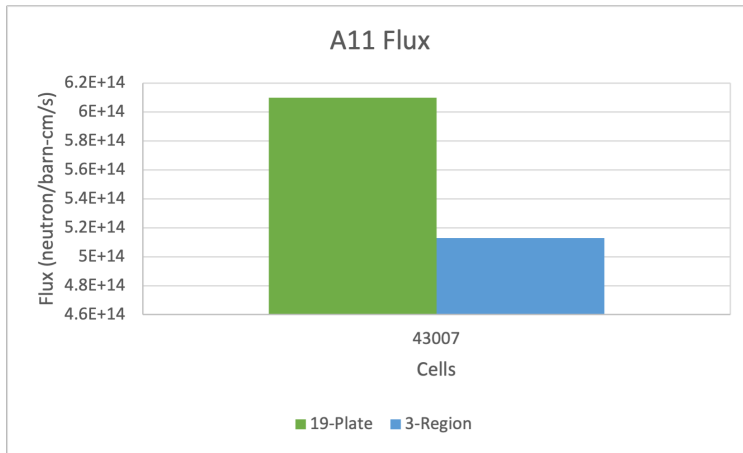


(a) Flux for the A10 position

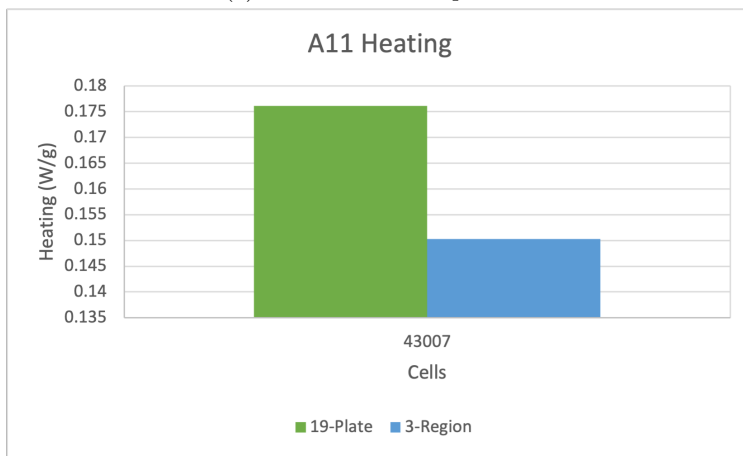


(b) Heat generation rates for the A10 position.

Figure 55: Flux and heat generation for the A10 position.

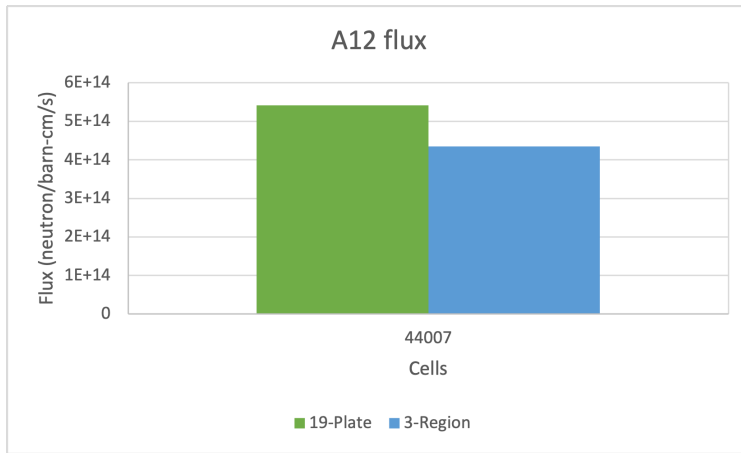


(a) Flux for the A11 position

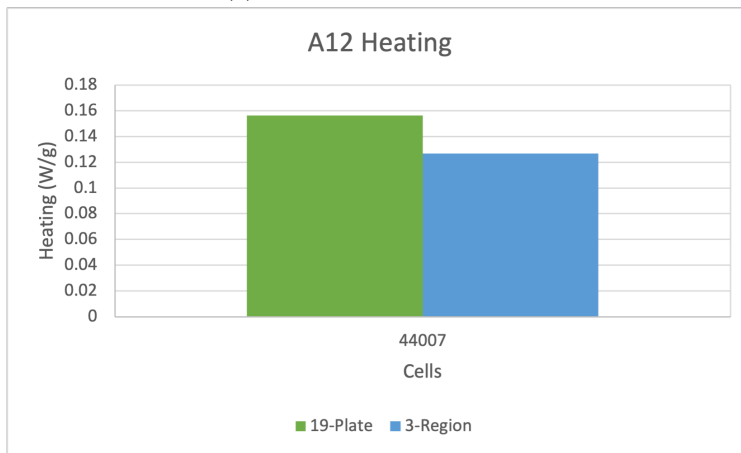


(b) Heat generation rates for the A11 position.

Figure 56: Flux and heat generation for the A11 position.

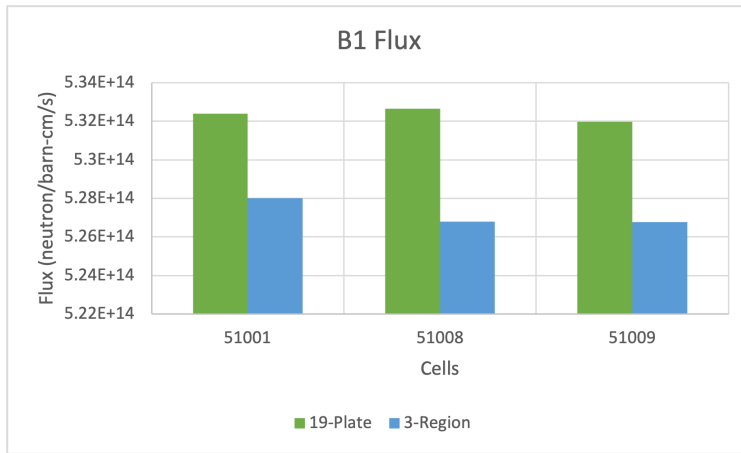


(a) Flux for the A12 position

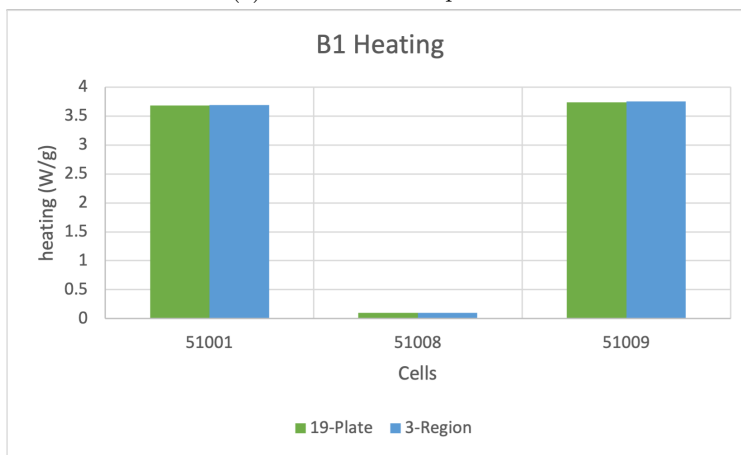


(b) Heat generation rates for the A12 position.

Figure 57: Flux and heat generation for the A12 position.

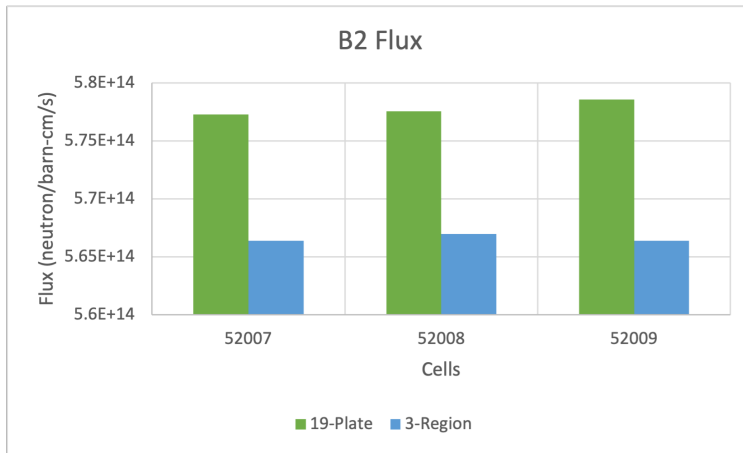


(a) Flux for the B1 position

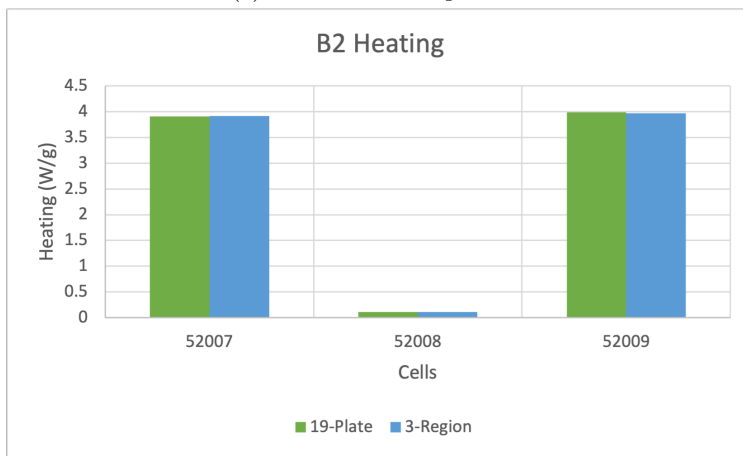


(b) Heat generation rates for the B1 position.

Figure 58: Flux and heat generation for the B1 position.

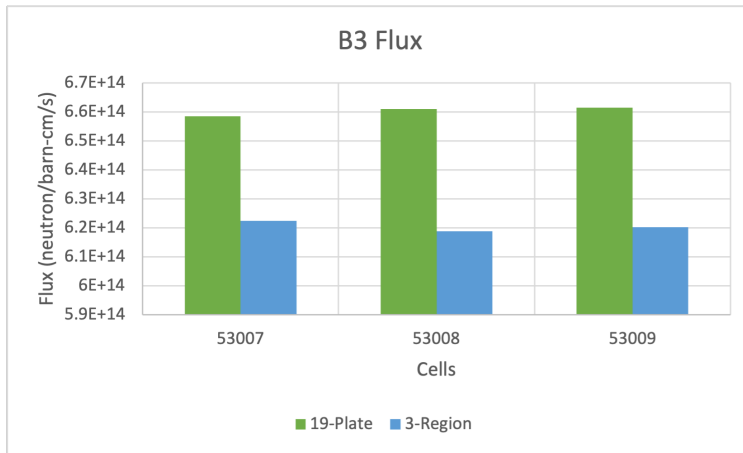


(a) Flux for the B2 position

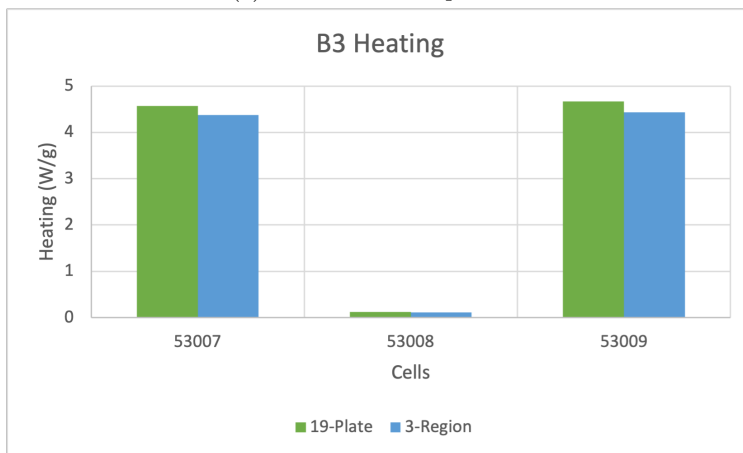


(b) Heat generation rates for the B2 position.

Figure 59: Flux and heat generation for the B2 position.

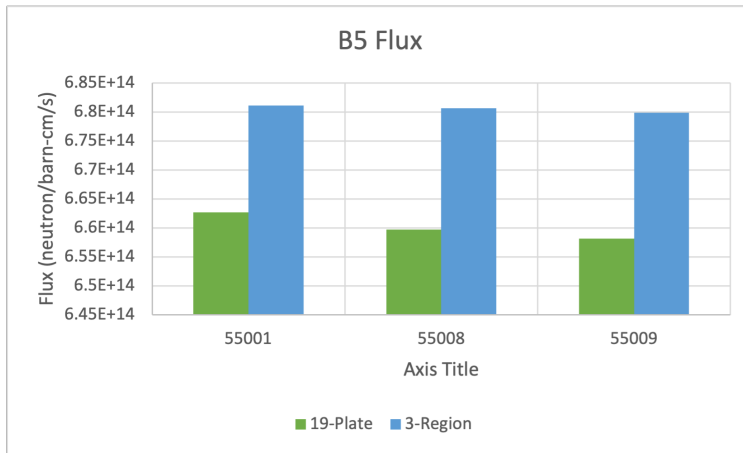


(a) Flux for the B3 position

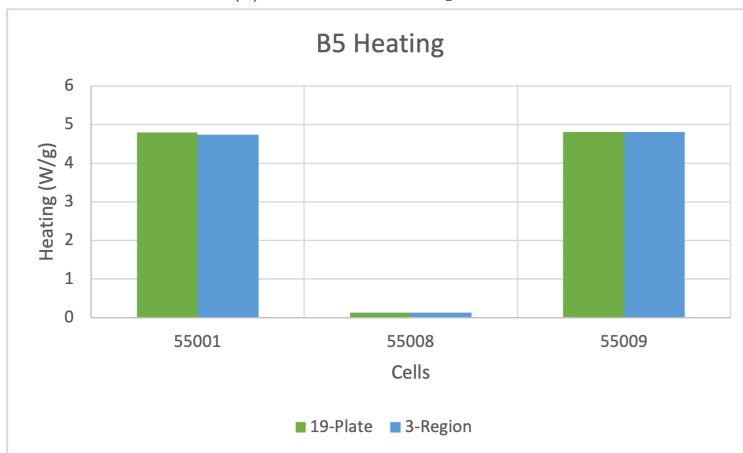


(b) Heat generation rates for the B3 position.

Figure 60: Flux and heat generation for the B3 position.

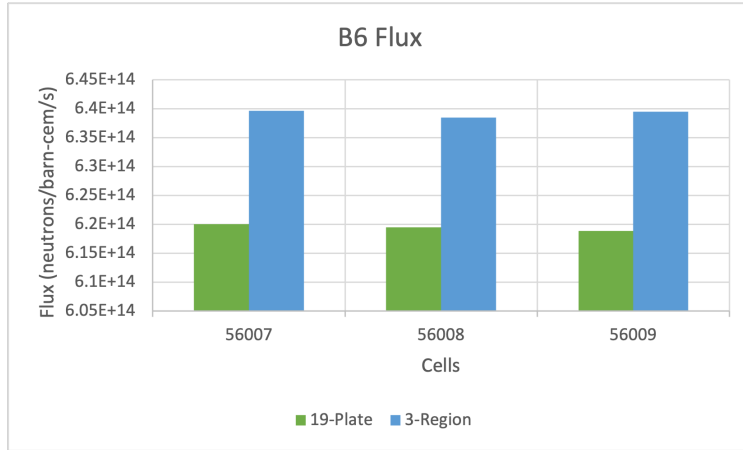


(a) Flux for the B5 position

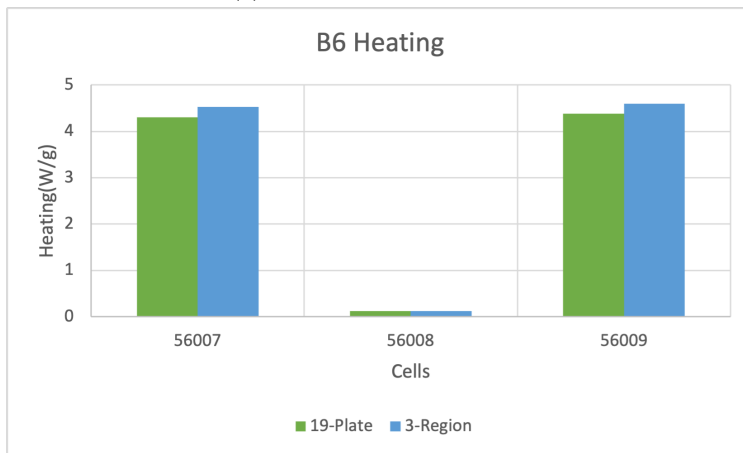


(b) Heat generation rates for the B5 position.

Figure 61: Flux and heat generation for the B5 position.

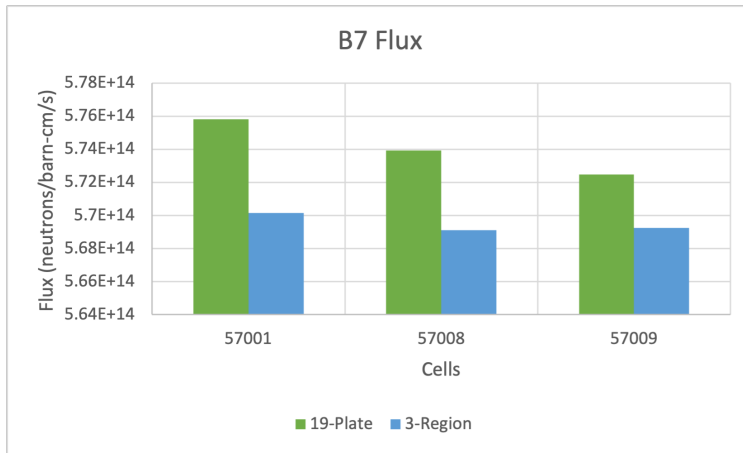


(a) Flux for the B6 position

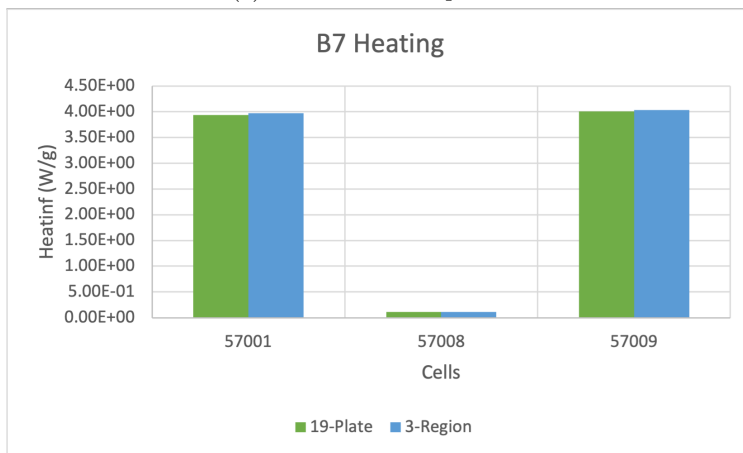


(b) Heat generation rates for the B6 position.

Figure 62: Flux and heat generation for the B6 position.

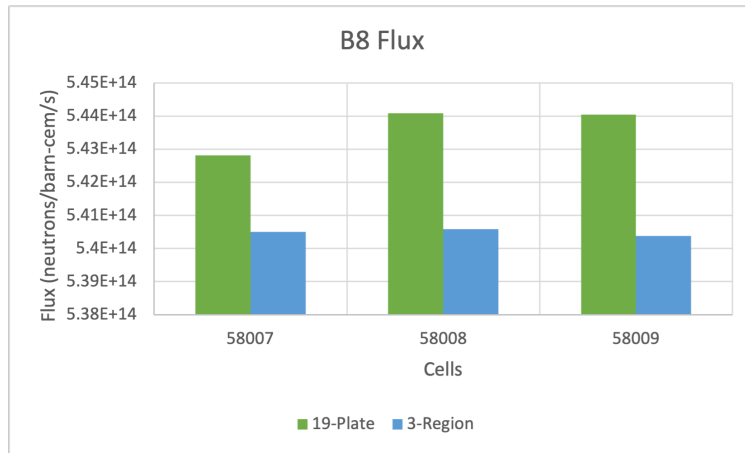


(a) Flux for the B7 position

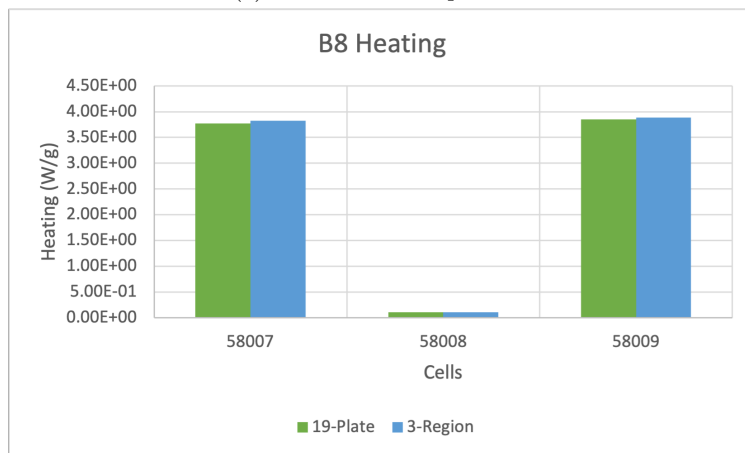


(b) Heat generation rates for the B7 position.

Figure 63: Flux and heat generation for the B7 position.

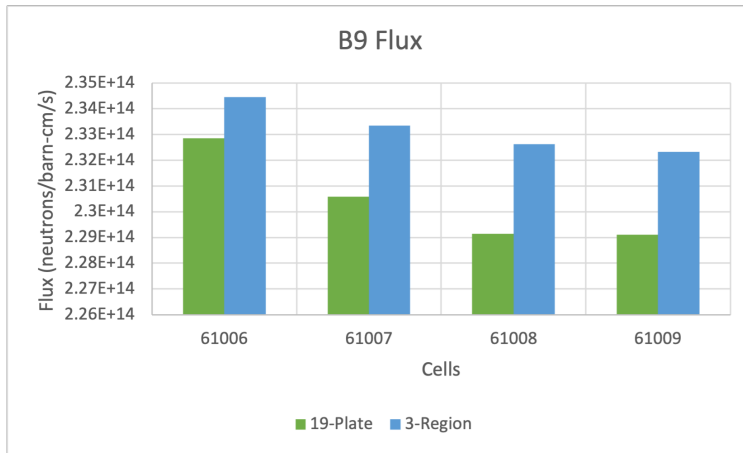


(a) Flux for the B8 position

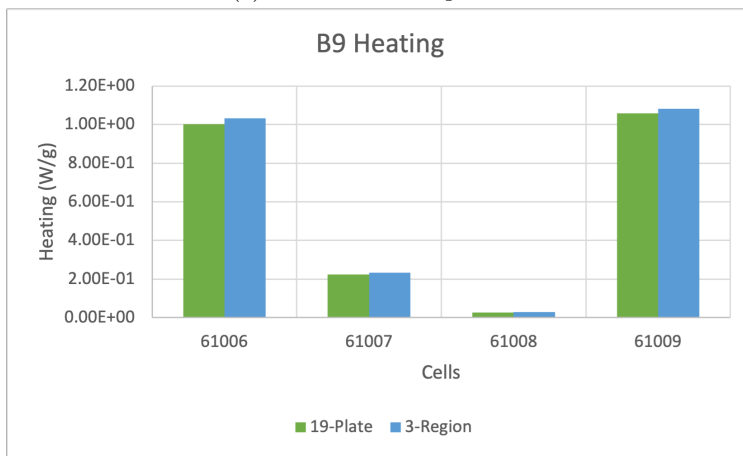


(b) Heat generation rates for the B8 position.

Figure 64: Flux and heat generation for the B8 position.

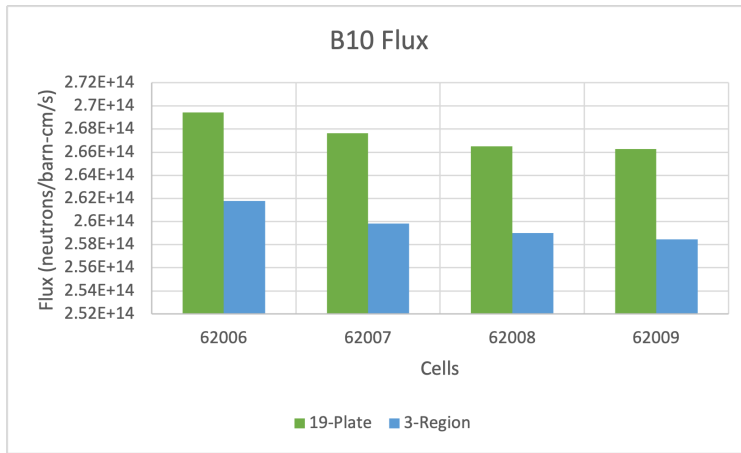


(a) Flux for the B9 position

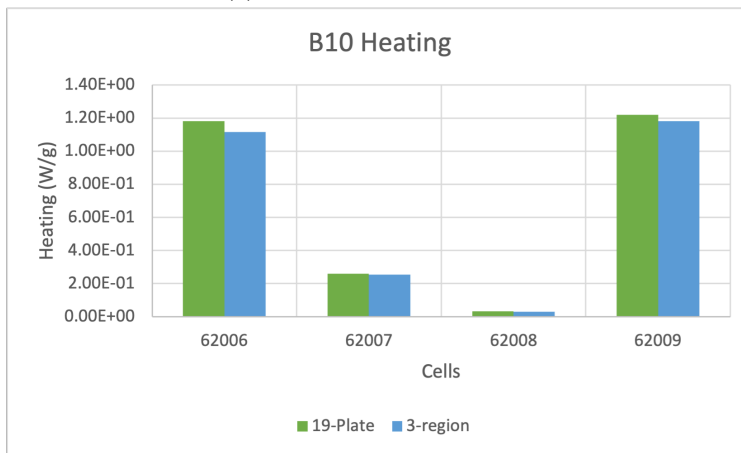


(b) Heat generation rates for the B9 position.

Figure 65: Flux and heat generation for the B9 position.

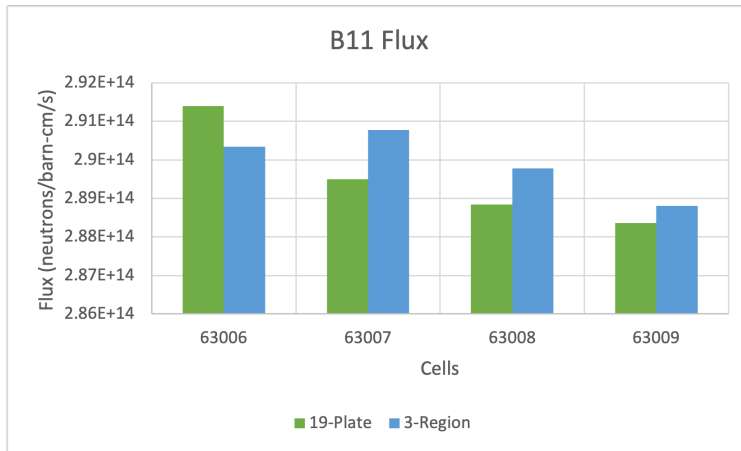


(a) Flux for the B10 position

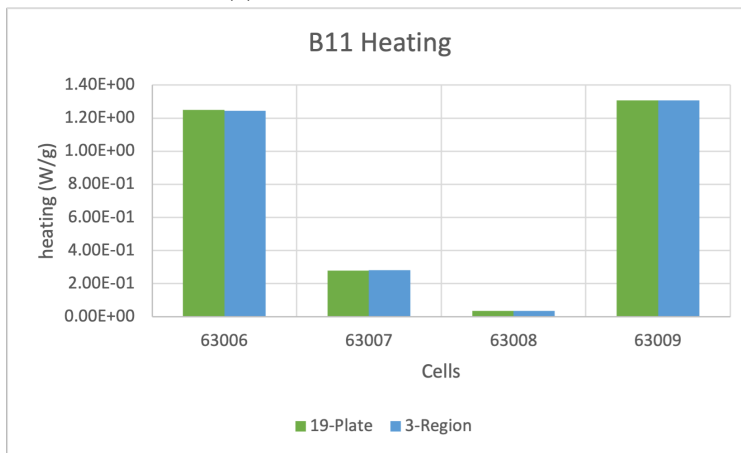


(b) Heat generation rates for the B10 position.

Figure 66: Flux and heat generation for the B10 position.

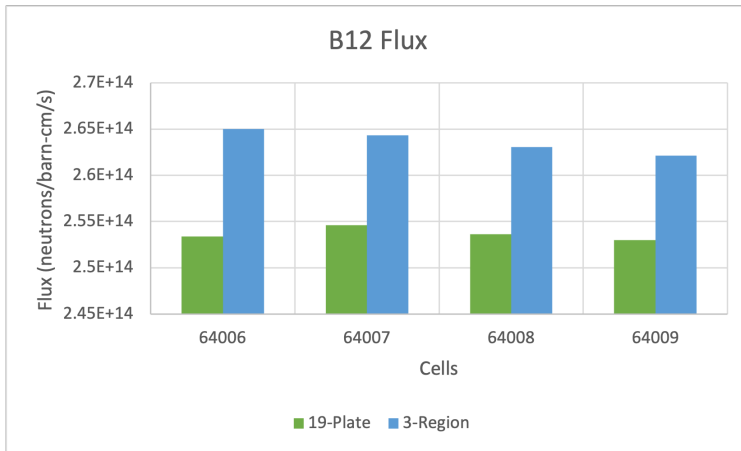


(a) Flux for the B11 position

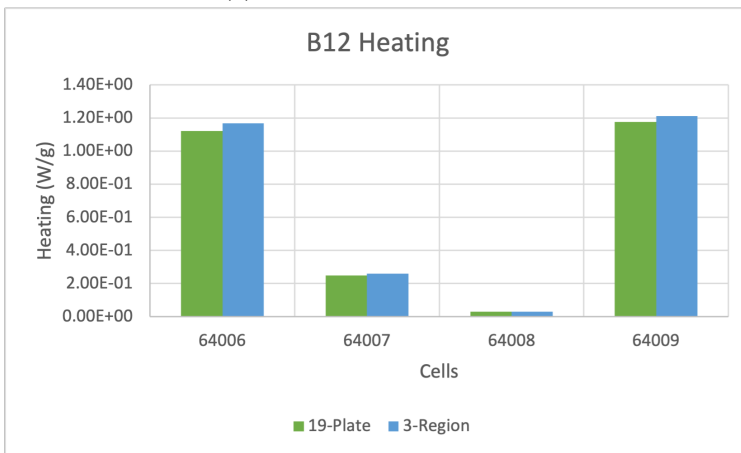


(b) Heat generation rates for the B11 position.

Figure 67: Flux and heat generation for the B11 position.

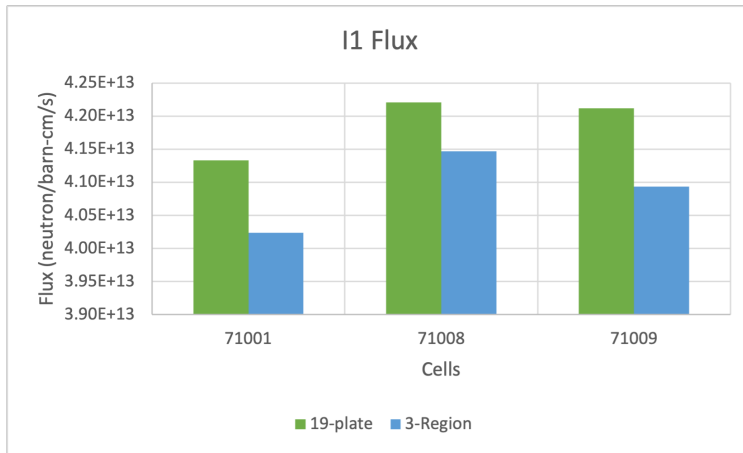


(a) Flux for the B12 position

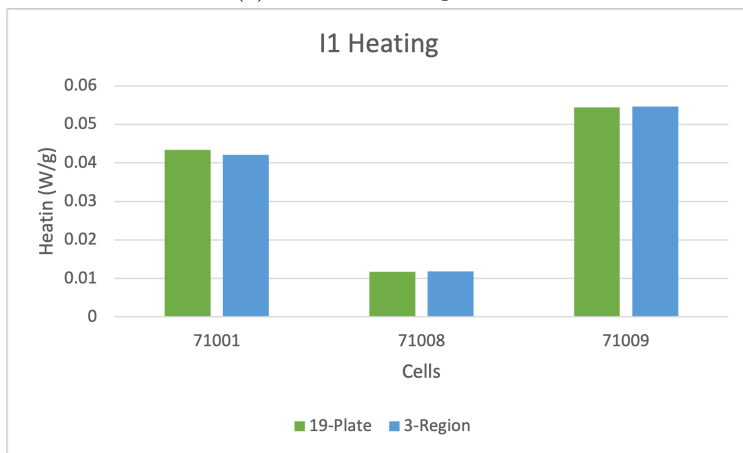


(b) Heat generation rates for the B12 position.

Figure 68: Flux and heat generation for the B12 position.

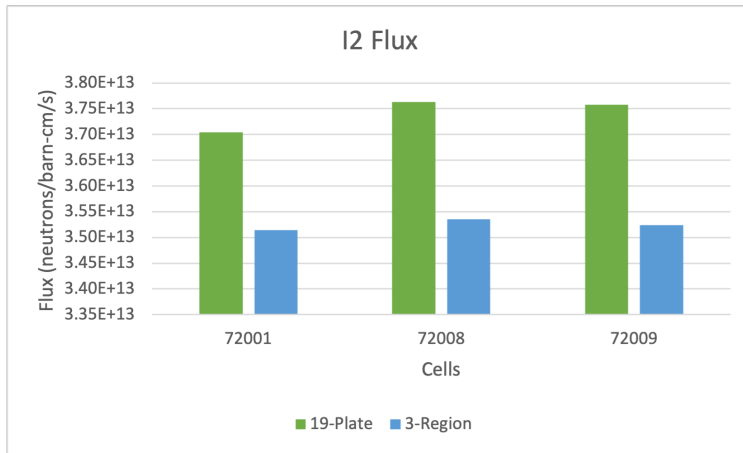


(a) Flux for the I1 position

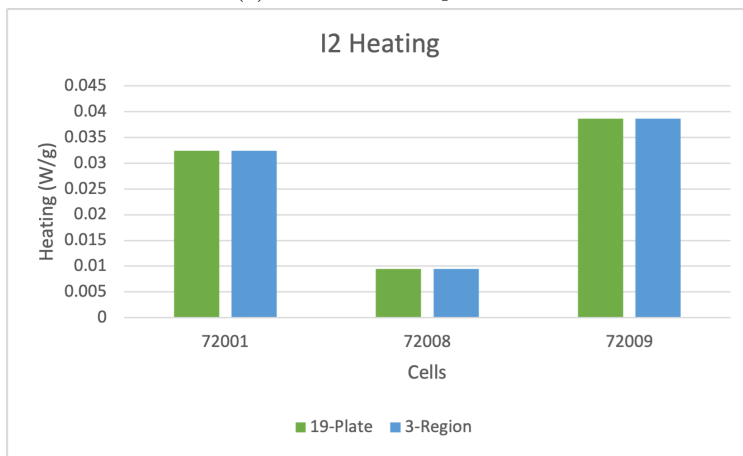


(b) Heat generation rates for the I1 position.

Figure 69: Flux and heat generation for the I1 position.

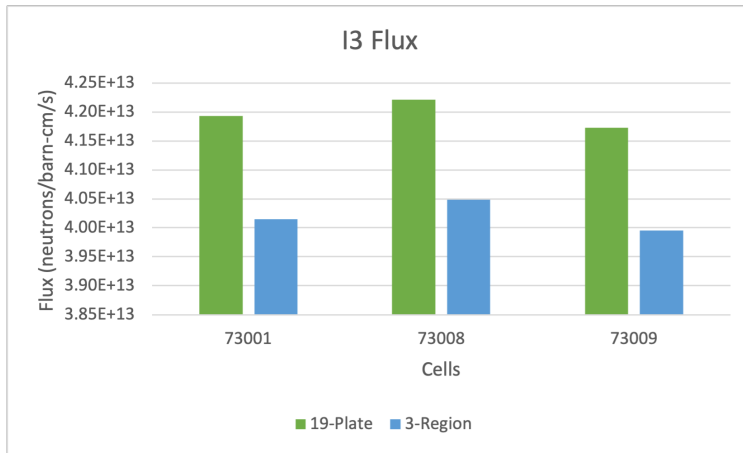


(a) Flux for the I2 position

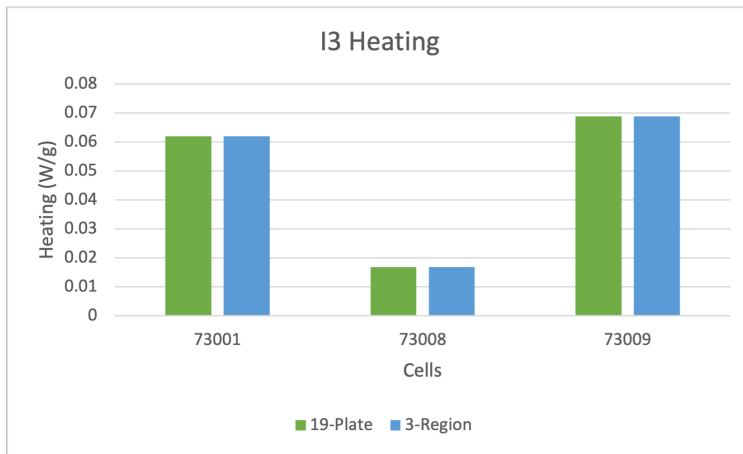


(b) Heat generation rates for the I2 position.

Figure 70: Flux and heat generation for the I2 position.

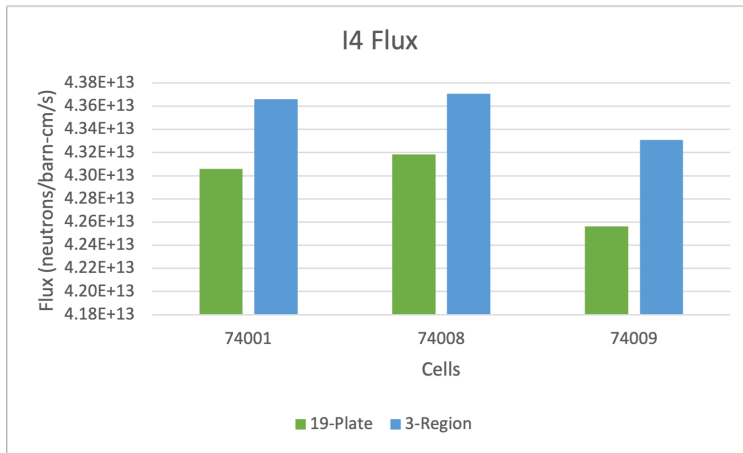


(a) Flux for the I3 position

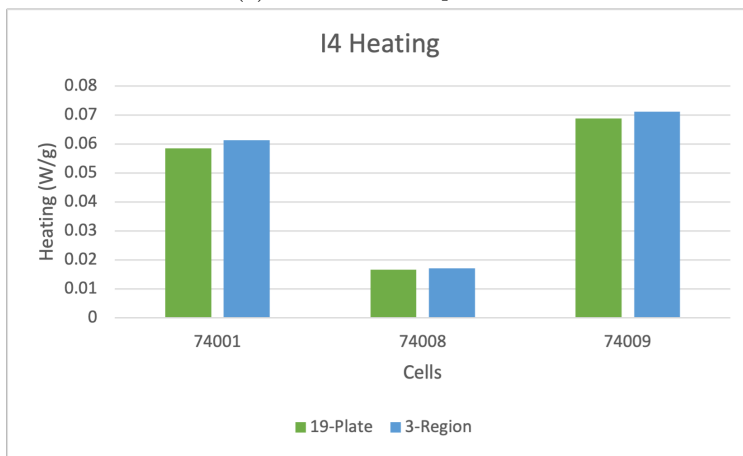


(b) Heat generation rates for the I3 position.

Figure 71: Flux and heat generation for the I3 position.

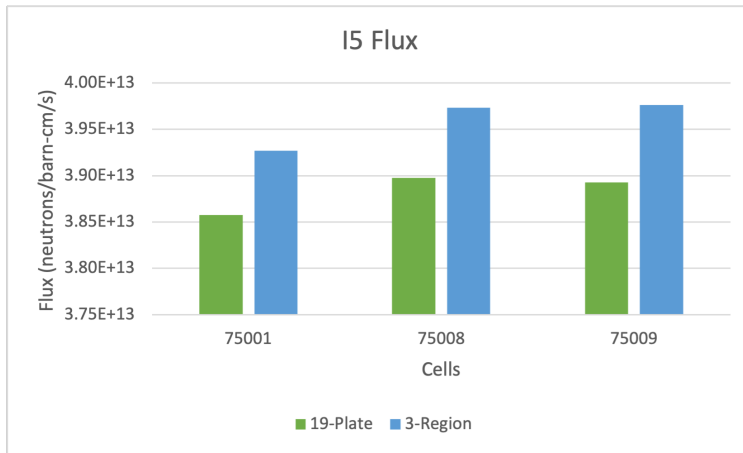


(a) Flux for the I4 position

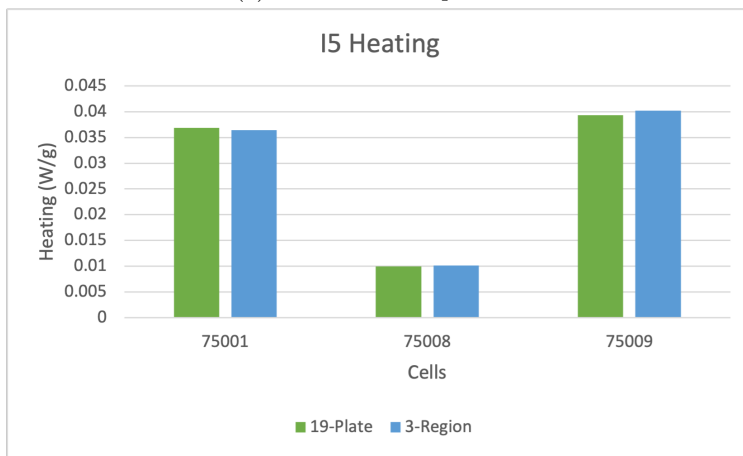


(b) Heat generation rates for the I4 position.

Figure 72: Flux and heat generation for the I4 position.

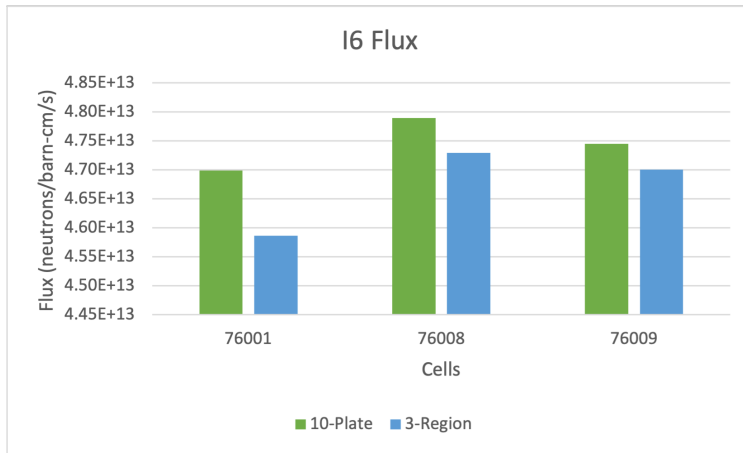


(a) Flux for the I5 position

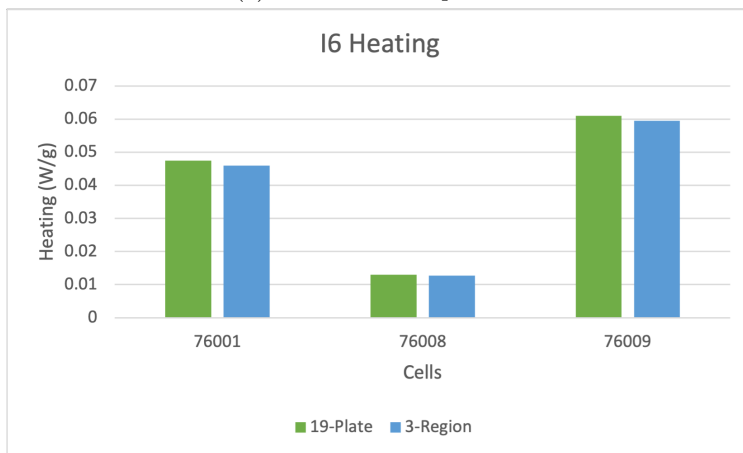


(b) Heat generation rates for the I5 position.

Figure 73: Flux and heat generation for the I5 position.

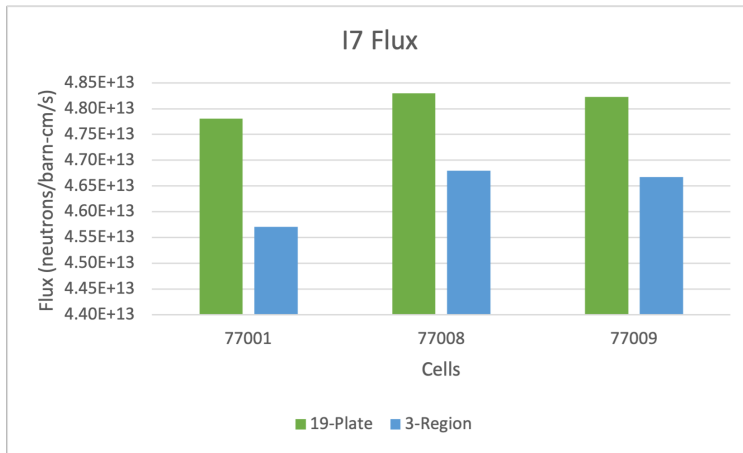


(a) Flux for the I6 position

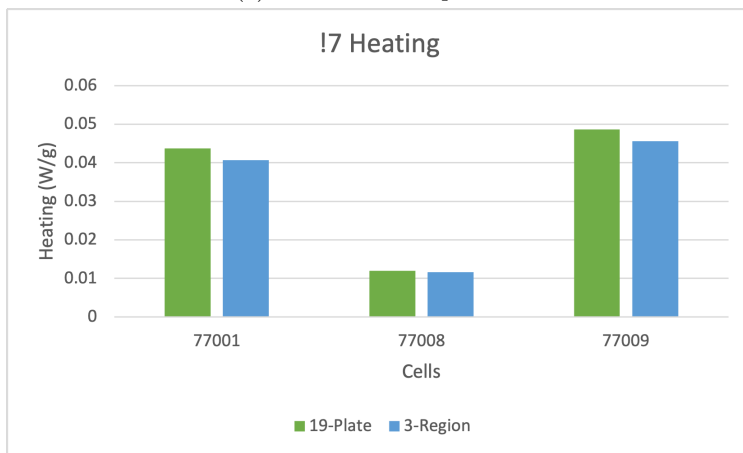


(b) Heat generation rates for the I6 position.

Figure 74: Flux and heat generation for the I6 position.

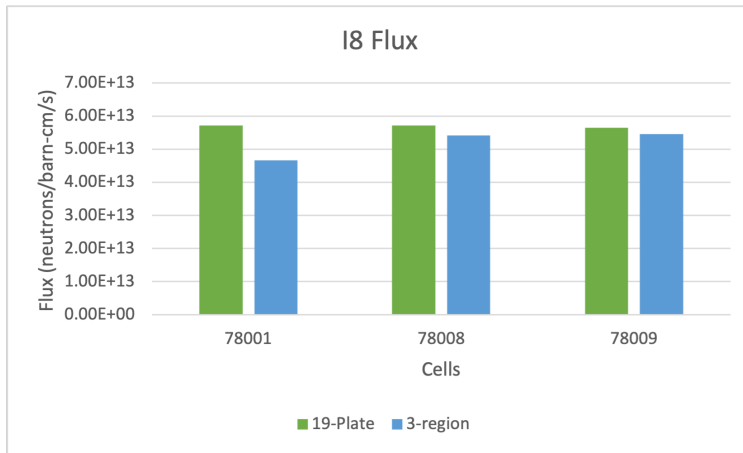


(a) Flux for the I7 position

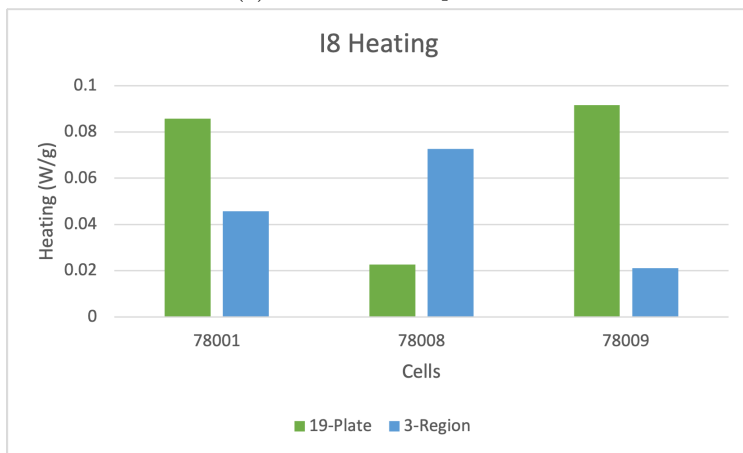


(b) Heat generation rates for the I7 position.

Figure 75: Flux and heat generation for the I7 position.

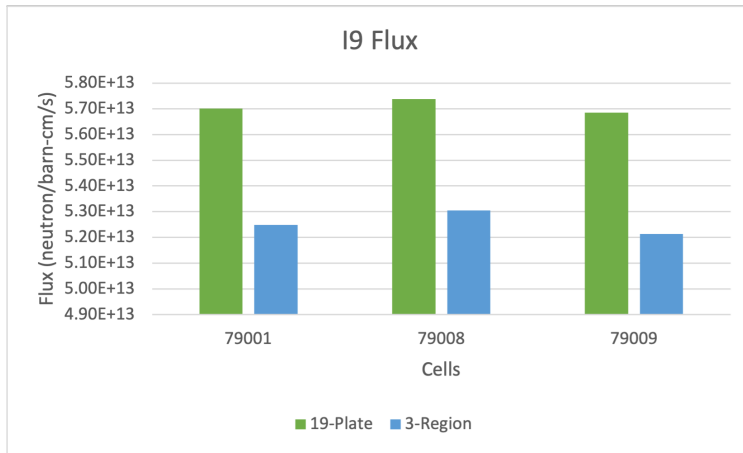


(a) Flux for the I8 position

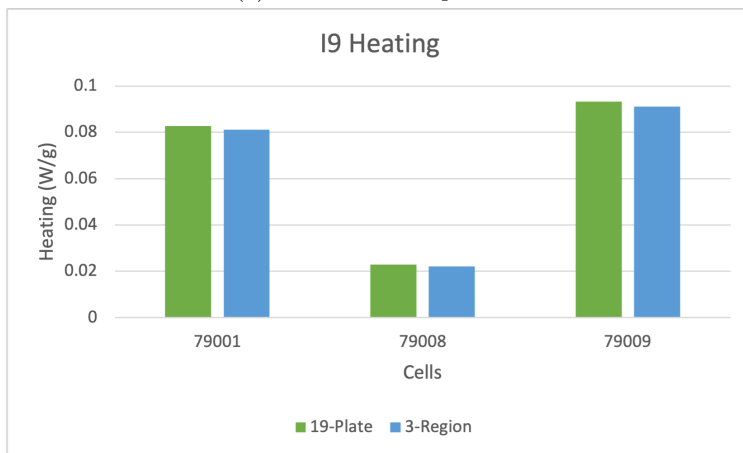


(b) Heat generation rates for the I8 position.

Figure 76: Flux and heat generation for the I8 position.

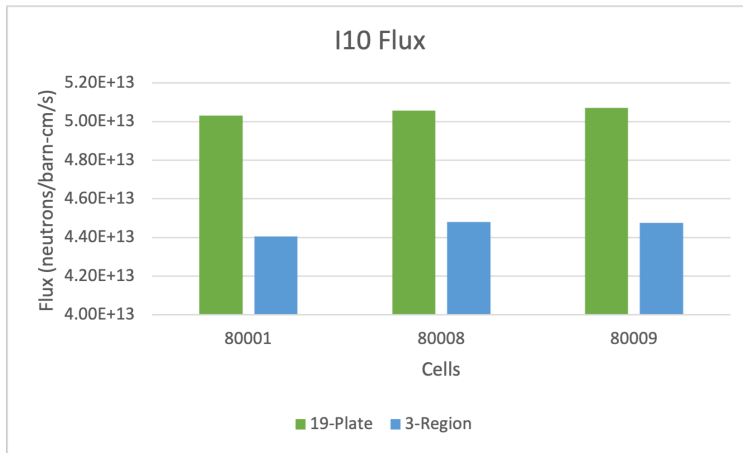


(a) Flux for the I9 position

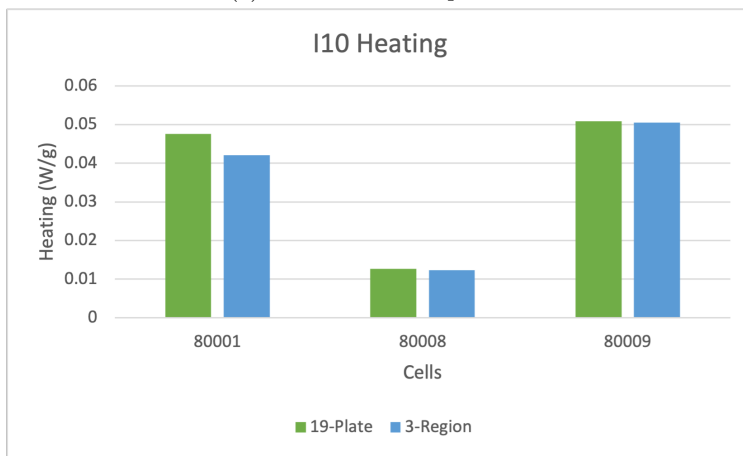


(b) Heat generation rates for the I9 position.

Figure 77: Flux and heat generation for the I9 position.

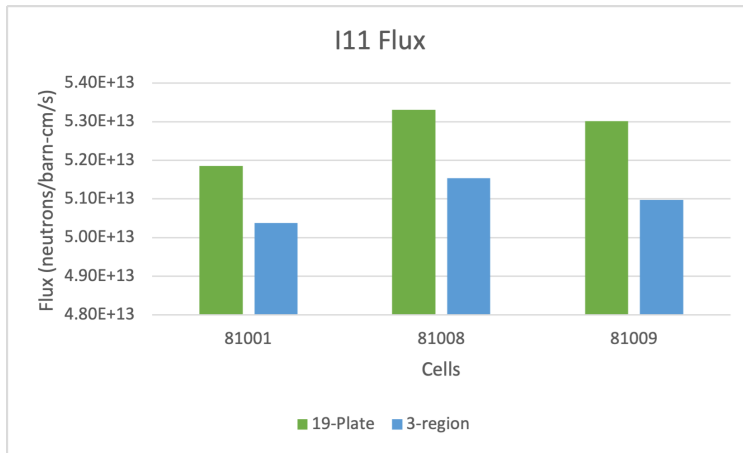


(a) Flux for the I10 position

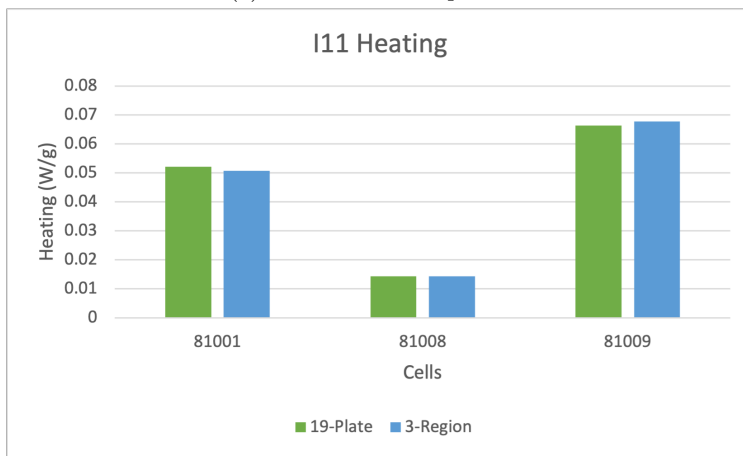


(b) Heat generation rates for the I10 position.

Figure 78: Flux and heat generation for the I10 position.

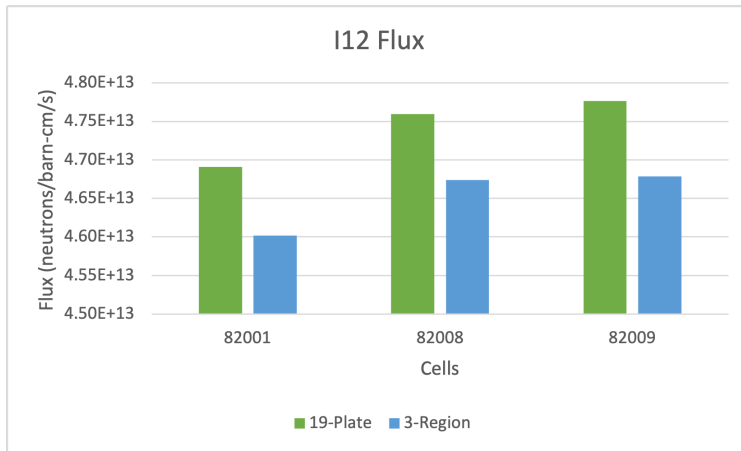


(a) Flux for the I11 position

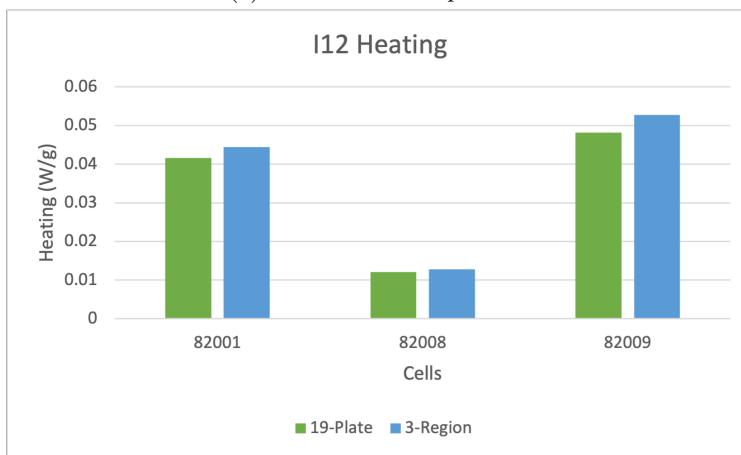


(b) Heat generation rates for the I11 position.

Figure 79: Flux and heat generation for the I11 position.

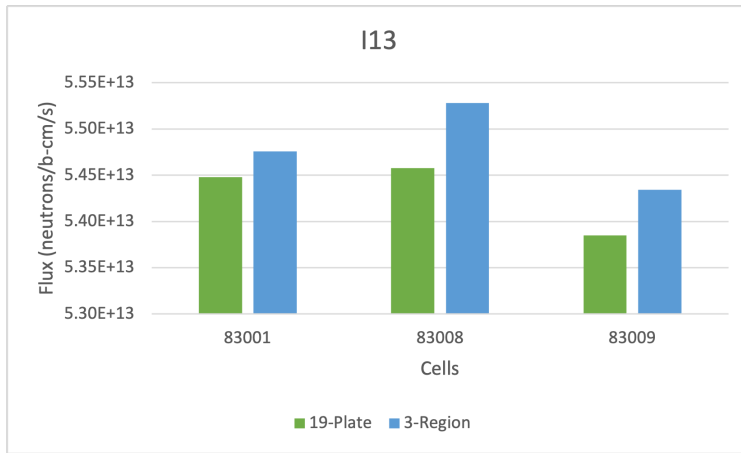


(a) Flux for the I12 position

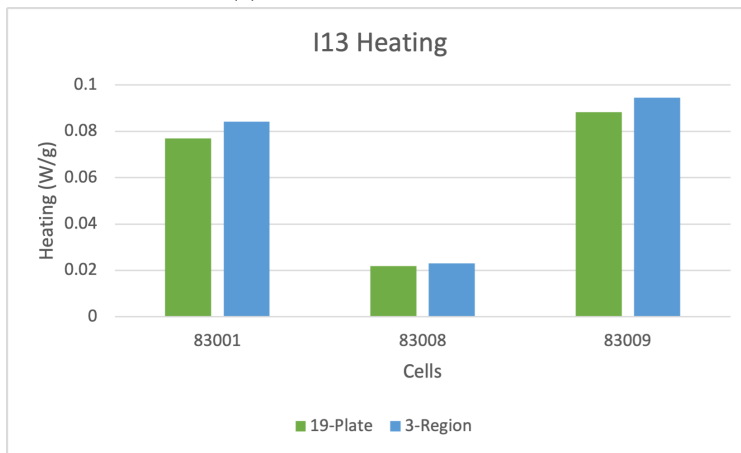


(b) Heat generation rates for the I12 position.

Figure 80: Flux and heat generation for the I12 position.

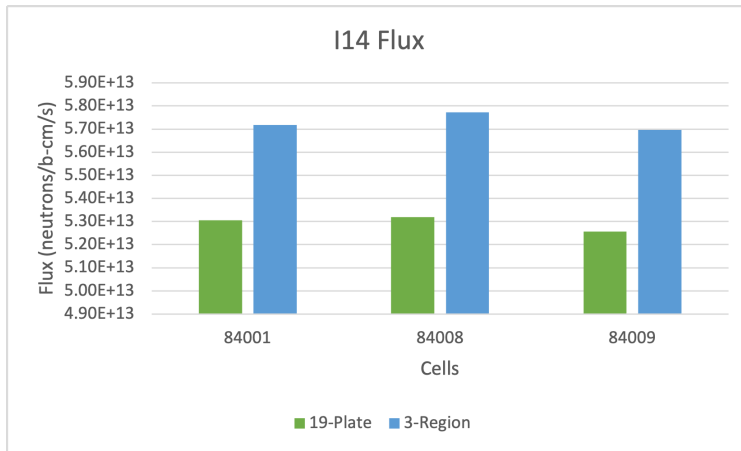


(a) Flux for the I13 position

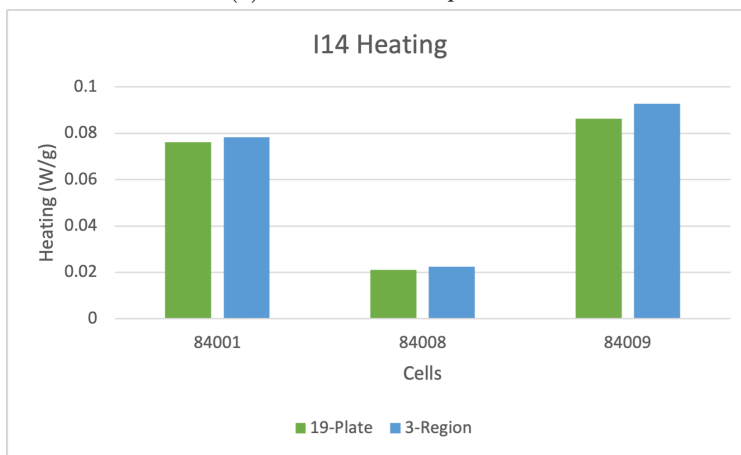


(b) Heat generation rates for the I13 position.

Figure 81: Flux and heat generation for the I13 position.

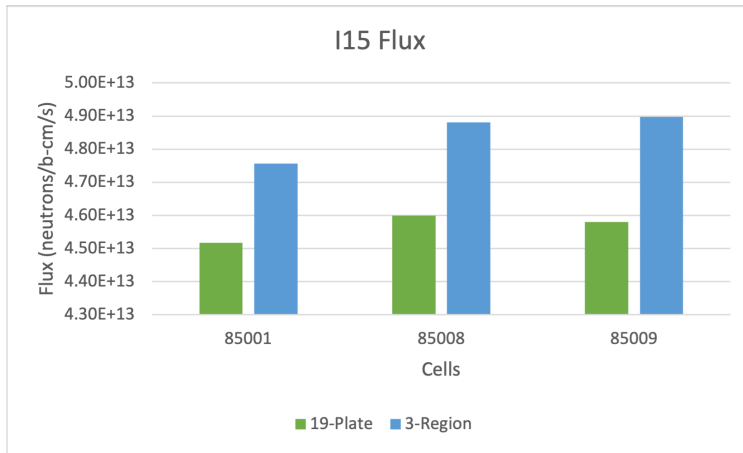


(a) Flux for the I14 position

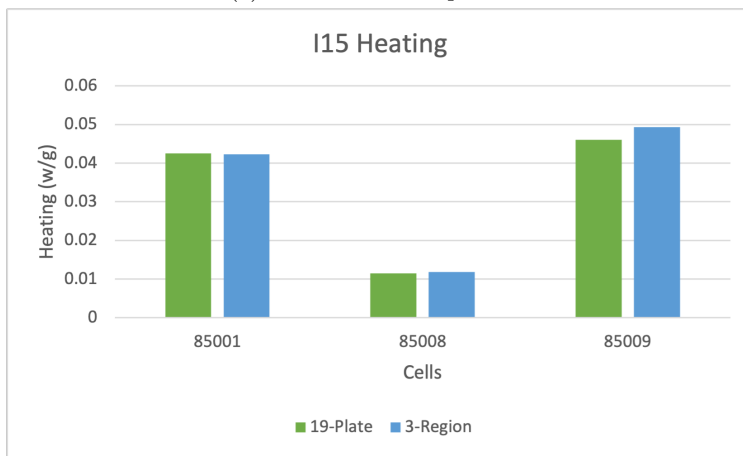


(b) Heat generation rates for the I14 position.

Figure 82: Flux and heat generation for the I14 position.

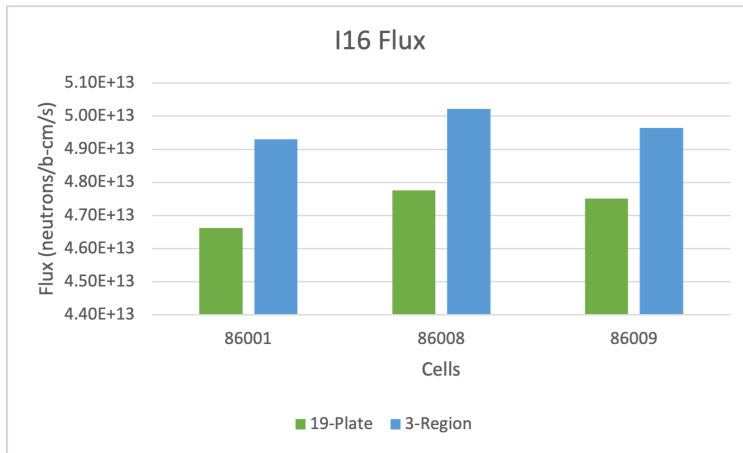


(a) Flux for the I15 position

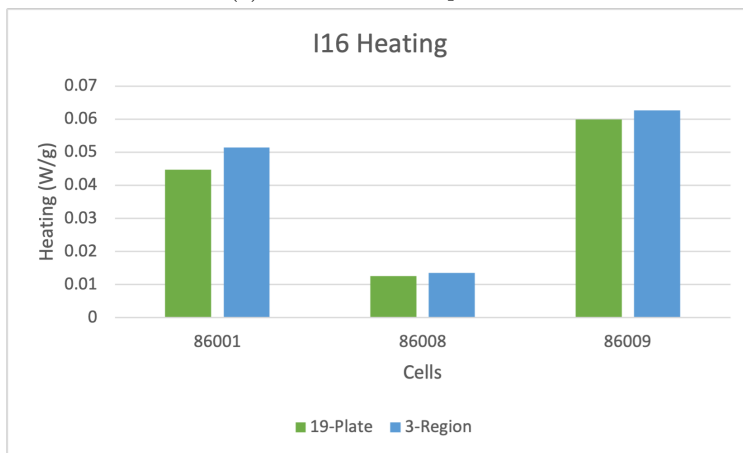


(b) Heat generation rates for the I15 position.

Figure 83: Flux and heat generation for the I15 position.

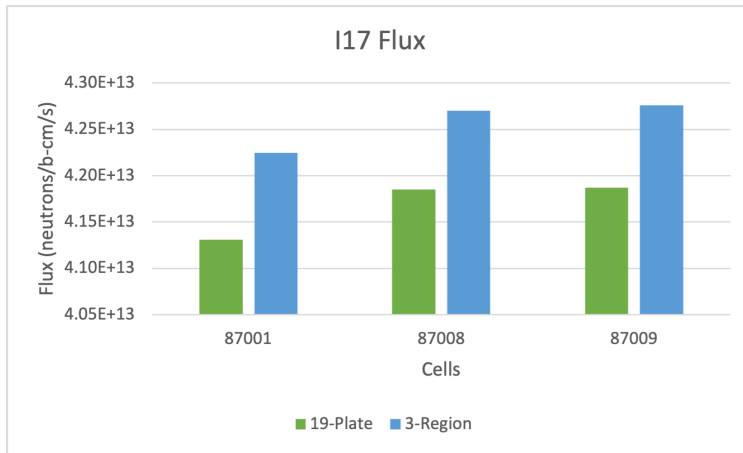


(a) Flux for the I16 position

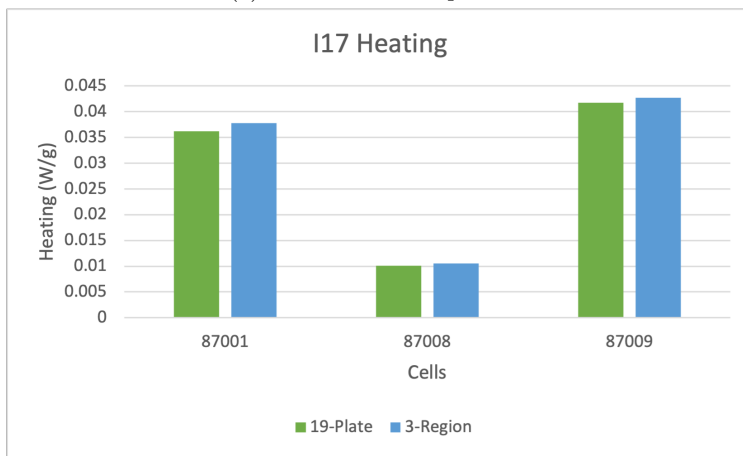


(b) Heat generation rates for the I16 position.

Figure 84: Flux and heat generation for the I16 position.

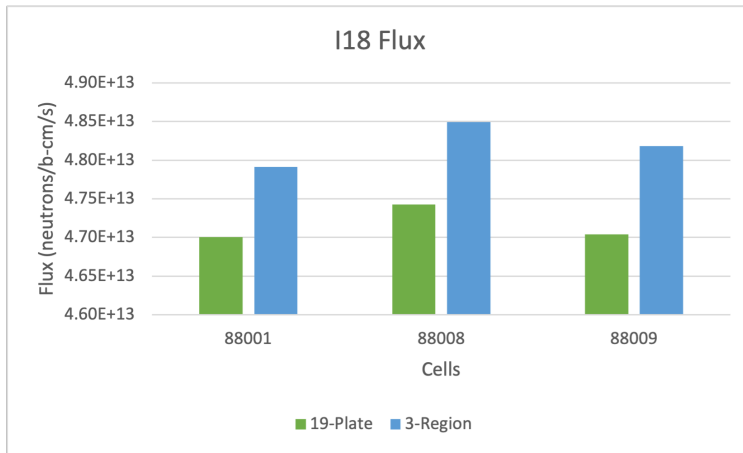


(a) Flux for the I17 position

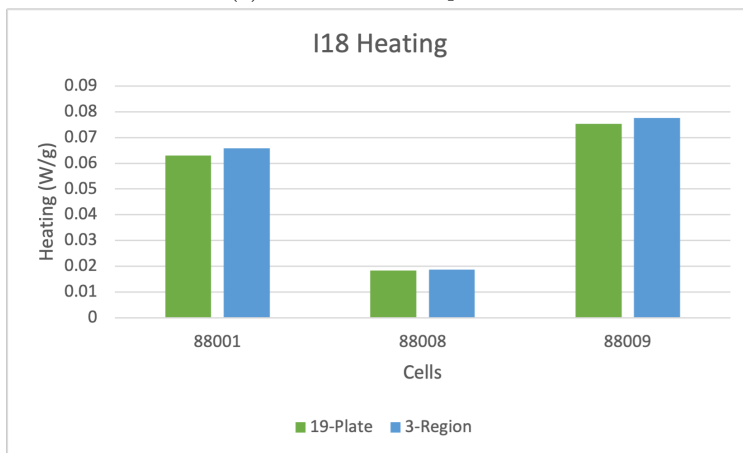


(b) Heat generation rates for the I17 position.

Figure 85: Flux and heat generation for the I17 position.

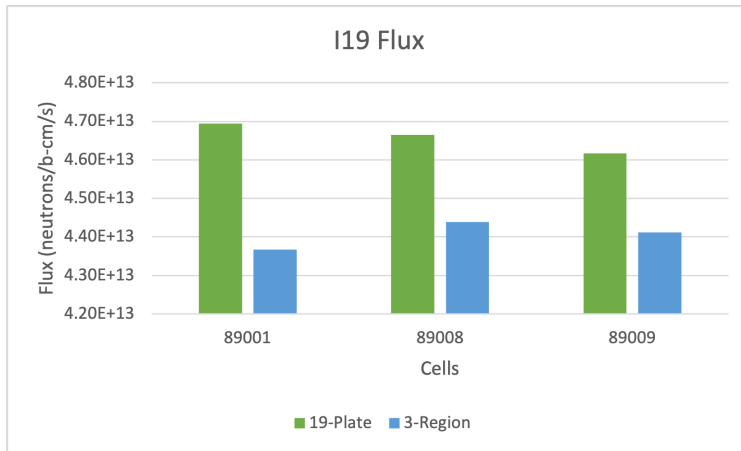


(a) Flux for the I18 position

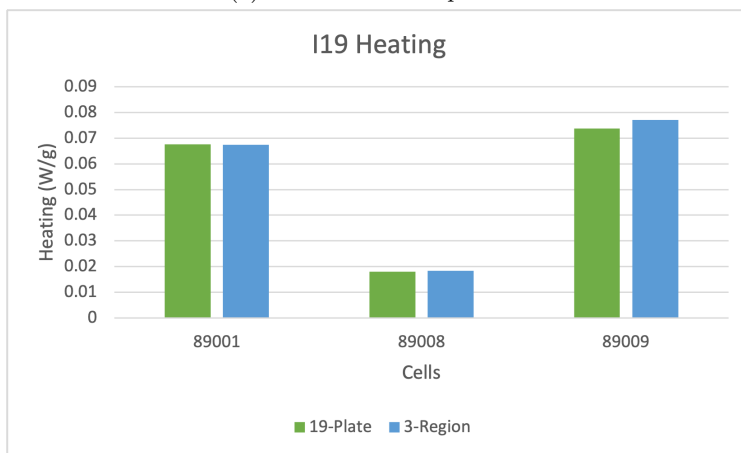


(b) Heat generation rates for the I18 position.

Figure 86: Flux and heat generation for the I18 position.

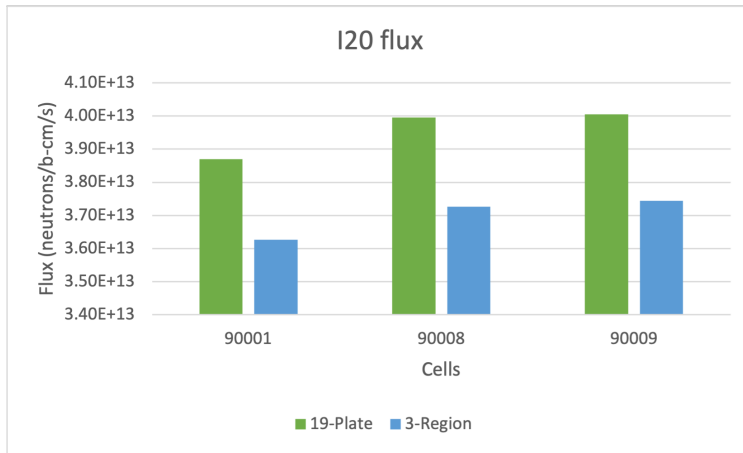


(a) Flux for the I19 position

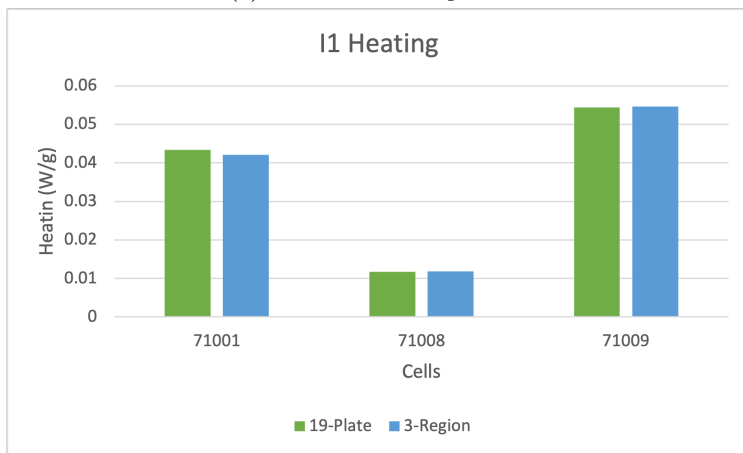


(b) Heat generation rates for the I19 position.

Figure 87: Flux and heat generation for the I19 position.

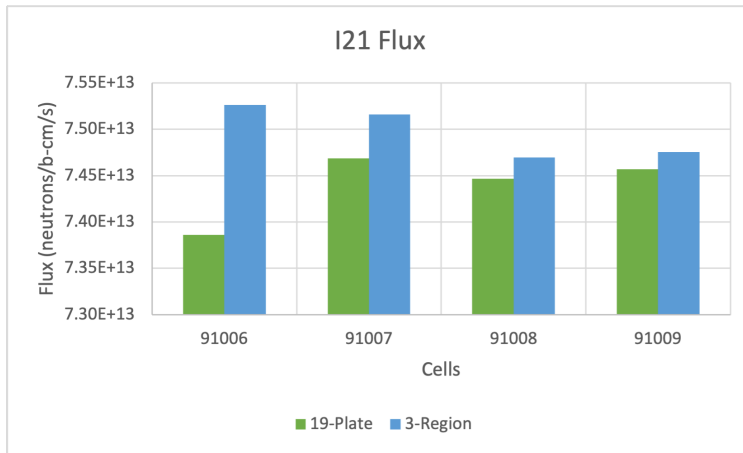


(a) Flux for the I20 position

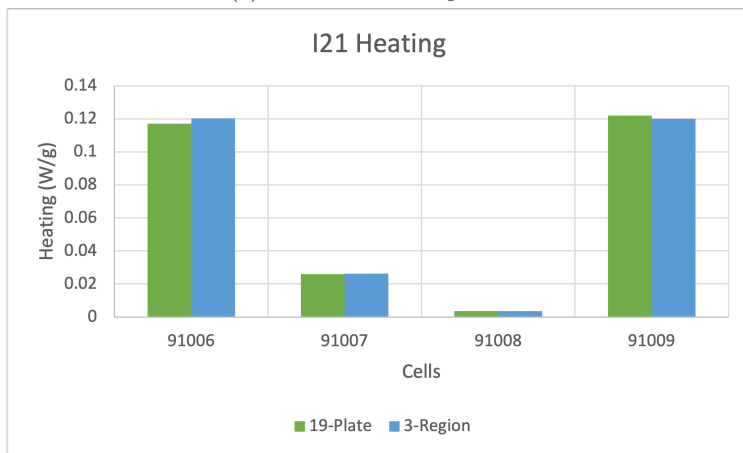


(b) Heat generation rates for the I20 position.

Figure 88: Flux and heat generation for the I20 position.

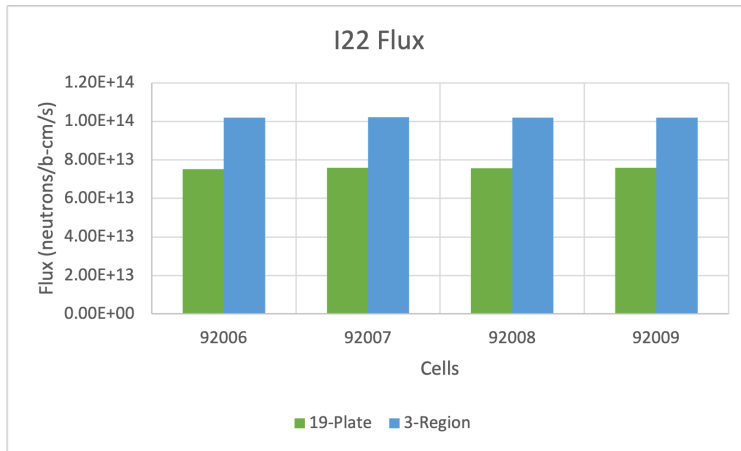


(a) Flux for the I21 position

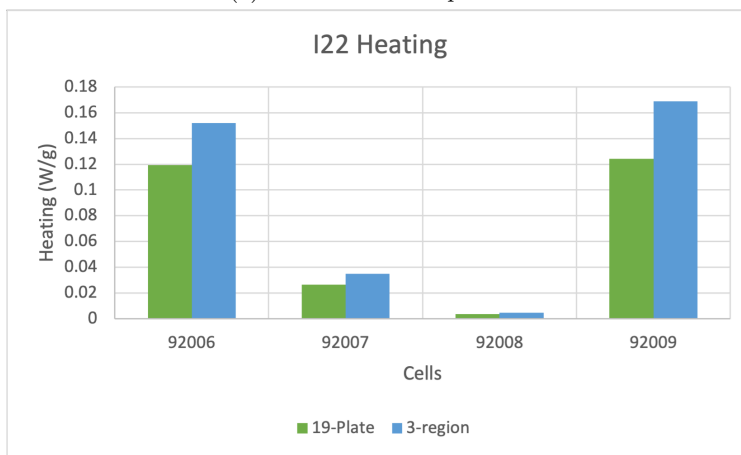


(b) Heat generation rates for the I21 position.

Figure 89: Flux and heat generation for the I21 position.

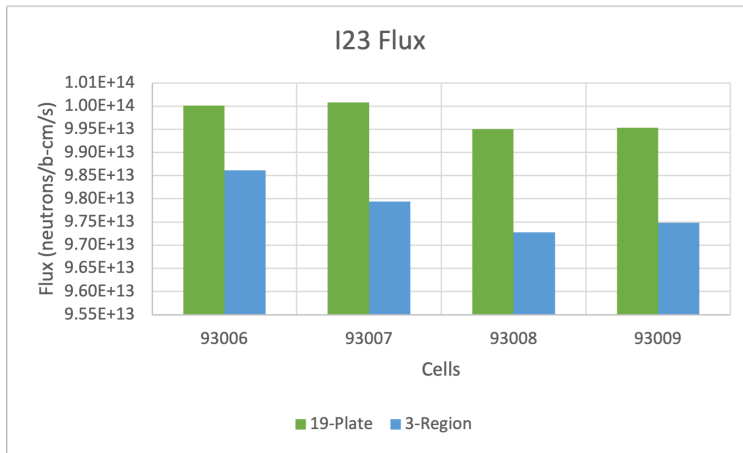


(a) Flux for the I22 position

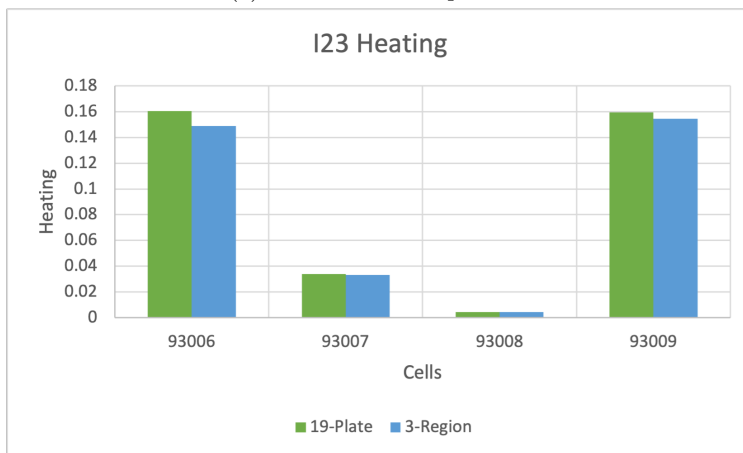


(b) Heat generation rates for the I22 position.

Figure 90: Flux and heat generation for the I22 position.

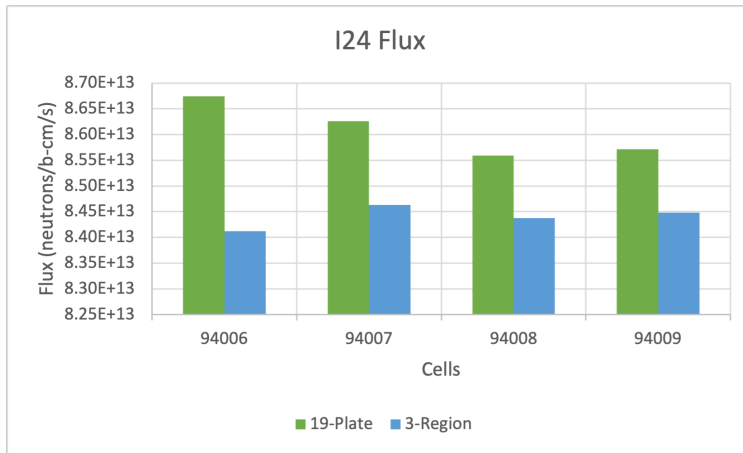


(a) Flux for the I23 position

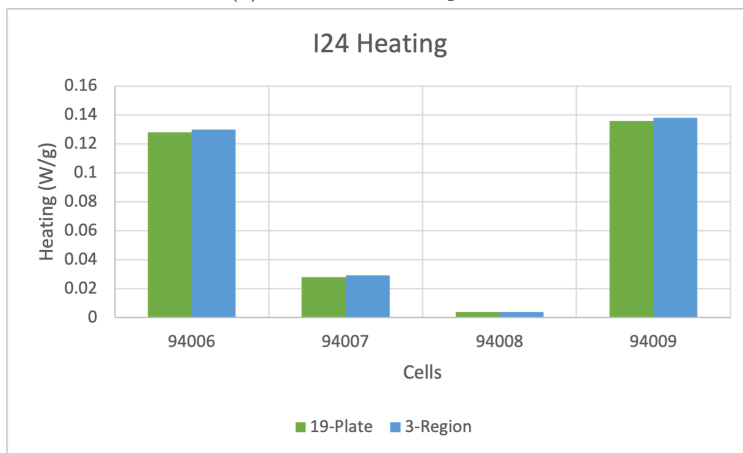


(b) Heat generation rates for the I23 position.

Figure 91: Flux and heat generation for the I23 position.

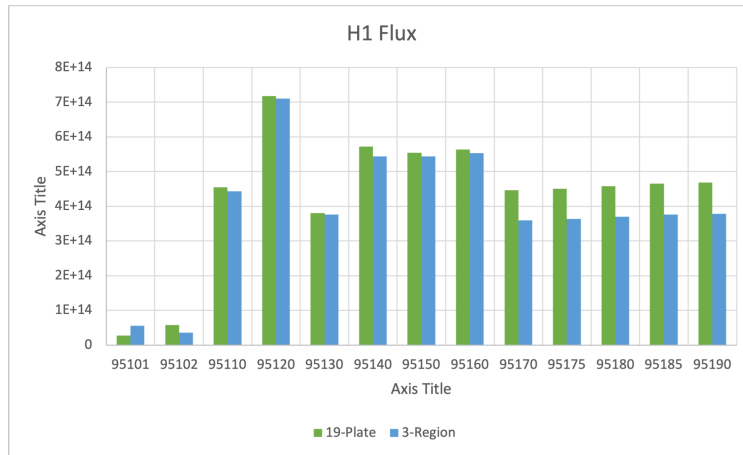


(a) Flux for the I24 position

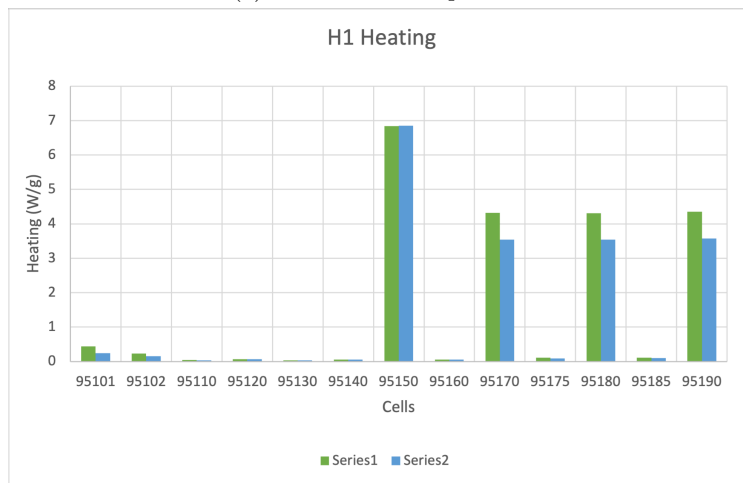


(b) Heat generation rates for the I24 position.

Figure 92: Flux and heat generation for the I24 position.

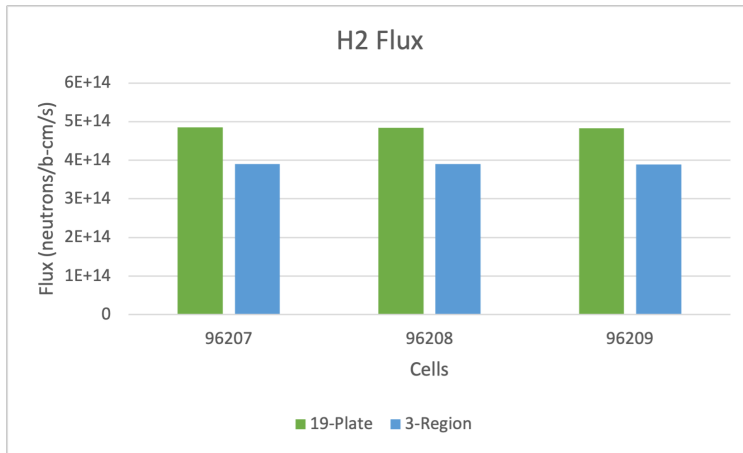


(a) Flux for the H1 position

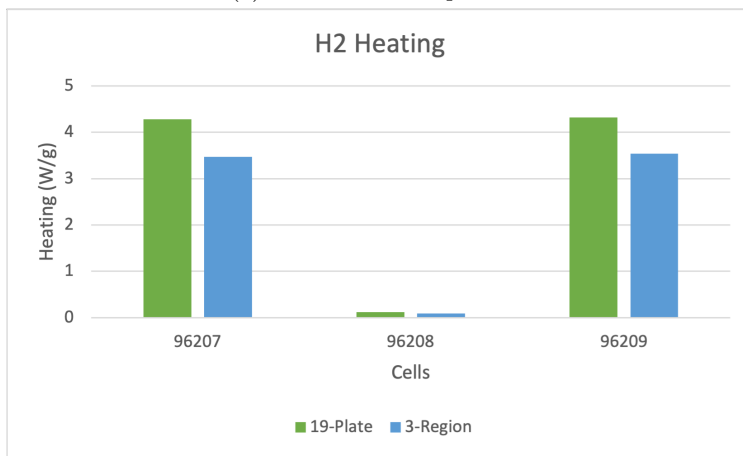


(b) Heat generation rates for the H1 position.

Figure 93: Flux and heat generation for the H1 position.

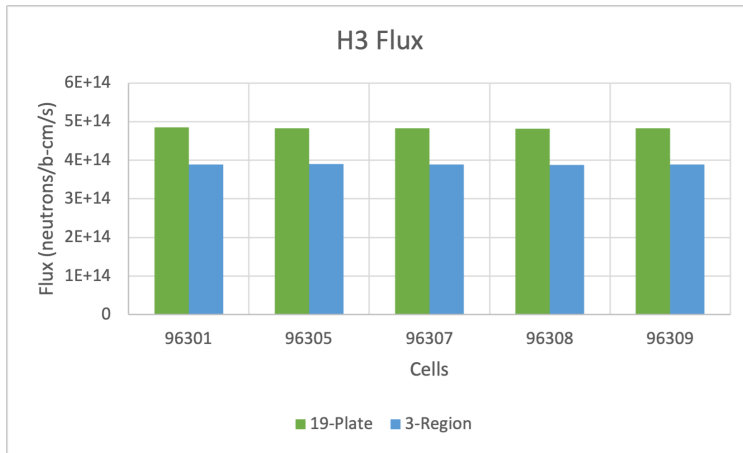


(a) Flux for the H2 position

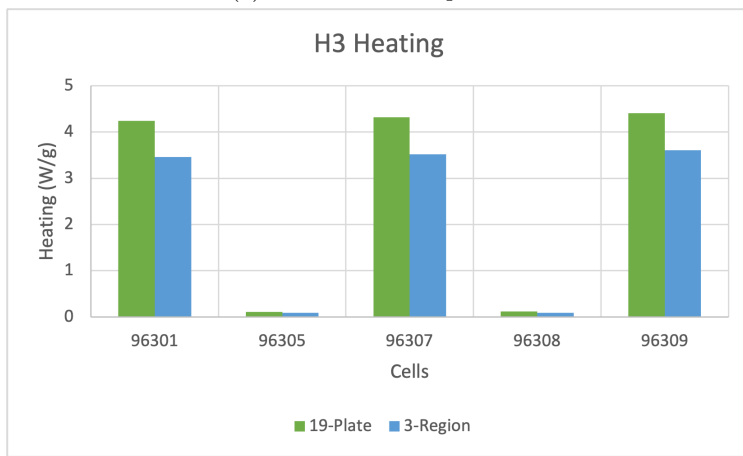


(b) Heat generation rates for the H2 position.

Figure 94: Flux and heat generation for the H2 position.

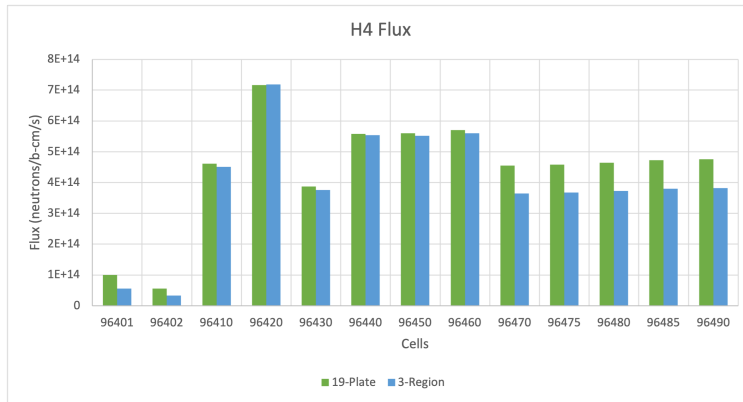


(a) Flux for the H3 position

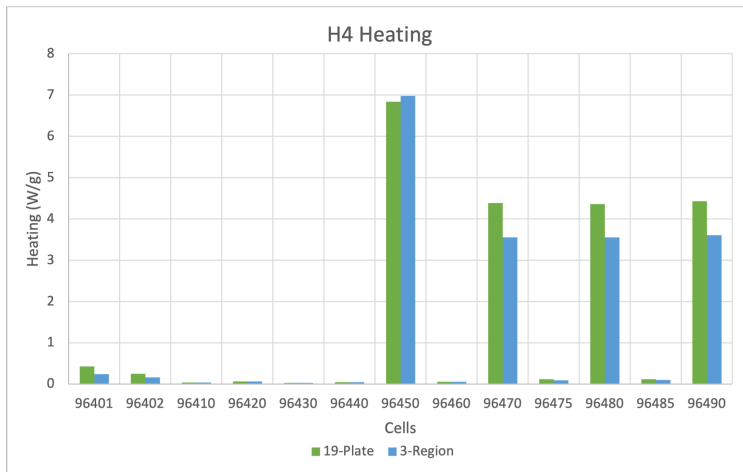


(b) Heat generation rates for the H3 position.

Figure 95: Flux and heat generation for the H3 position.

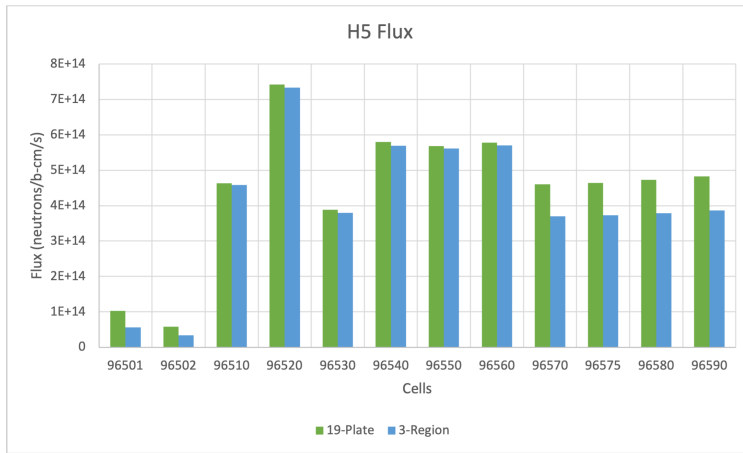


(a) Flux for the H4 position

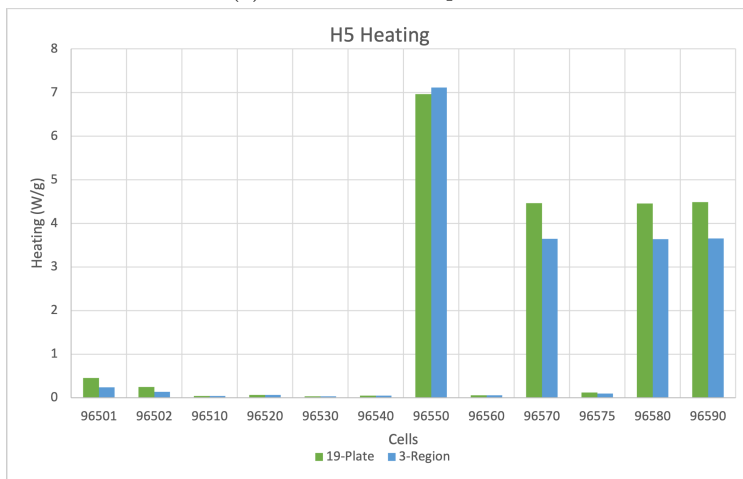


(b) Heat generation rates for the H4 position.

Figure 96: Flux and heat generation for the H4 position.

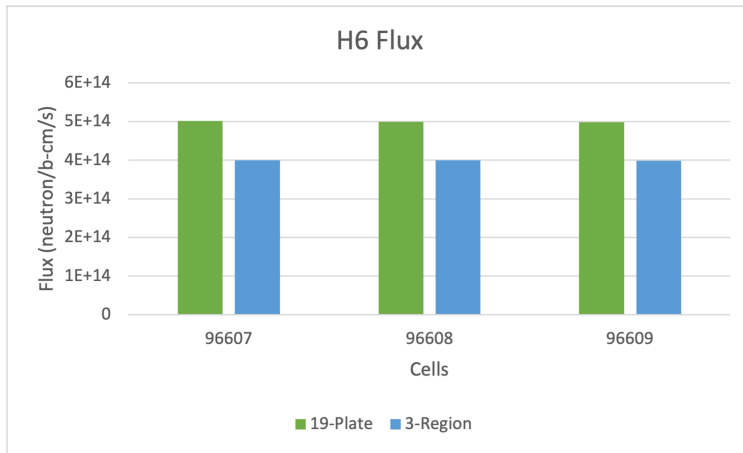


(a) Flux for the H5 position

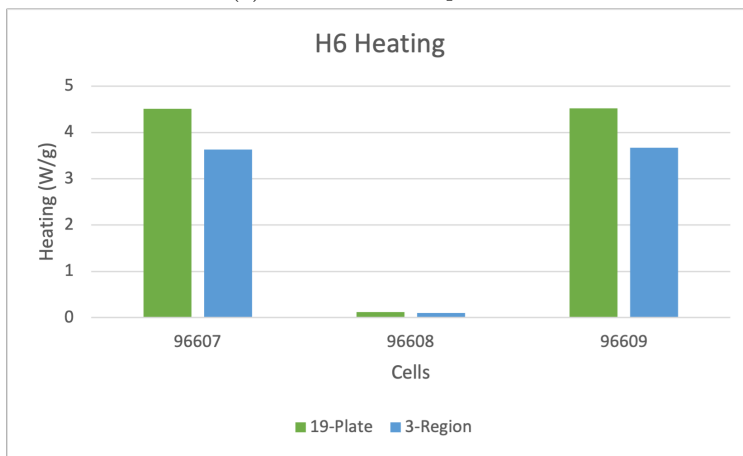


(b) Heat generation rates for the H5 position.

Figure 97: Flux and heat generation for the H5 position.

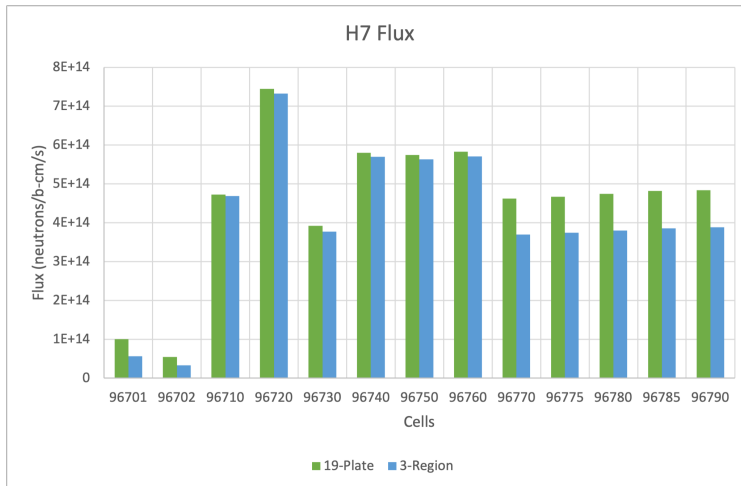


(a) Flux for the H6 position

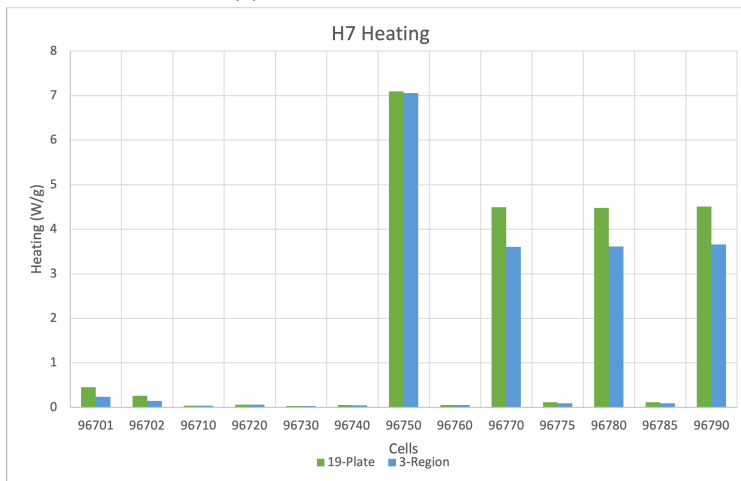


(b) Heat generation rates for the H6 position.

Figure 98: Flux and heat generation for the H6 position.

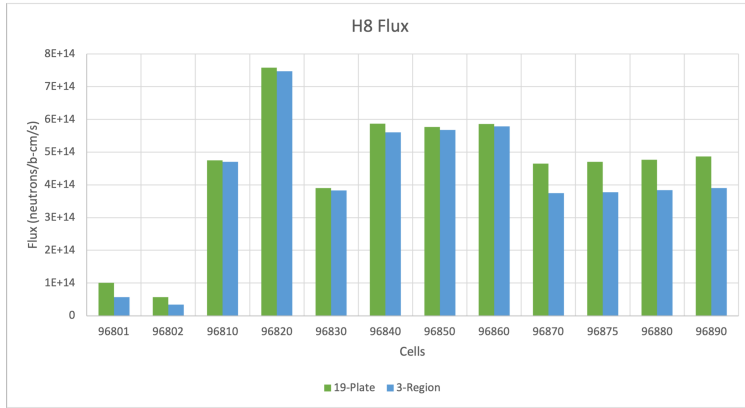


(a) Flux for the H7 position

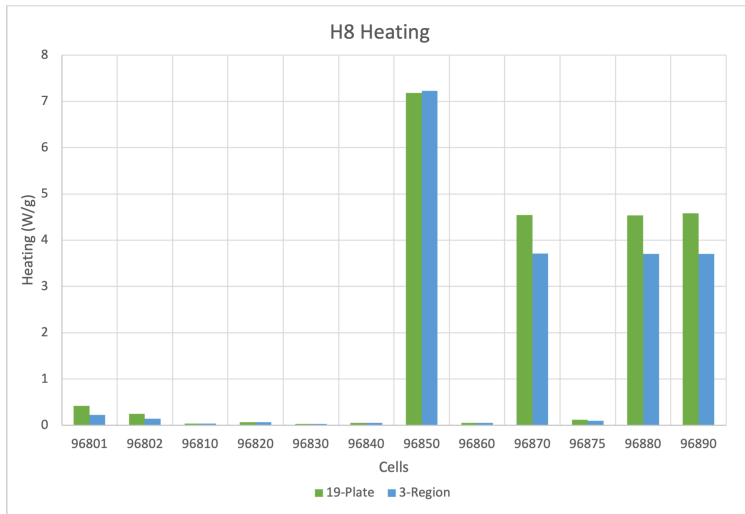


(b) Heat generation rates for the H7 position.

Figure 99: Flux and heat generation for the H7 position.

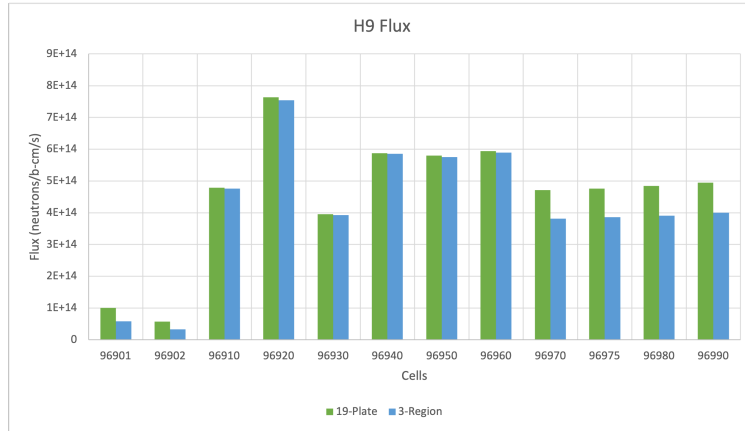


(a) Flux for the H8 position

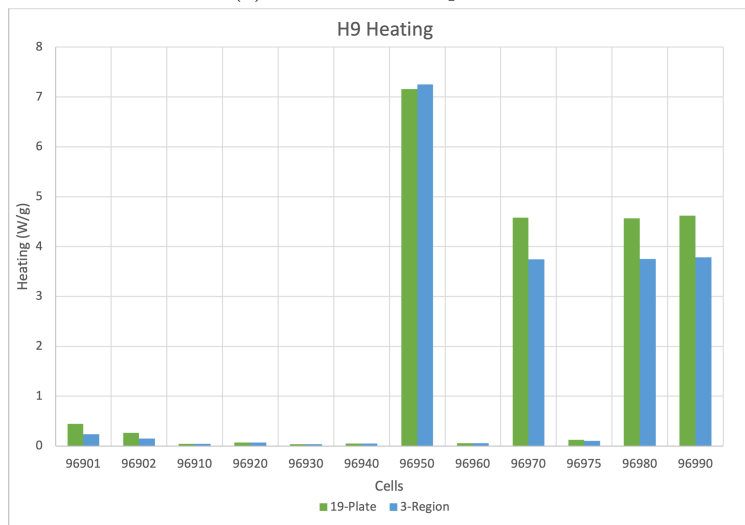


(b) Heat generation rates for the H8 position.

Figure 100: Flux and heat generation for the H8 position.

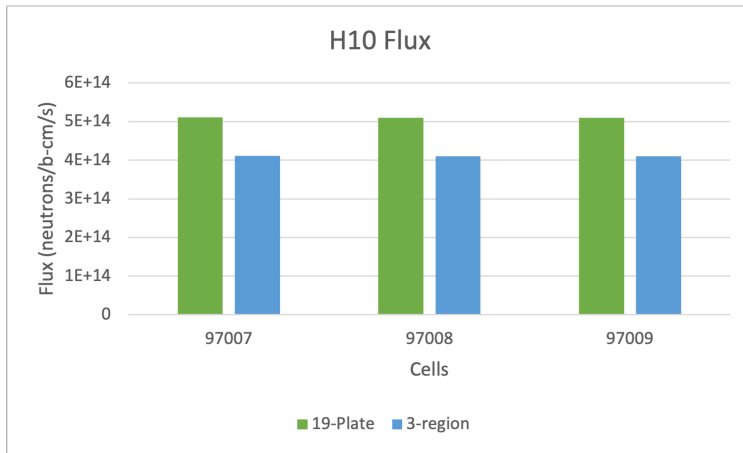


(a) Flux for the H9 position

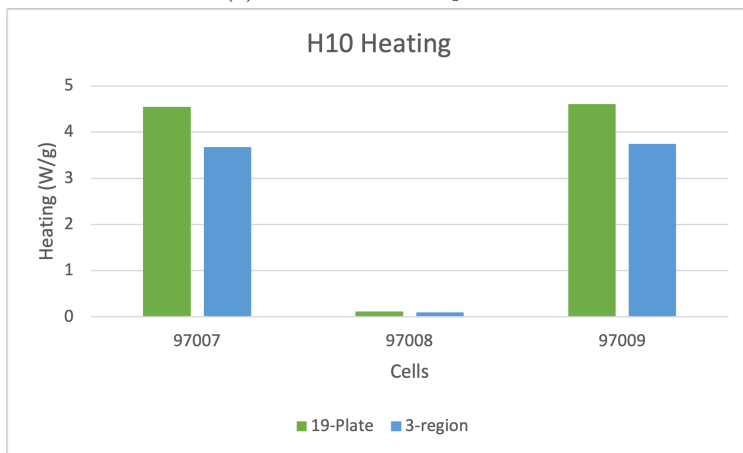


(b) Heat generation rates for the H9 position.

Figure 101: Flux and heat generation for the H9 position.

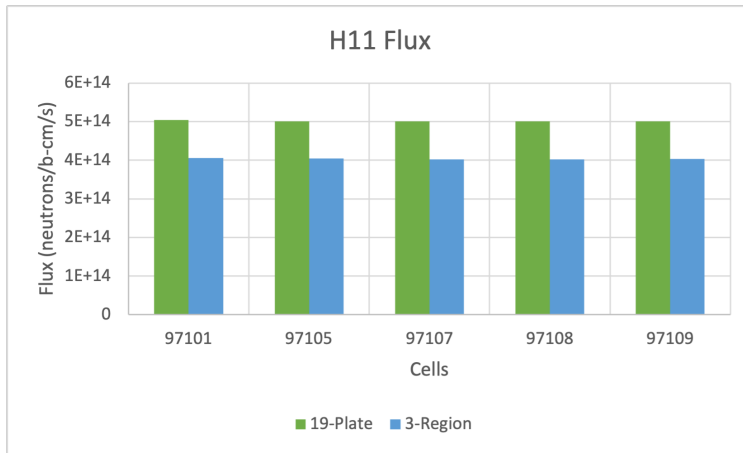


(a) Flux for the H10 position

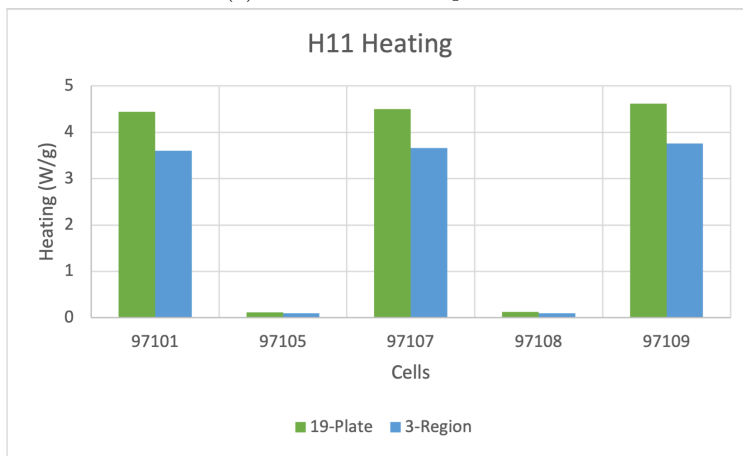


(b) Heat generation rates for the H10 position.

Figure 102: Flux and heat generation for the H10 position.

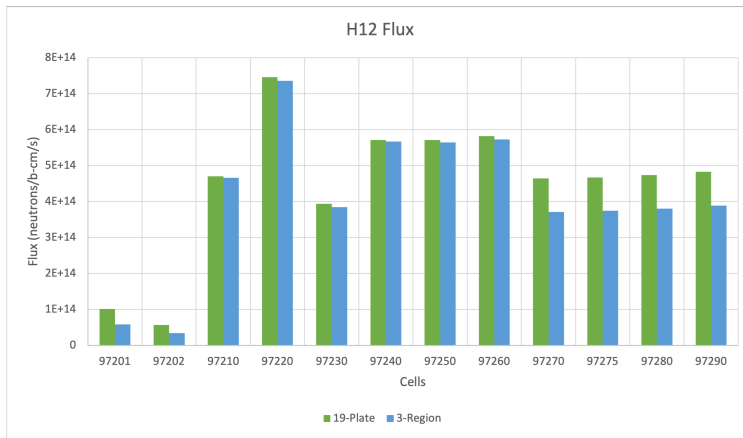


(a) Flux for the H11 position

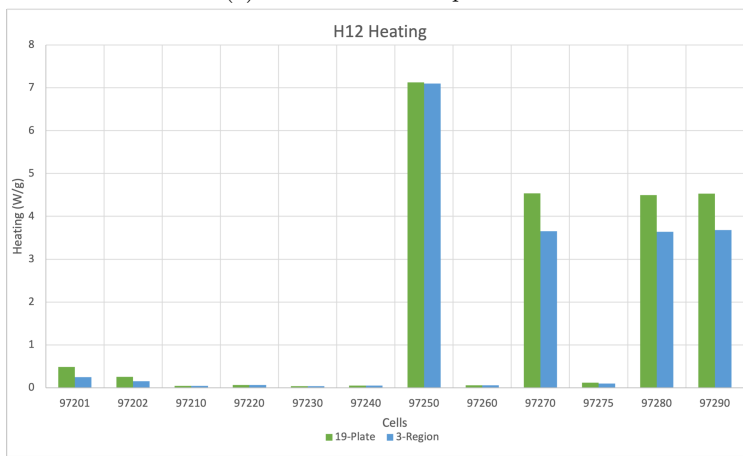


(b) Heat generation rates for the H11 position.

Figure 103: Flux and heat generation for the H11 position.



(a) Flux for the H12 position

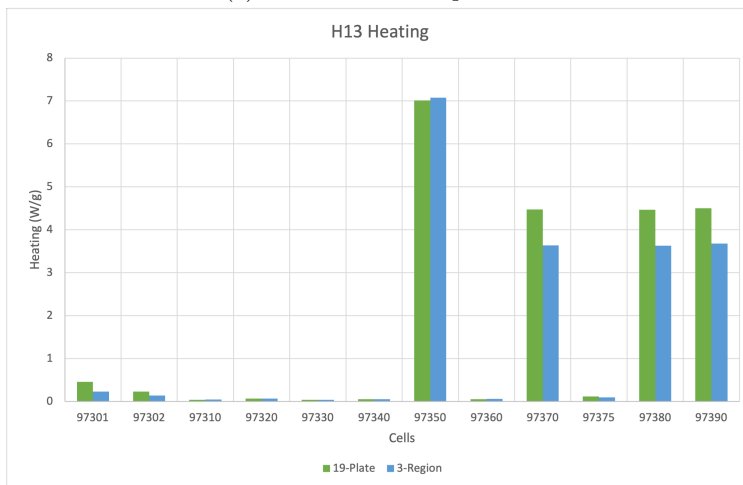


(b) Heat generation rates for the H12 position.

Figure 104: Flux and heat generation for the H12 position.

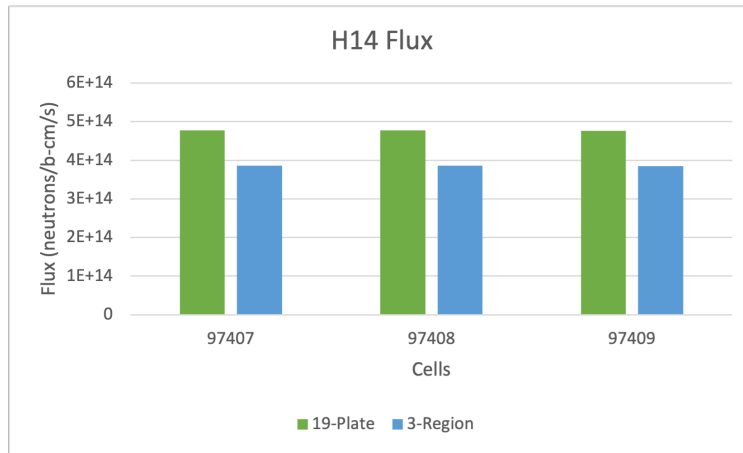


(a) Flux for the H13 position

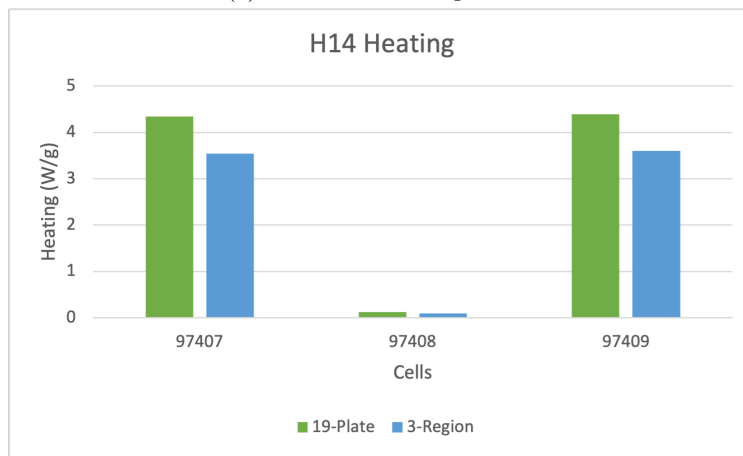


(b) Heat generation rates for the H13 position.

Figure 105: Flux and heat generation for the H13 position.

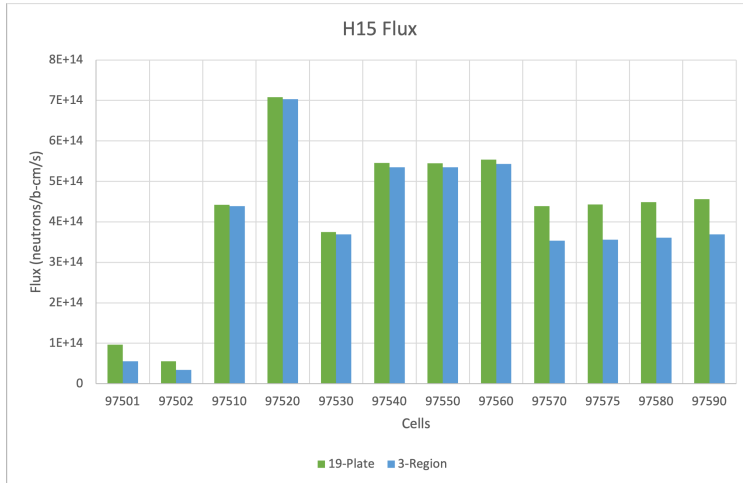


(a) Flux for the H14 position

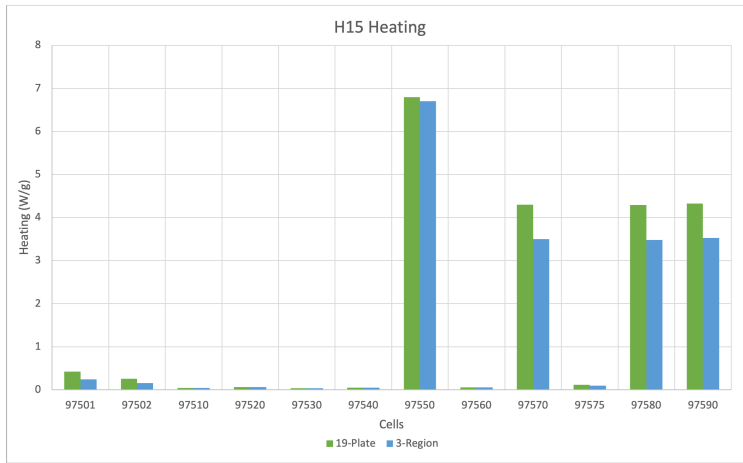


(b) Heat generation rates for the H14 position.

Figure 106: Flux and heat generation for the H14 position.

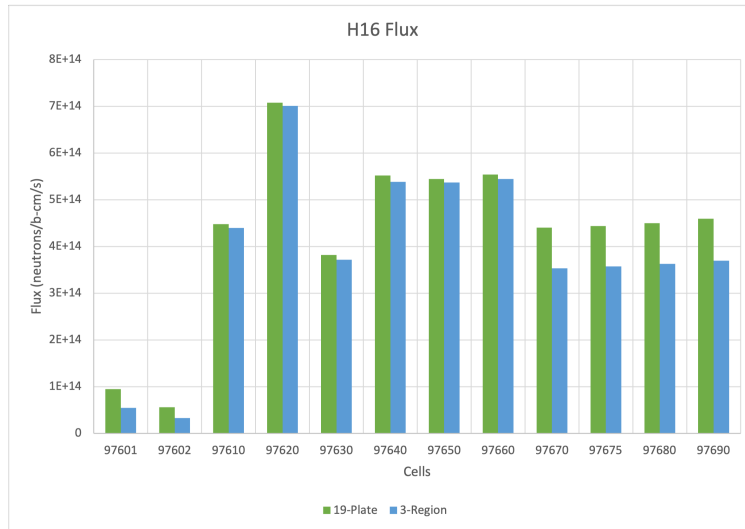


(a) Flux for the H15 position

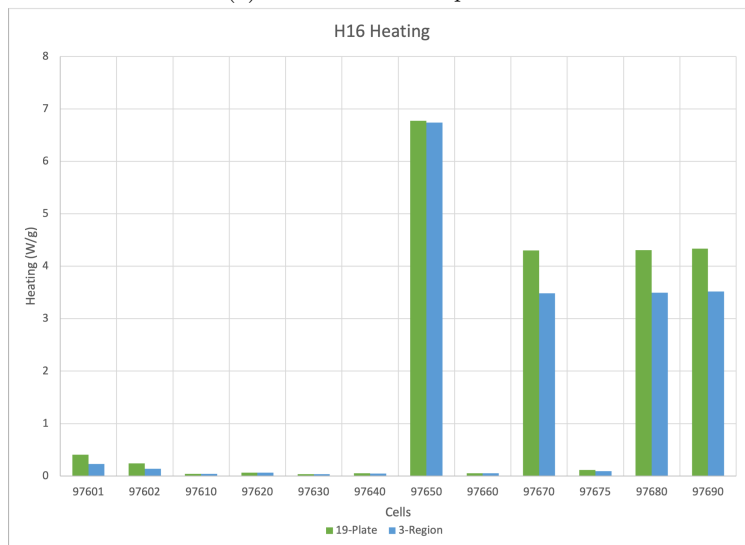


(b) Heat generation rates for the H15 position.

Figure 107: Flux and heat generation for the H15 position.

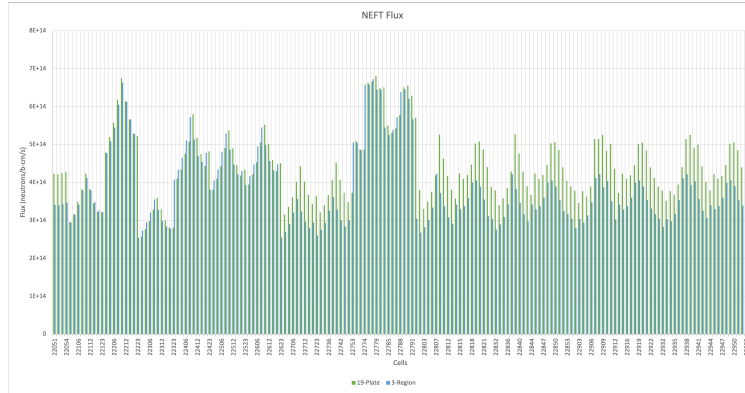


(a) Flux for the H16 position

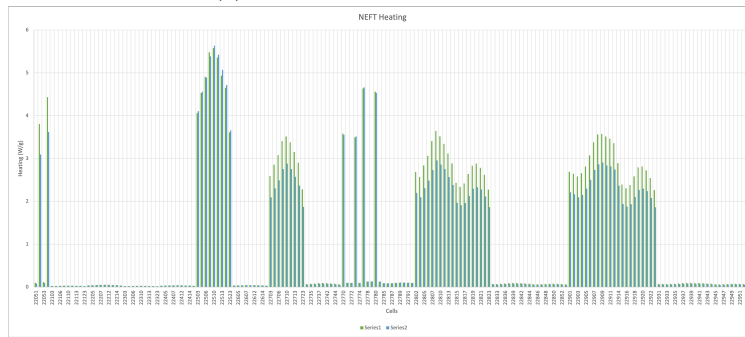


(b) Heat generation rates for the H16 position.

Figure 108: Flux and heat generation for the H16 position.

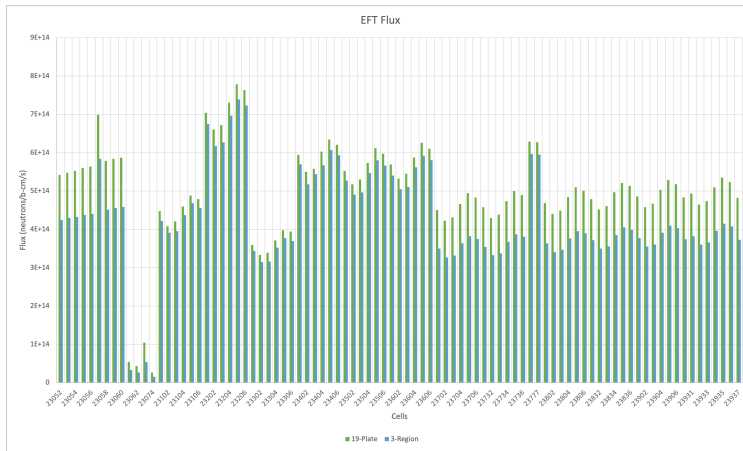


(a) Flux for the NEFT position

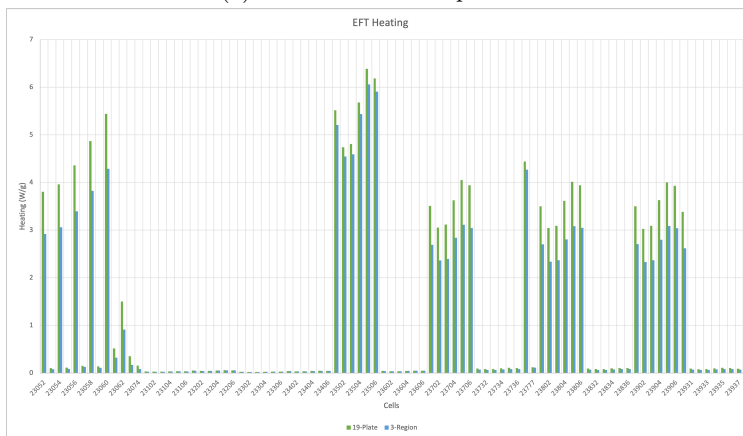


(b) Heat generation rates for the NEFT position.

Figure 110: Flux and heat generation for the NEFT position.



(a) Flux for the EFT position

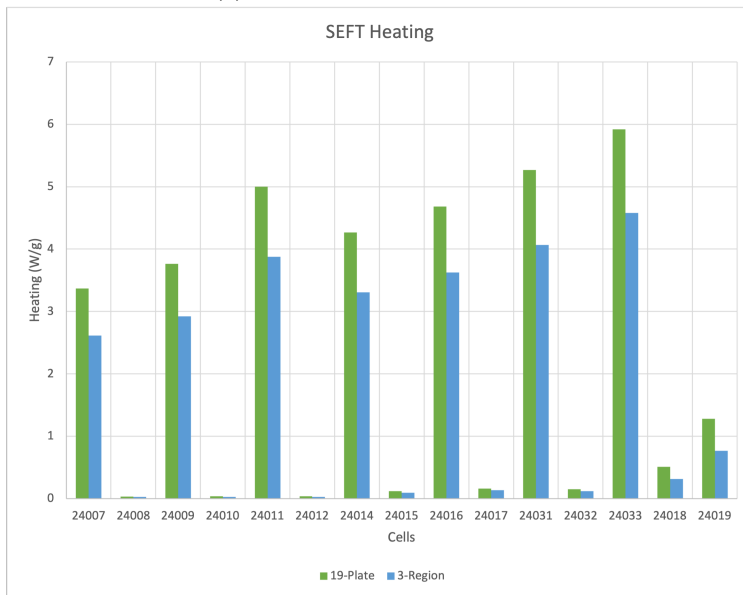


(b) Heat generation rates for the EFT position.

Figure 111: Flux and heat generation for the EFT position.

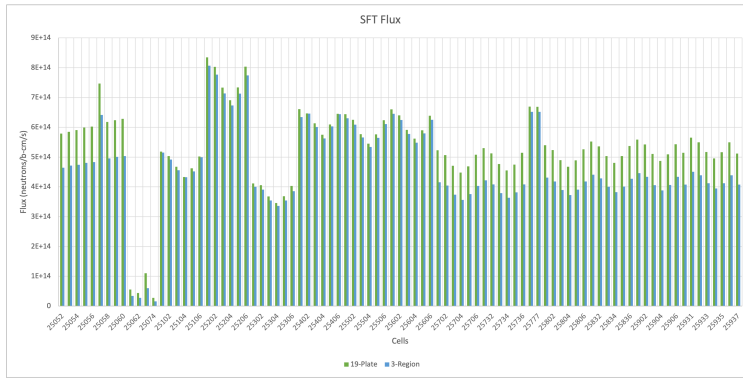


(a) Flux for the SEFT position

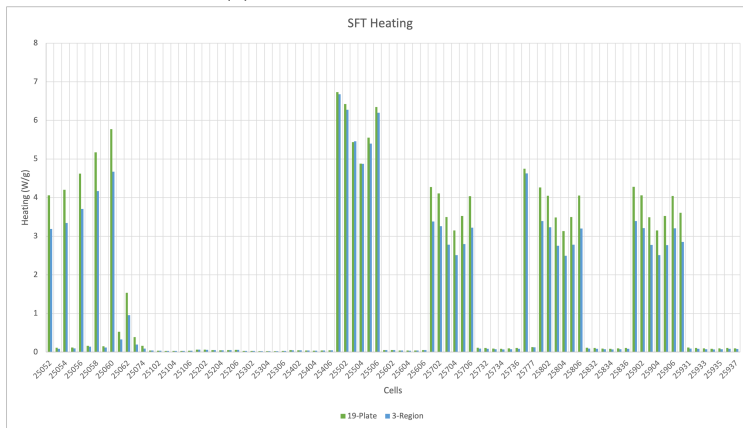


(b) Heat generation rates for the SEFT position.

Figure 112: Flux and heat generation for the SEFT position.

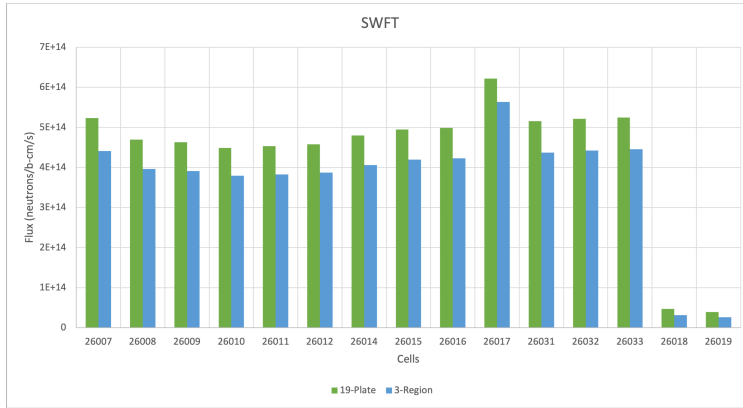


(a) Flux for the SFT position



(b) Heat generation rates for the SFT position.

Figure 113: Flux and heat generation for the SFT position.

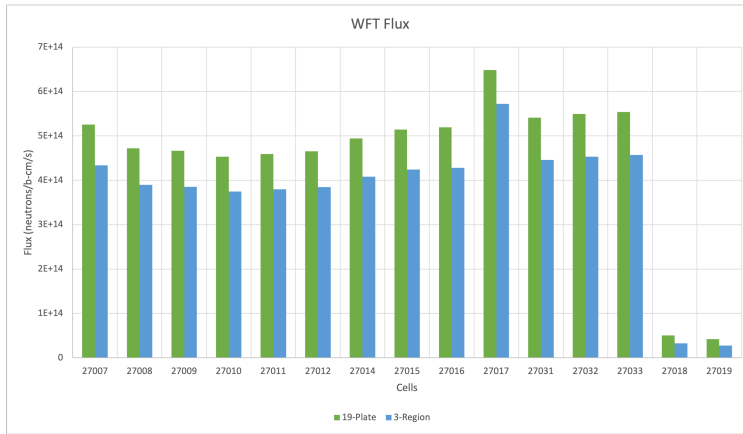


(a) Flux for the SWFT position

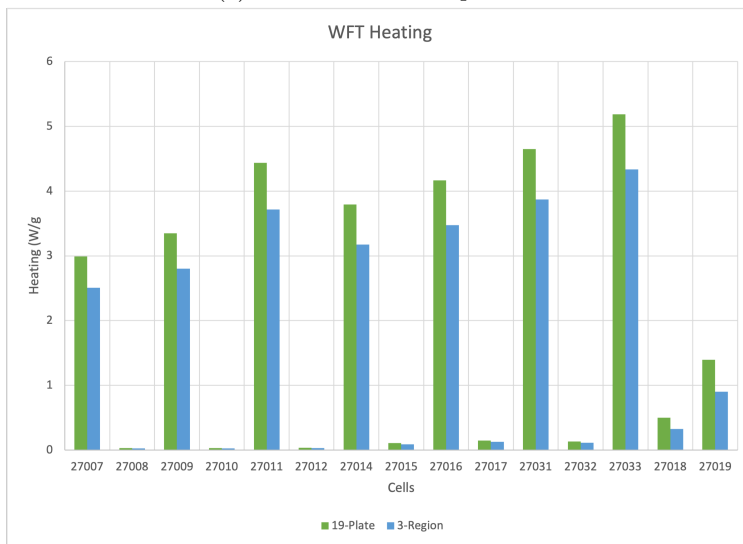


(b) Heat generation rates for the SWFT position.

Figure 114: Flux and heat generation for the SWFT position.

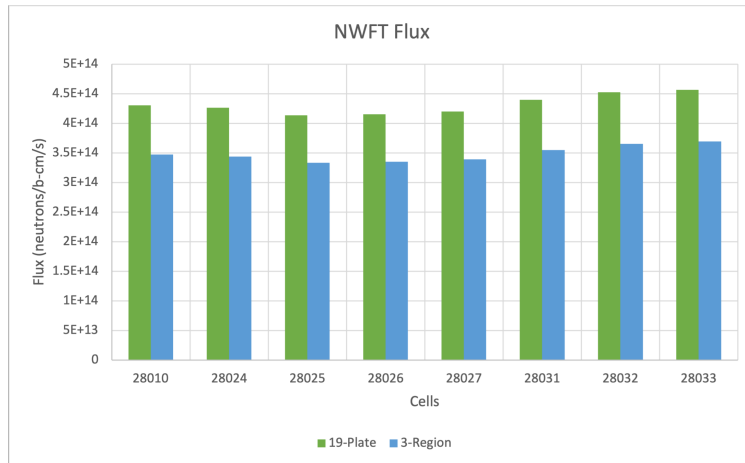


(a) Flux for the WFT position

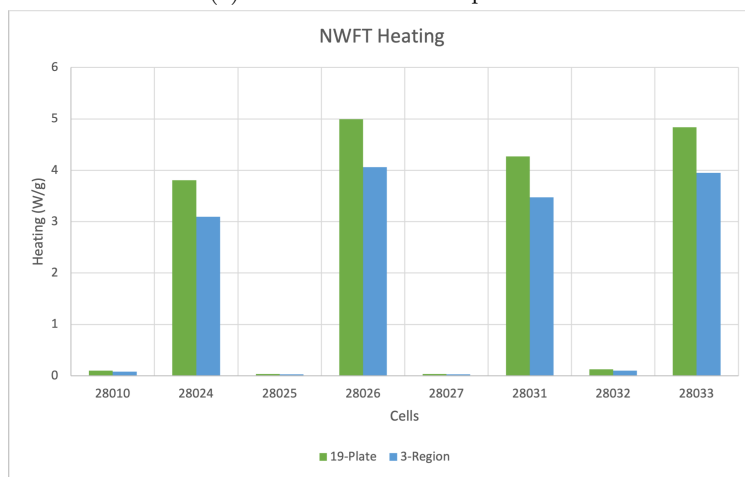


(b) Heat generation rates for the WFT position.

Figure 115: Flux and heat generation for the WFT position.

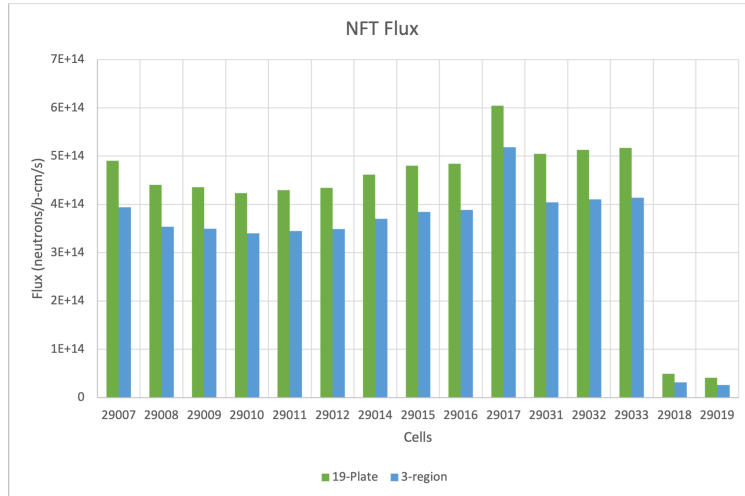


(a) Flux for the NWFT position

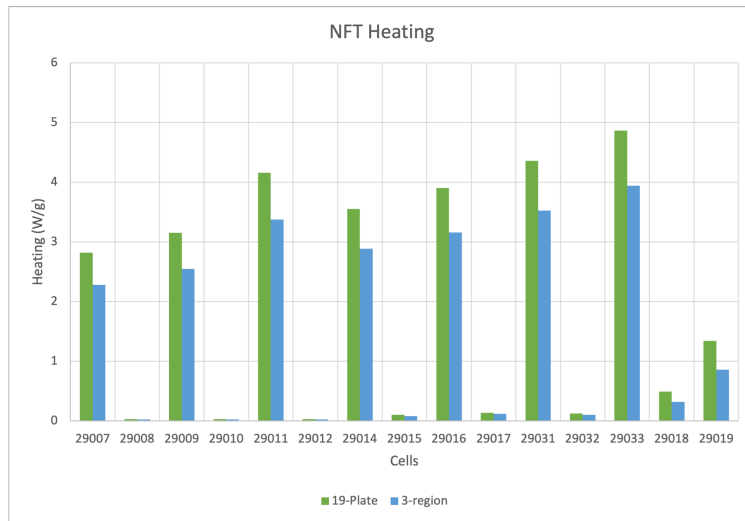


(b) Heat generation rates for the NWFT position.

Figure 116: Flux and heat generation for the NWFT position.



(a) Flux for the NFT position



(b) Heat generation rates for the NFT position.

Figure 117: Flux and heat generation for the NFT position.

B Percent Error by Cell

Position	Cell	Flux error	Heat error
A1	31007	19.48	18.33
A1	31009	19.42	18.7
A2	32007	20.04	18.83
A2	32009	19.96	19.29
A3	33007	19.83	18.89
A3	33009	19.81	19.49
A4	34007	19.76	18.95
A4	34009	19.85	19.25
A5	35007	19.42	18.33
A5	35009	19.13	18.41
A6	36007	19.49	18.18
A6	36009	19.19	18.36
A7	37007	19.48	18.26
A7	37009	19.33	18.51
A8	38007	19.22	18.46
A8	38009	19.36	18.9
A9	41007	20.02	19.07
A10	42007	23.47	22.2
A11	43007	15.89	14.68
A12	44007	19.87	19.02
B1	51001	0.82	0.33
B1	51008	1.1	0.1
B1	51009	0.98	0.48
B2	52007	1.89	0.17
B2	52008	1.84	0.02
B2	52009	2.11	0.55
B3	53007	5.51	4.36
B3	53008	6.37	4.61
B3	53009	6.24	5.03
B5	55001	2.78	1.1
B5	55008	3.18	0.13
B5	55009	3.3	0.15
B6	56007	3.17	5.15
B6	56008	3.06	5.26
B6	56009	3.33	4.81
B7	57001	0.98	0.8
B7	57008	0.84	0.83
B7	57009	0.56	0.64
B8	58007	0.43	1.54
B8	58008	0.64	0.83
B8	58009	0.67	1.01

Table 24: Percent error for flux and heating tallies.

Position	Cell	Flux error	Heat error
B9	61006	0.69	3.09
B9	61007	1.2	3.59
B9	61008	1.52	3.38
B9	61009	1.41	2.13
B10	62006	2.84	5.56
B10	62007	2.92	2.76
B10	62008	2.81	2.32
B10	62009	2.94	3.22
B11	63006	0.36	0.58
B11	63007	0.44	0.32
B11	63008	0.32	0.24
B11	63009	0.16	0
B12	64006	4.6	4.29
B12	64007	3.81	4.12
B12	64008	3.72	3.41
B12	64009	3.6	2.97
I1	71001	2.65	2.81
I1	71008	1.75	0.84
I1	71009	2.81	0.38
I2	72001	5.13	9.14
I2	72008	6.04	2.83
I2	72009	6.23	1.43
I3	73001	4.25	7.25
I3	73008	4.08	0.57
I3	73009	4.24	1.89
I4	74001	1.4	4.64
I4	74008	1.21	2.48
I4	74009	1.75	3.5
I5	75001	1.81	1.22
I5	75008	1.94	1.36
I5	75009	2.15	2.24
I6	76001	2.39	3.23
I6	76008	1.27	2.01
I6	76009	0.95	2.33
I7	77001	4.4	7.06
I7	77008	3.11	3.44
I7	77009	3.23	6.15
I8	78001	18.43	46.84
I8	78008	5.45	220.42
I8	78009	3.49	77.02

Table 25: Percent error for flux and heating tallies.

Position	Cell	Flux error	Heat error
I9	79001	7.93	2.01
I9	79008	7.52	3.27
I9	79009	8.27	2.28
I10	80001	12.42	11.72
I10	80008	11.43	2.49
I10	80009	11.77	0.51
I11	81001	2.84	2.49
I11	81008	3.32	0.93
I11	81009	3.84	1.92
I12	82001	1.9	6.92
I12	82008	1.79	6.45
I12	82009	2.06	9.35
I13	83001	0.52	9.32
I13	83008	1.29	5.78
I13	83009	0.91	7.1
I14	84001	7.76	2.85
I14	84008	8.51	6.13
I14	84009	8.37	7.57
I15	85001	5.29	0.6
I15	85008	6.1	3.4
I15	85009	6.94	7.08
I16	86001	5.76	14.75
I16	86008	5.14	7.69
I16	86009	4.5	4.64
I17	87001	2.27	4.28
I17	87008	2.04	4.88
I17	87009	2.11	2.28
I18	88001	1.93	4.58
I18	88008	2.24	2.53
I18	88009	2.43	3.08
I19	89001	6.99	0.03
I19	89008	4.84	2.18
I19	89009	4.47	4.53
I20	90001	6.27	6.43
I20	90008	6.74	8.38
I20	90009	6.54	5.66
I21	91006	1.9	2.59
I21	91007	0.63	0.42
I21	91008	0.31	0.17
I21	91009	0.25	1.62

Table 26: Percent error for flux and heating tallies.

Position	Cell	Flux error	Heat error
I22	92006	35.62	27.49
I22	92007	34.48	31.27
I22	92008	34.37	34.63
I22	92009	34.23	36.01
I23	93006	1.39	7.19
I23	93007	2.14	2.58
I23	93008	2.24	0.86
I23	93009	2.07	2.93
I24	94006	3.02	1.42
I24	94007	1.89	4.01
I24	94008	1.42	0.94
I24	94009	1.44	1.72
H1	95101	101.09	46.25
H1	95102	37.95	35.1
H1	95110	2.5	2.02
H1	95120	0.96	2.75
H1	95130	1.21	1.5
H1	95140	4.93	5.49
H1	95150	1.92	0.15
H1	95160	1.71	0.72
H1	95170	19.42	18.12
H1	95175	19.4	18
H1	95180	19.34	17.92
H1	95185	19.14	17.33
H1	95190	19.22	17.89
H2	96207	19.55	18.99
H2	96208	19.51	18.48
H2	96209	19.24	18.11
H3	96301	19.77	18.37
H3	96305	19.36	17.86
H3	96307	19.33	18.38
H3	96308	19.47	18.03
H3	96309	19.42	18.12
H4	96401	43.81	44.24
H4	96402	40.46	34.34
H4	96410	2.09	0.75
H4	96420	0.21	1.7
H4	96430	2.83	1
H4	96440	0.74	7.08

Table 27: Percent error for flux and heating tallies.

Position	Cell	Flux error	Heat error
H4	96450	1.44	2.04
H4	96460	1.74	2.22
H4	96470	19.92	18.83
H4	96475	19.81	17.89
H4	96480	19.7	18.45
H4	96485	19.58	17.77
H4	96490	19.7	18.56
H5	96501	45.35	46.65
H5	96502	42.53	43.19
H5	96510	1.03	1.15
H5	96520	1.06	2.93
H5	96530	2.37	0.5
H5	96540	1.88	0.79
H5	96550	1.12	2.18
H5	96560	1.41	2.29
H5	96570	19.63	18.23
H5	96575	19.71	18.13
H5	96580	19.78	18.39
H5	96590	19.87	18.64
H6	96607	20.15	19.55
H6	96608	19.98	18.18
H6	96609	20.02	18.77
H7	96701	43.72	46.73
H7	96702	39.37	44.24
H7	96710	0.8	1.05
H7	96720	1.68	0.74
H7	96730	3.77	2.87
H7	96740	1.83	2.59
H7	96750	1.86	0.52
H7	96760	2	0.45
H7	96770	20.03	19.91
H7	96775	19.97	19.16
H7	96780	20	19.25
H7	96785	19.97	18.59
H7	96790	19.75	18.92
H8	96801	43.94	46.31
H8	96802	40.57	41.68
H8	96810	0.83	1.75
H8	96820	1.45	1.13

Table 28: Percent error for flux and heating tallies.

Position	Cell	Flux error	Heat error
H8	96830	1.9	1.31
H8	96840	4.43	1.85
H8	96850	1.61	0.62
H8	96860	1.29	2.2
H8	96870	19.48	18.35
H8	96875	19.63	17.84
H8	96880	19.49	18.36
H8	96890	19.85	19.12
H9	96901	41.93	46.11
H9	96902	42.06	44.05
H9	96910	0.51	3.15
H9	96920	1.17	0.99
H9	96930	0.65	1.81
H9	96940	0.31	1.88
H9	96950	0.85	1.23
H9	96960	0.82	2.31
H9	96970	19.17	18.18
H9	96975	18.98	17.23
H9	96980	19.24	17.85
H9	96990	19.2	18.12
H10	97007	19.4	19.19
H10	97008	19.66	18.66
H10	97009	19.46	18.51
H11	97101	19.5	18.9
H11	97105	19.33	18
H11	97107	19.62	18.55
H11	97108	19.65	18.11
H11	97109	19.61	18.56
H12	97201	42.34	49.13
H12	97202	41.08	40.22
H12	97210	0.84	1.63
H12	97220	1.34	1.3
H12	97230	2.18	0.24
H12	97240	0.81	3.45
H12	97250	1.04	0.4
H12	97260	1.61	0.78
H12	97270	20.04	19.44
H12	97275	19.94	18.76
H12	97280	19.74	19
H12	97290	19.47	18.74

Table 29: Percent error for flux and heating tallies.

Position	Cell	Flux error	Heat error
H13	97301	42.09	49.47
H13	97302	39.67	40.18
H13	97310	0.38	0.9
H13	97320	0.96	0.16
H13	97330	1.98	0.87
H13	97340	1.5	3.53
H13	97350	1.18	0.96
H13	97360	1.25	2.04
H13	97370	19.33	18.78
H13	97375	19.24	17.7
H13	97380	19.6	18.67
H13	97390	19.52	18.36
H14	97407	19.22	18.37
H14	97408	19.2	17.29
H14	97409	19.14	17.99
H15	97501	42.2	43.27
H15	97502	38.22	40.27
H15	97510	0.76	0.71
H15	97520	0.76	1.89
H15	97530	1.61	0.52
H15	97540	1.91	1.54
H15	97550	1.74	1.43
H15	97560	1.81	1.36
H15	97570	19.44	18.67
H15	97575	19.59	18.22
H15	97580	19.51	18.97
H15	97590	19.14	18.42
H16	97601	42.02	43.92
H16	97602	41.24	43.14
H16	97610	1.75	0.12
H16	97620	0.9	2.46
H16	97630	2.68	0.07
H16	97640	2.51	4.02
H16	97650	1.29	0.51
H16	97660	1.69	0.48
H16	97670	19.74	19.02
H16	97675	19.39	18.28
H16	97680	19.48	18.83
H16	97690	19.62	18.81

Table 30: Percent error for flux and heating tallies.

Position	Cell	Flux error	Heat error
CFT	21053	19.48	17.84
CFT	21054	19.47	18.41
CFT	21071	43.9	45.85
CFT	21072	39.78	45.62
CFT	11106	0.94	0.56
CFT	11206	0.73	0.57
CFT	11306	1.75	2
CFT	21406	0.67	1.02
CFT	11506	1.32	0.38
CFT	11606	1.46	0.31
CFT	11706	19.76	18.66
CFT	11736	19.66	18.2
CFT	21771	1.22	2.12
CFT	21772	1.54	1.41
CFT	21773	1.58	0.74
CFT	21774	1.46	0.71
CFT	21775	1.33	1.04
CFT	21776	1.26	1.45
CFT	21777	1.39	1.39
CFT	21801	19.41	17.69
CFT	21802	19.64	17.88
CFT	21803	20.1	19.13
CFT	21804	19.62	18.61
CFT	21805	19.43	17.84
CFT	21806	19.51	18.58
CFT	21831	19.46	17.35
CFT	21832	19.64	17.77
CFT	21833	19.89	18.39
CFT	21834	19.59	17.89
CFT	21835	19.51	17.65
CFT	21836	19.39	18.38
CFT	21901	19.36	17.8
CFT	21902	19.61	18.21
CFT	21903	19.72	18.24
CFT	21904	19.62	18.12
CFT	21905	19.58	18.42
CFT	21906	19.46	18.59
CFT	21907	19.5	17.65

Table 31: Percent error for flux and heating tallies.

Position	Cell	Flux error	Heat error
CFT	21931	19.3	17.56
CFT	21932	19.72	18.15
CFT	21933	19.83	17.79
CFT	21934	19.5	17.87
CFT	21935	19.67	18.5
CFT	21936	19.36	18.32
CFT	21937	19.7	17.34
NEFT	22051	19.42	18.46
NEFT	22052	19.39	18.69
NEFT	22053	19.36	18.15
NEFT	22054	19.2	18.39
NEFT	22103	0.35	0.29
NEFT	22105	0.3	0.14
NEFT	22106	2.18	0.22
NEFT	22107	0.63	1.48
NEFT	22110	2.68	0.76
NEFT	22112	0.93	2.43
NEFT	22113	0.95	4.74
NEFT	22114	1.08	0.18
NEFT	22123	0.33	3.95
NEFT	22203	0.32	0.34
NEFT	22205	2.16	0.98
NEFT	22206	2.33	0.51
NEFT	22207	2.24	0.6
NEFT	22210	1.75	2.01
NEFT	22212	0.21	3.27
NEFT	22213	0.1	0.74
NEFT	22214	0.17	1.87
NEFT	22223	51.33	1.91
NEFT	22303	6.38	0.31
NEFT	22305	6.51	0.86
NEFT	22306	7.93	3.44
NEFT	22307	7.94	1.42
NEFT	22310	8.66	1.15
NEFT	22312	9.25	5.44
NEFT	22313	5.35	2.2
NEFT	22314	1.3	0
NEFT	22323	45.27	1.49

Table 32: Percent error for flux and heating tallies.

Position	Cell	Flux error	Heat error
NEFT	22403	5.83	3.36
NEFT	22405	7.32	0.37
NEFT	22406	7.28	2.71
NEFT	22407	12.7	6.56
NEFT	22410	11.58	4.12
NEFT	22412	9.34	1.13
NEFT	22413	4.25	4.75
NEFT	22414	7.81	1.06
NEFT	22423	20.84	4.04
NEFT	22503	6.57	1.17
NEFT	22505	5.96	0.68
NEFT	22506	8.76	0.47
NEFT	22507	7.8	1.78
NEFT	22510	9.52	0.95
NEFT	22512	8.77	1.29
NEFT	22513	5.47	2.84
NEFT	22514	3.02	1.33
NEFT	22523	9.35	1.25
NEFT	22603	5.78	1.29
NEFT	22605	6.2	0.08
NEFT	22606	9.27	1.87
NEFT	22607	8.05	0.84
NEFT	22610	9.85	1.94
NEFT	22612	9.11	3.07
NEFT	22613	5.93	1.75
NEFT	22614	4.14	1.51
NEFT	22623	43.32	1.44
NEFT	22703	14.28	19.14
NEFT	22705	13.55	19.25
NEFT	22706	11.14	19.09
NEFT	22707	11.18	19.15
NEFT	22710	26.91	17.99
NEFT	22712	26.32	18.54
NEFT	22713	23.95	18.29
NEFT	22714	14.41	18.37
NEFT	22723	28.53	17.88
NEFT	22733	14.37	18.21

Table 33: Percent error for flux and heating tallies.

Position	Cell	Flux error	Heat error
NEFT	22735	13.69	18.94
NEFT	22736	11.26	19.81
NEFT	22737	11.15	18.9
NEFT	22740	27.29	17.69
NEFT	22742	26.26	17.18
NEFT	22743	23.77	18.86
NEFT	22744	13.88	17.18
NEFT	22753	35.45	18.09
NEFT	22770	0.96	0.79
NEFT	22773	0.3	0.54
NEFT	22774	35.03	0.46
NEFT	22775	0.88	0.52
NEFT	22778	0.96	0.53
NEFT	22779	5.36	0.25
NEFT	22780	0.58	0.62
NEFT	22781	16.29	0.98
NEFT	22785	4.42	0.97
NEFT	22786	1.56	2.05
NEFT	22787	5.32	0.35
NEFT	22788	10.54	0.68
NEFT	22789	0.85	0.91
NEFT	22790	5.3	0.47
NEFT	22791	9.9	1.55
NEFT	22792	46.75	1.21
NEFT	22802	29.58	18.07
NEFT	22803	14.67	18.4
NEFT	22805	13.8	18.64
NEFT	22806	10.9	18.8
NEFT	22807	1.05	19.79
NEFT	22809	29.32	18.86
NEFT	22810	27.26	18.73
NEFT	22812	26.26	17.62
NEFT	22813	23.56	17.58
NEFT	22814	4.48	17.54
NEFT	22815	22.28	19.15
NEFT	22816	17.58	18.4
NEFT	22817	14.54	18.88
NEFT	22818	10.55	19.42
NEFT	22819	19.39	18.96
NEFT	22820	23.42	19.14

Table 34: Percent error for flux and heating tallies.

Position	Cell	Flux error	Heat error
NEFT	22821	27.1	18.11
NEFT	22822	29.3	19.35
NEFT	22823	21.67	18.03
NEFT	22832	27.49	17.99
NEFT	22833	14.81	17.74
NEFT	22835	13.64	17.75
NEFT	22836	11.01	18.25
NEFT	22837	1.67	19.09
NEFT	22839	27.34	18.53
NEFT	22840	27.4	18.48
NEFT	22842	26.26	17.63
NEFT	22843	23.77	17.7
NEFT	22844	6.9	17.56
NEFT	22845	22.27	18.5
NEFT	22846	17.54	17.38
NEFT	22847	14.27	18.96
NEFT	22848	10.47	19
NEFT	22849	19.54	19.14
NEFT	22850	23.07	18.73
NEFT	22851	26.95	17.68
NEFT	22852	26.37	18.59
NEFT	22853	21.7	18.21
NEFT	22901	21.92	17.81
NEFT	22902	26.18	18.09
NEFT	22903	12.24	18.92
NEFT	22904	22.08	19.1
NEFT	22905	13.77	18.34
NEFT	22906	10.72	18.46
NEFT	22907	19.92	19.05

Table 35: Percent error for flux and heating tallies.

Position	Cell	Flux error	Heat error
NEFT	22908	17.95	19.57
NEFT	22909	26.24	18.68
NEFT	22910	16.44	19.29
NEFT	22911	30.17	18.59
NEFT	22912	30.61	18.25
NEFT	22914	8.34	18.16
NEFT	22915	22.24	18.91
NEFT	22916	17.61	18.49
NEFT	22917	14.16	18.81
NEFT	22918	10.31	18.66
NEFT	22919	19.23	18.82
NEFT	22920	22.88	18.4
NEFT	22921	26.9	17.79
NEFT	22922	24.58	18.34
NEFT	22923	23.34	17.77
NEFT	22931	21.76	17.38
NEFT	22932	25.13	18.25
NEFT	22933	13.79	18.23
NEFT	22934	21.03	19
NEFT	22935	13.68	18.39
NEFT	22936	10.41	18.21
NEFT	22937	6.69	18.47
NEFT	22938	18.11	18.58
NEFT	22939	25.16	19.29
NEFT	22940	17.88	18.91
NEFT	22941	28.71	18.1
NEFT	22942	26.34	17.33
NEFT	22943	23.77	17.45
NEFT	22944	10.19	17.76
NEFT	22945	21.82	17.96
NEFT	22946	17.58	18.05
NEFT	22947	13.89	18.77
NEFT	22948	10.46	18.83
NEFT	22949	19.22	19.31
NEFT	22950	22.85	17.9
NEFT	22951	27.02	17.11
NEFT	22952	22.99	17.87
NEFT	22953	19.64	17.61
EFT	23052	21.75	23.29
EFT	23053	21.49	22.11

Table 36: Percent error for flux and heating tallies.

Position	Cell	Flux error	Heat error
EFT	23054	21.77	22.68
EFT	23055	21.83	21.66
EFT	23056	21.93	22.13
EFT	23057	16.42	15.95
EFT	23058	21.91	21.5
EFT	23059	21.94	20.89
EFT	23060	21.88	21.17
EFT	23061	38.71	37.19
EFT	23062	38.75	39.24
EFT	23073	48.81	51.27
EFT	23074	41.83	45.54
EFT	23101	5.63	4.62
EFT	23102	4.11	3.32
EFT	23103	6.05	2.47
EFT	23104	4.84	1.33
EFT	23105	4.15	3.97
EFT	23106	4.97	2.52
EFT	23201	4.13	3.71
EFT	23202	6.57	6.48
EFT	23203	6.63	5.1
EFT	23204	4.7	4.66
EFT	23205	5.1	5.2
EFT	23206	5.24	3.43
EFT	23301	4.26	5.84
EFT	23302	5.61	3.53
EFT	23303	6.81	4.44
EFT	23304	5.23	2.55
EFT	23305	5.17	3.95
EFT	23306	6.41	8.55
EFT	23401	4.13	3.39
EFT	23402	5.93	2.72
EFT	23403	2.57	5.78
EFT	23404	5.89	8.46
EFT	23405	4.34	10.66
EFT	23406	4.46	0.85
EFT	23501	4.58	5.6
EFT	23502	5.17	4.04
EFT	23503	6.32	4.56
EFT	23504	4.59	4.28
EFT	23505	5.24	5.12

Table 37: Percent error for flux and heating tallies.

Position	Cell	Flux error	Heat error
EFT	23506	5.17	4.5
EFT	23601	5.03	4.24
EFT	23602	5.27	3.13
EFT	23603	6.35	4.13
EFT	23604	4.33	1.59
EFT	23605	5.46	4.39
EFT	23606	4.85	3.16
EFT	23701	22.39	23.21
EFT	23702	22.7	22.61
EFT	23703	23.12	23.14
EFT	23704	21.9	21.66
EFT	23705	22.74	23.18
EFT	23706	22.48	22.76
EFT	23731	22.62	22.64
EFT	23732	22.5	22.43
EFT	23733	22.96	23.2
EFT	23734	22.39	22.18
EFT	23735	22.6	22.82
EFT	23736	22.19	22.3
EFT	23776	5.12	3.89
EFT	23777	5.14	4.34
EFT	23801	22.49	22.87
EFT	23802	22.6	23.24
EFT	23803	22.79	23.4
EFT	23804	22.27	22.42
EFT	23805	22.53	23.18
EFT	23806	22.21	22.62
EFT	23831	22.34	21.88
EFT	23832	22.62	23.14
EFT	23833	22.79	22.57
EFT	23834	22.5	22.24
EFT	23835	22.2	22.17
EFT	23836	22.38	22.18
EFT	23901	22.43	22.74
EFT	23902	22.45	23.05
EFT	23903	22.75	23.35
EFT	23904	22.19	22.91
EFT	23905	22.49	22.82
EFT	23906	22.2	22.65
EFT	23907	22.62	22.56

Table 38: Percent error for flux and heating tallies.

Position	Cell	Flux error	Heat error
EFT	23931	22.55	22.15
EFT	23932	22.44	22.16
EFT	23933	22.76	22.78
EFT	23934	22.2	22.46
EFT	23935	22.45	22.67
EFT	23936	22.14	22.17
EFT	23937	22.67	22.66
SEFT	24007	23.4	22.51
SEFT	24008	23.4	21.84
SEFT	24009	23.22	22.28
SEFT	24010	23.28	21.63
SEFT	24011	23.21	22.4
SEFT	24012	23.22	21.48
SEFT	24014	23.2	22.39
SEFT	24015	23.3	22.07
SEFT	24016	23.29	22.55
SEFT	24017	17.92	16.91
SEFT	24031	23.38	22.75
SEFT	24032	23.32	22.3
SEFT	24033	23.28	22.61
SEFT	24018	39.38	38.5
SEFT	24019	39.28	40
SFT	25052	19.71	21.37
SFT	25053	19.46	20.27
SFT	25054	19.67	20.46
SFT	25055	19.77	19.59
SFT	25056	19.8	19.83
SFT	25057	14.15	13.55
SFT	25058	19.79	19.37
SFT	25059	19.79	18.84
SFT	25060	19.8	19.13
SFT	25061	38.22	37.84
SFT	25062	37.83	37.72
SFT	25073	45.47	49.62
SFT	25074	41.28	44.18
SFT	25101	0.65	0.52
SFT	25102	2.4	1.25
SFT	25103	2.58	2.69
SFT	25104	0.23	3.83
SFT	25105	2.25	1.38

Table 39: Percent error for flux and heating tallies.

Position	Cell	Flux error	Heat error
SFT	25106	0.51	0.58
SFT	25201	3.35	1
SFT	25202	3.23	1.38
SFT	25203	2.61	0.69
SFT	25204	2.59	1.48
SFT	25205	2.83	2.15
SFT	25206	3.64	1.99
SFT	25301	2.63	0.63
SFT	25302	3.69	3.52
SFT	25303	3.7	1.19
SFT	25304	2.9	3.12
SFT	25305	3.81	3.42
SFT	25306	4.37	5.52
SFT	25401	4.03	7.19
SFT	25402	0.13	0.46
SFT	25403	2	2.32
SFT	25404	2.15	3.07
SFT	25405	1.09	8.96
SFT	25406	0.2	2.9
SFT	25501	2.14	0.82
SFT	25502	2.54	2.31
SFT	25503	1.98	0.43
SFT	25504	2.1	0.12
SFT	25505	2.11	2.75
SFT	25506	2.11	2.36
SFT	25601	2.26	0.99
SFT	25602	2.41	0.57
SFT	25603	2.37	0.36
SFT	25604	2.45	0.68
SFT	25605	1.82	2.11
SFT	25606	2.17	0.03
SFT	25701	20.5	20.82
SFT	25702	20.17	20.72
SFT	25703	20.67	20.58
SFT	25704	20.46	20.4
SFT	25705	19.92	20.66
SFT	25706	20.59	20.19
SFT	25731	20.34	19.85
SFT	25732	20.3	19.97
SFT	25733	20.5	20.29

Table 40: Percent error for flux and heating tallies.

Position	Cell	Flux error	Heat error
SFT	25734	20.2	19.37
SFT	25735	19.63	20.21
SFT	25736	20.63	20.18
SFT	25776	2.63	2.64
SFT	25777	2.53	1.94
SFT	25801	20.12	20.43
SFT	25802	20.1	20.19
SFT	25803	20.43	21.05
SFT	25804	20.35	20.46
SFT	25805	20.15	20.47
SFT	25806	20.49	21.02
SFT	25831	20.17	20.15
SFT	25832	20.06	20.35
SFT	25833	20.45	20.05
SFT	25834	20.37	20.38
SFT	25835	20.34	21.13
SFT	25836	20.46	20.94
SFT	25901	20.24	20.74
SFT	25902	20.06	20.88
SFT	25903	20.47	20.55
SFT	25904	20.3	20.33
SFT	25905	20.14	21.29
SFT	25906	20.2	20.77
SFT	25907	20.72	20.92
SFT	25931	20.24	20.65
SFT	25932	20.1	19.99
SFT	25933	20.17	19.61
SFT	25934	20.38	19.93
SFT	25935	20.09	20.57
SFT	25936	20.16	20.43
SFT	25937	20.28	19.83
SWFT	26007	15.69	14.53
SWFT	26008	15.59	13.8
SWFT	26009	15.62	14.59
SWFT	26010	15.5	13.9
SWFT	26011	15.45	14.48
SWFT	26012	15.4	13.59
SWFT	26014	15.31	14.52
SWFT	26015	15.22	14.21
SWFT	26016	15.26	14.64

Table 41: Percent error for flux and heating tallies.

Position	Cell	Flux error	Heat error
SWFT	26017	9.39	8.32
SWFT	26031	15.24	14.48
SWFT	26032	15.11	13.96
SWFT	26033	15	14.37
SWFT	26018	32.75	32.79
SWFT	26019	32.76	32.47
WFT	27007	17.47	16.12
WFT	27008	17.38	15.5
WFT	27009	17.44	16.33
WFT	27010	17.41	15.75
WFT	27011	17.35	16.29
WFT	27012	17.36	15.28
WFT	27014	17.41	16.32
WFT	27015	17.58	16.25
WFT	27016	17.53	16.65
WFT	27017	11.73	10.56
WFT	27031	17.55	16.77
WFT	27032	17.49	16.16
WFT	27033	17.43	16.39
WFT	27018	35.18	34.27
WFT	27019	34.84	35.44
NWFT	28010	19.27	18.42
NWFT	28024	19.27	18.7
NWFT	28025	19.31	17.66
NWFT	28026	19.28	18.66
NWFT	28027	19.28	17.57
NWFT	28031	19.31	18.57
NWFT	28032	19.2	18.15
NWFT	28033	19.12	18.36
NFT	29007	19.63	19.05
NFT	29008	19.74	18.33
NFT	29009	19.75	19.13
NFT	29010	19.73	18.26
NFT	29011	19.72	18.82
NFT	29012	19.66	18.4
NFT	29014	19.79	18.88
NFT	29015	19.83	18.9
NFT	29016	19.79	19.06
NFT	29017	14.18	13.24
NFT	29031	19.92	19.15

Table 42: Percent error for flux and heating tallies.

Position	Cell	Flux error	Heat error
NFT	29032	19.92	18.77
NFT	29033	19.87	19.01
NFT	29018	36.07	34.99
NFT	29019	36.19	35.98

Table 43: Percent error for flux and heating tallies.